# FRICTION AND SLIDING WEAR OF WC-Co INSERTS CONTAINING MIXED CARBIDES (TiC, TaC, NbC)

**Roxane van der Merwe**

A research report submitted to the Faculty of Engineering and the Built Environment, of the University of the Witwatersrand, in partial fulfilment of the requirements for the degree of Master of Science in Engineering.

Johannesburg, 2011

I declare this research report is my own unaided work. It is being submitted to the Degree of Master of Science to the University of the Witwatersrand, Johannesburg. It has not been submitted before for any degree or examination to any other University.

..........................................................................................................................

Roxane van der Merwe

........................... day of ........................... year ..............................

# Abstract

Improving the wear resistance of materials subject to friction and sliding wear plays an important role in extending the life cycles of equipment used for demanding applications. The focus of this project was to systematically investigate the friction and sliding wear characteristics of three grades of WC-Co alloys to which refractory carbides TiC, TaC and NbC were added. The wear behaviour was characterized by sliding the carbide alloys against two grades of steel in a pin-on-disc configuration and determining the associated wear mechanisms. The influence of applied load and sliding velocity on the friction and wear response was also analyzed. The 304 stainless steel sliding pairs experienced 50% more friction than the bright mild steel sliding pairs under all operating conditions. An increase in load caused a non-linear decrease in friction while an increase in sliding velocity did not have a significant effect. The WC-Co alloy to which small amounts of TaC and NbC were added was found to have the highest wear resistance under all the operating conditions tested. The wear mechanisms for the steels were predominantly smearing and groove formation caused by ploughing of the wear particles. The predominant wear mechanisms for the cemented carbides were preferential binder removal, followed by carbide grain cracking and carbide grain pull-out with the occasional tribofilm.

Dedicated to my grandparents, Rensché and Jan le Roux and Mona and Leslie Schreiber, for all the love they have given me and for affording me with such wonderful parents.

To my parents Nada and Basil Schreiber, who have always steadfastly supported me in all that I do and who have always been my best friends.

Aan my man Johann, my sielsgenoot en beste vriend, vir al sy liefde, ondersteuning en geduld.

# Acknowledgements

I would like to thank my supervisor, Dr Natasha Sacks, for all her support, and guidance throughout this research project. I am grateful for her willingness and dedication to take me on as a part time student. Her commitment to her students is inspirational.

It is with gratitude towards my company, Foster Wheeler South Africa, and specifically my manager, Herman Bothma, and my Lead Engineer, Stuart South, for their understanding and support. I thank them for allowing me all the time away from work in order to accomplish a personal goal.

I would sincerely like to thank my parents for all the phone calls of support, the messages of encouragement and all the love they have given me over the years; I love them greatly.

Aan my man Johann, vir wie ek verskriklik lief is, wil ek baie dankie se vir al sy onwrikbare ondersteuning, aanmoediging en geduld. Ek is God ewig dankbaar vir sy liefde en sien uit na nog baie advonture saam!

# Contents

# List of Figures

# List of Tables

# Chapter 1

# Introduction

One of the unique attributes of modern day engineering is the increasing focus on the field of materials science and engineering. With the growing financial demand on cost saving, engineers and scientists are pursuing newer and improved materials to satisfy both the economic and technical demands of society. One area that has received extensive interest is that of industrial machinery and manufacturing tools which form a critical part of the manufacturing and fabrication industry. Equipment is expected to have longer life cycles under increasingly demanding applications. In order to achieve this, wear resistance should be a major focus point early in the design phase [1]. By increasing a component's wear resistance its life cycle is extended and in turn maintenance and component replacement costs are reduced.

Considering the manufacturing industry, sliding wear is generally of interest. This type of wear is often encountered within the industrial and manufacturing processes where machining and cutting tools, wire drawing, drilling, to name a few are employed. The cause of tool degradation can often be attributed to wear. Factors that influence the degree of wear are the material properties such as hardness, microstructure and composition, lubrication or lack thereof, as well as the operating conditions [1]. Drill bits, for example, operate at high speed and are exposed to high temperatures, demanding loads and friction. The materials used for the manufacturing of drill bits must therefore be able to withstand these conditions to reduce excessive wear.

Tungsten carbide-cobalt (WC-Co), well known for its high hardness and excellent wear resistance, is successfully being used to manufacture drill bit inserts. The wear resistance properties of WC-Co can be enhanced by adding refractory metals such as Ti, Ta and Nb [2]. Based on preliminary investigations it has been found that the combined effect of adding these refractories to WC-Co is not well researched. In addition when sliding wear specifically is considered, limited published information is available.

The focus of this project is to systematically investigate the friction and sliding wear characteristics of WC-Co alloys to which refractory metals have been added. The sliding wear will be evaluated against common engineering materials encountered in industrial applications. The influence of applied load and sliding velocity on friction and wear will also be analysed. The results of this project will broaden the existing scientific knowledge base on cemented carbides. In addition research in this field could enhance current insert applications and possibly result in new applications.

The remainder of this research report is structured in the following manner: Chapter 2 reviews the fundamentals of friction and sliding wear as well as published literature on the production and properties of cemented carbides. Chapter 3 describes the experimental procedures followed throughout this project. The summarised results are presented in Chapter 4 and discussed and analyzed in Chapter 5. The conclusions that have been drawn are presented in Chapter 6. Detailed test results are provided in appendices.

# Chapter 2

# Literature Review

Tribology, defined as 'the science and technology of interacting surfaces in relative motion' [1], involves the study of friction, wear and lubrication. These three factors are fundamentally linked together and each contributes significantly to the success or failure of a given system of surfaces in relative motion to each other.

Many applications existing today do not allow for lubrication. In the absence of lubrication, as is the case with dry sliding wear, the friction and wear response of the system will be more significant in determining the failure modes and lifetimes of the system components. Thus the material properties and the parameters of the operating system which affect friction and wear become vital to improve the tibological response within the system.

Cemented carbides have been developed for such applications and are widely used throughout industry for its high wear resistance properties. In search for greater efficiencies and new applications, cemented carbides are constantly being modified to improve material performance.

This chapter reviews the fundamentals of tribology and cemented carbides which are the focus of this research project. This chapter is divided into three sections. The first two sections review the main components of the researched tribological system namely, friction and dry sliding wear. The third section reviews the investigated materials namely, cemented carbides with emphasis being placed on the sliding wear characteristics.

## 2.1 Friction

Friction can be defined as the resistance experienced by one body when moving against another body [1]. Friction is usually described or compared by using μ, known as the coefficient of friction. This coefficient of friction is indicative of the relationship between the frictional force experienced, F, and the normal load on the object, W [1,3,4]:

$$\mu = F/W \tag{2.1}$$

For most common materials sliding in air, the value of μ usually lies between 0.1 and 1 [1]. Equation (2.1) is an expression of the Laws of Friction as described below.

There are two types of coefficients of friction that are required to accurately describe a system experiencing friction. The first is the static coefficient of friction, $\mu_s$, which describes the system in which an object remains stationary although a force is being exerted against it. The second is the kinetic coefficient of friction, $\mu_k$, which is used to describe the system when an object is moved from its point of rest due to a force being exerted against it and the object continues to move under the applied force. It is common knowledge that $\mu_s$ is usually larger than $\mu_k$ as the force required to initiate motion is larger than the force required to maintain motion [1,4].

There are three Laws of Friction generally applied to metals [1,3,5]. The laws state that the frictional forces are:

i. Proportional to the normal load on the object,
ii. Independent of the area of contact and
iii. Independent of the sliding velocity.

The third law only applies once motion has started [5] and thus only kinetic friction with its kinetic coefficient of friction $\mu_k$ is independent of sliding velocity and does not change for moderate speeds [1].

It is important to acknowledge that friction is not a material property but rather a system response [5]. There are various factors that influence the friction properties of materials. For example, oxide films, composition, microstructure, environmental conditions and the applied loads all affect how the material will respond to the friction experienced [1]. With metals, temperature has a significant effect on friction. When the temperature of a metal increases it changes the mechanical properties and the rate of oxidation and there is the possibility of phase transformations, all of which affect frictional behaviour [1].

Friction plays a contributory role to the rate of wear within a given system although no accurate relationship, producing realistic results, has been defined [3]. Although sliding velocity does not usually affect friction it does affect the frictional energy dissipation which in turn affects the temperature at the sliding interface [1]. Measuring the friction coefficient during a wear test allows changes in the sliding behaviour of the material to be monitored and often corresponds to changes in the wear pattern and hence the wear mechanisms which often renders valuable information of the material properties [1].

When considering sliding friction it has been accepted that the total intrinsic frictional force consists of two components [5]. That of the force required to shear the asperities known as the adhesive friction component and that of the force required to supply the energy of deformation known as the ploughing component. For brittle materials the fracture of adhesive contacts and brittle deformation need to be considered. Therefore fracture toughness plays a vital role.

The pattern of a friction response graph during dry sliding wear can often provide detailed information. These graphs are typically presented in an S-shaped curve as shown in Figure 2.1 [5]. The shape of these friction curves may be influenced by the interface materials as well as the operating conditions. During sliding, changes occur between the surfaces and within the surface materials that affect the friction and wear properties. The initial sliding period during which the frictional forces stabilize is often referred to as the run-in period. During this time high asperities may be worn down, surface films may be removed or new films formed or structural changes within the material may occur. After this initial period new changes may occur at the interfaces of the two sliding bodies such as roughening and/or the presence of trapped wear particles which may lead to an increase in the friction level or causing it to increase to a new steady state plateau [5].

The transitions that friction could possibly undergo during a wear test can generally be grouped into four patterns as illustrated in Figure 2.1 [5].

The first pattern (I) shows that friction stays at an initial level for a period of time and then slowly increases to another steady state value. This pattern is often associated with identical metals sliding against each other. This response is a result of ploughing due to roughening of the surface and entrapped wear particles. In smooth surfaces involving elastic deformation with a dominant adhesive component of friction an increase in the friction level is associated with the smoothing of the surfaces resulting in a larger component of adhesive friction [5].

The second pattern (II) shows that friction stays at an initial level for a period of time and then increases to a higher level after which it decreases slightly and then levels off. This decrease in friction is due to the smoothing of two hard surfaces experiencing plastic deformation which results in a decrease in the ploughing component. If the surfaces experience elastic contact where the adhesive component is dominant a decrease in the adhesive component of the friction is due to the decreased real contact area as a result of the ploughing which is due to the roughening and wear debris [5].

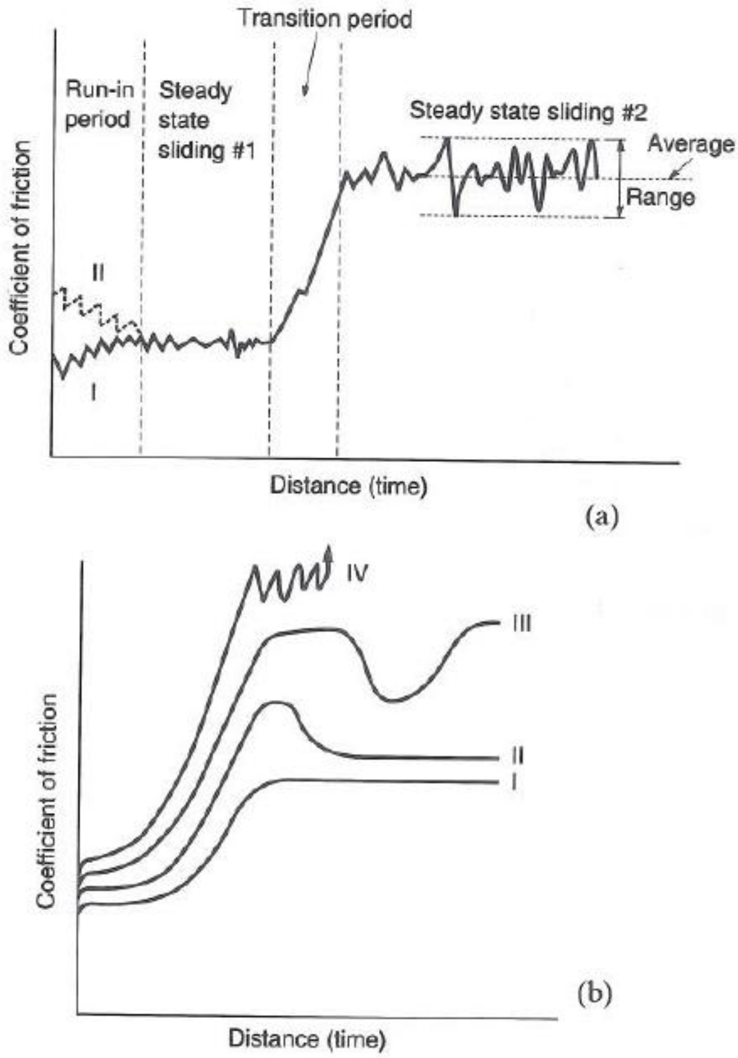


*Figure 2.1 The coefficient of friction as a function of sliding distance. (a) A typical S-shaped curve illustrating the running in period. (b) Four hypothetical patterns that can be expected [5].*

Pattern three (III) shows that friction increases to a high value at which it remains for a period of time and then decreases to a lower value. Shortly afterward it increases again to a high level. This pattern can often be repetitive. The decrease in the friction level during plastic contact is thought to be due to the ejection of wear particles from the contact surfaces and then subsequently the formation of new wear particles contributes to the increase in the friction levels [5].

Pattern four (IV) is similar to pattern (III) however the high and low levels are not repetitive but rather unpredictable. The sharp rise in the friction level and its erratic behaviour is usually associated with incompatible material pairing [5].

## 2.2 Sliding wear

Sliding wear refers to the wear that occurs when one body is sliding over another body [1]. It results in deformation of a material's surface generally due to a breakdown of lubrication which is often referred to as scuffing when it occurs at high speeds. Galling is a result of severe sliding wear and causes harsh surface damage due to localized welding during un-lubricated conditions at low speeds [1].

Tests executed to investigate sliding wear can be performed using numerous test configurations as indicated in Figure 2.2. The geometries may differ but the basic principle remains the same; one body is held stationary whilst the other body is in motion. One of the most common configurations used is that of the pin-on-disc (Figure 2.2(a)), which is also used in the current project. It consists of a stationary pin, to which a load is applied, pressed against a rotating disc. The pin can also be a non-rotating ball or a hemispherically tipped rider [5].

Several mechanisms have been proposed to explain how sliding wear operates. Although the specific details of material removal differ for each mechanism, plastic deformation is shown to be the main cause of sliding wear [1]. One mechanism involves shearing of the asperities on the interface either with no wear occurring (1) or with the irregular shaped sheared particles adhering to the opposite surface (2) as shown in Figure 2.3 [5].

A second mechanism attributes wear to the plastic shearing of successive layers of an asperity with complete detachment of the wedge shaped fragment. The plastic shearing occurs in conjunction with a shear crack which occurs along a slip line field along which the fragment detaches as illustrated in Figure 2.4. This fragment can become attached to the opposite surface due to adhesion [5].

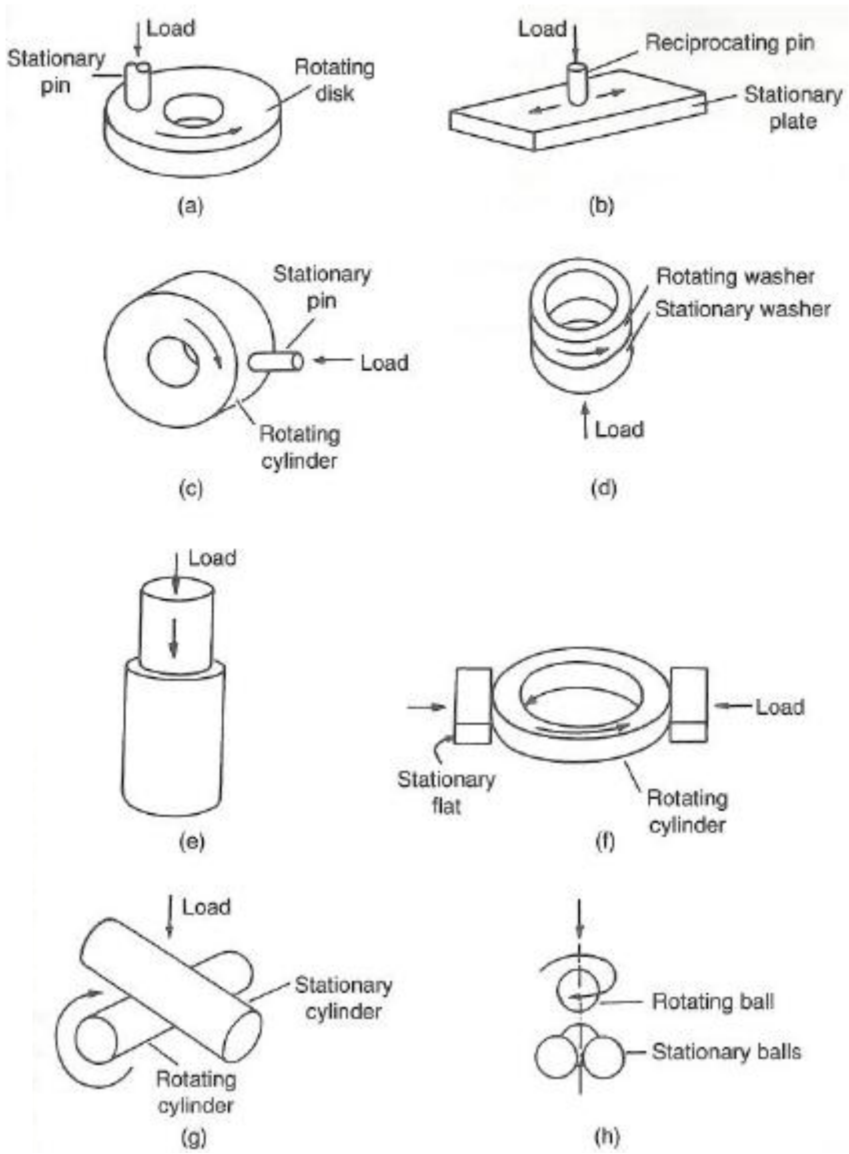


*Figure 2.2. Typical geometries used for sliding friction and wear tests; a) pin-on-disc, b) pin-on-flat, c) pin-on-cylinder, d) thrust washers, e) pin-into-bushing, f) rectangular flats on rotating cylinder, g) crossed cylinder and h) four ball [5].*

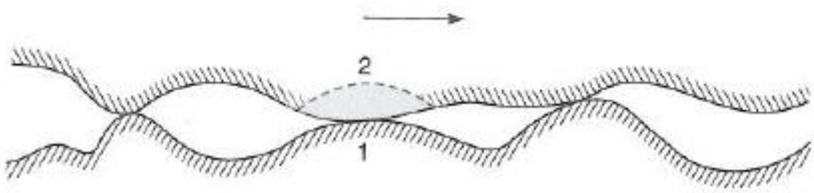


*Figure 2.3. Illustrating two possibilities of breaks during shearing of an interface [5].*

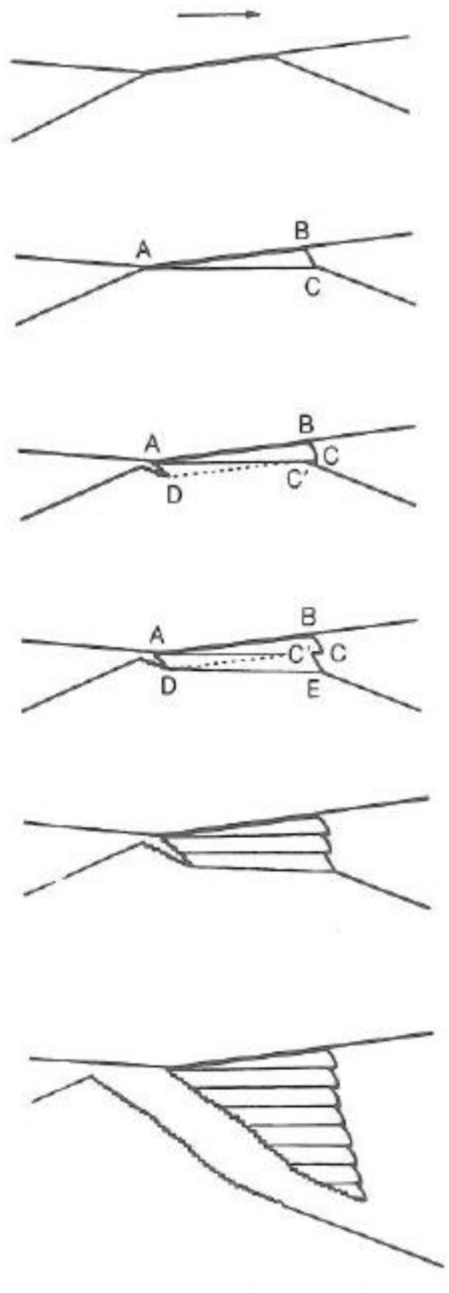


*Figure 2.4 Illustrating detachment of a fragment due to plastic shearing of successive layers of an asperity contact [5].*

These two mechanisms can be repetitive and can result in these fragments finally being released as wear particles which are roughly equal in size [5].

A fragment will remain attached to a surface if the adhesive energy between the fragment and the surface exceeds that of the fragment's elastic energy and will become detached if the elastic energy is greater [6]. The adhesion of fragments to the surface indicates the presence of strong bonds. The absence of a fragment implies the absence of such a bond. This is likely due to chemical changes occurring on the surface of the fragment. The large area of the surface promotes oxidation. With extensive oxidation the oxides, instead of the original material, attach to the surface and form a weaker bond which reduces the fragment's adhesive strength and thus the fragments break loose. Another possible reason for the breakaway of fragments from a surface is due to residual elastic energy of adherent fragments. These fragments are heavily stressed when trapped between the two opposing surfaces. When the sliding surface moves on residual stresses remain within the fragment. If these residual stresses are greater than the adhesive strength attaching it to the surface the fragment will break away [5-6]. Particle size may also play a contributing role in determining whether a fragment will become detached. Particles less than a critical size will remain adhered to the surface, however, particles larger than the critical size will break loose due to more elastic energy being present [6].

When these fragments break free and/or while they are still attached to a surface, it is possible for abrasive wear to be initiated [1]. Visually, abrasive wear can be identified by scratches or grooves on the softer surface, parallel to the sliding direction, referred to as ploughing or cutting. [5]. Fatigue wear, due to cyclic loading that may occur during the sliding motion, may also cause fragments to break off [5].

In sliding wear there is no singular wear mechanism that operates at a given time but rather a combination of mechanisms. These mechanisms depend on certain dominating factors and can change as these factors are changed. In un-lubricated wear of metals the wear mechanisms depend largely on the applied mechanical stresses, interface temperature and the oxidation rates of the surfaces in contact. These factors are interrelated and are influenced by changes in the sliding condition parameters such as the normal load, sliding velocity and often the sliding time or distance as Figure 2.5 illustrates [1].

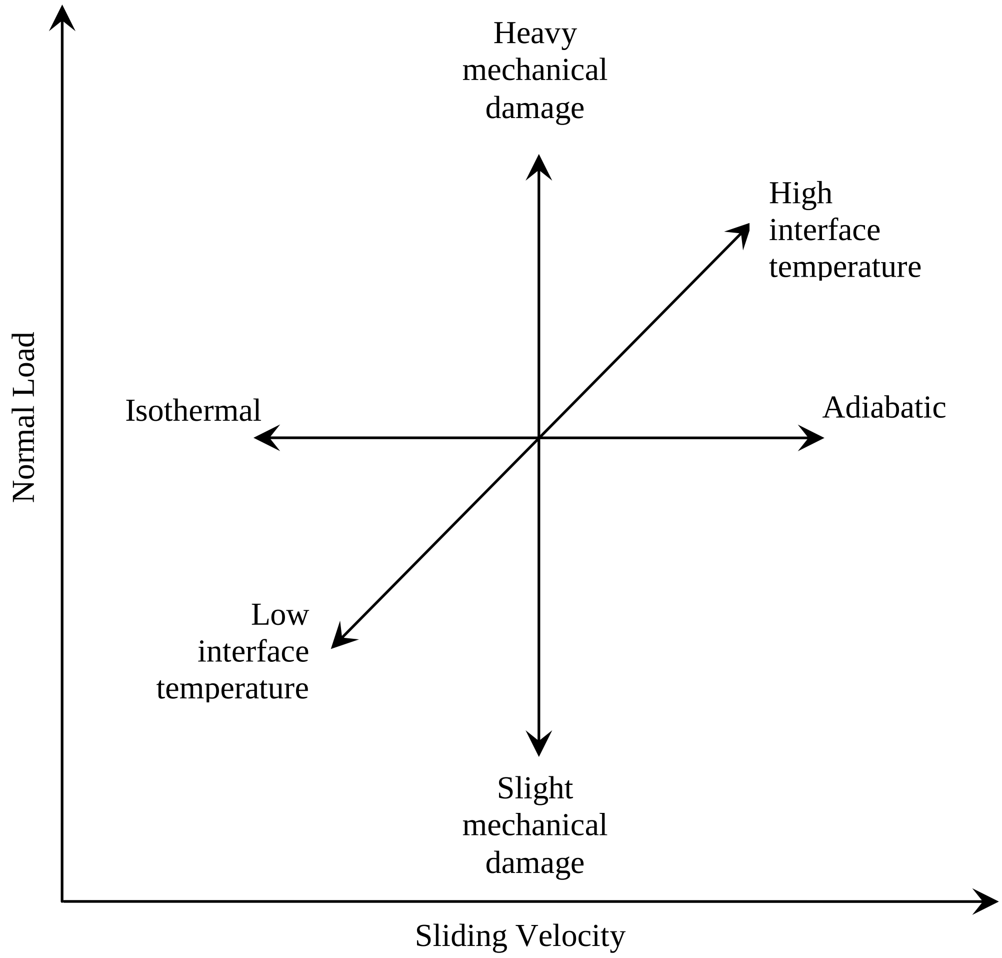


*Figure 2.5 Illustrating the combined influences that load and sliding velocity have on the sliding wear process in metals [1].*

An increase in the applied load has a direct correlation to an increase in the stress experienced. Load and sliding velocity both influence the interface temperature. The interface temperature in conjunction with the sliding velocity will affect oxidation that may occur. At low sliding velocities the heat generated at the surface will be rapidly conducted away resulting in an isothermal process. At high sliding velocities the heat generated will not be able to dissipate and will result in an adiabatic process. A high interface temperature promotes rapid growth of oxide layers and may decrease the mechanical strength of asperities. Occasionally hot spots might occur where the temperature at certain asperities may be significantly higher than the rest of the material [1].

These factors contribute to the degree of severity of the wear experienced. Most metals portray a wear rate transition area when subjected to an increasing applied load. Wear at loads below this transition region will be mild, whilst wear above this transition region will be severe. All sliding processes start with a layer of the softer material being transferred to the harder material. For mild wear this layer transfers back to the softer material which has oxidized during sliding. The oxide provides low shear strength at the sliding interface thereby reducing friction due to limited metallic contact. For severe wear the transferred layer becomes hardened and new material is transferred from the softer material to this hardened layer. This transferred material eventually breaks off leaving the system in plate-like forms of debris. Mild wear is characterised by fine debris which predominantly consists of oxide particles and very few metal particles. Mild wear occurs when a balance is achieved between the exposure of a fresh metal surface caused by severe wear and that of the rate of oxidation of the newly exposed surface. Severe wear debris constitutes mainly of large metallic particles as a result of extensive metallic contact due to either the absence of an oxide layer or the penetration of the oxide layer under the high applied forces [1].

Figure 2.6 shows a type of wear-regime map that may be developed for the sliding wear of metals. The map in Figure 2.6 is specific to the sliding system being tested and cannot be generalized for all sliding systems as the boundaries between mild and severe wear will differ depending on the specific materials being tested. However the shape may be similar for many metals sliding against each other in air in a pin-on-disc test configuration. This map serves to illustrate the complexity of the interactions between the factors that influence sliding wear [1].

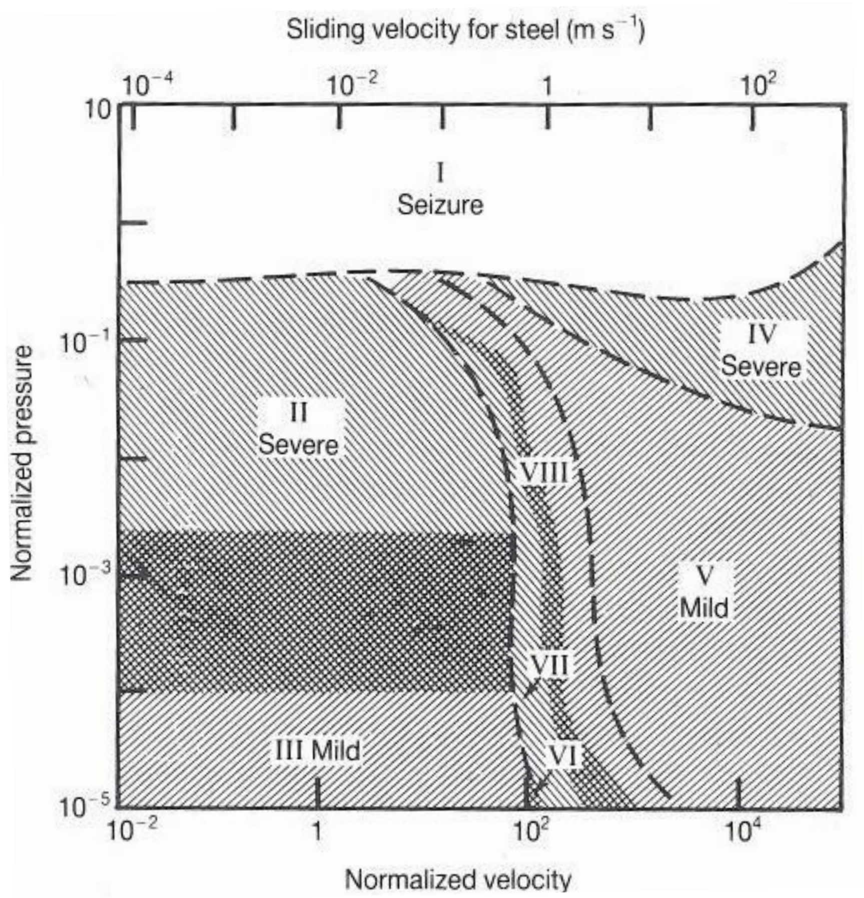


*Figure 2.6 Wear-regime map for dry sliding of steel-on-steel in a pin-on-disc set up [1].*

Figure 2.6 employs dimensionless variables. Normalised pressure is defined by the normal load applied on the pin divided by the nominal contact area multiplied by the indentation hardness of the softer material. Normalised velocity is defined by the sliding velocity divided by the velocity of heat flow [1].

Eight distinct wear regimes are defined for the sliding system in Figure 2.6 [1]:

Regime I represents very high contact pressures and complete seizure of the surfaces.

Regime II corresponds to severe wear. High loads, low sliding velocities and thin oxide layers which are easily pierced by asperities are experienced.

Regime III represents mild wear. The conditions experienced are similar to regime II with the exception that the loads are low. Consequently the oxide layer is not pierced and wear is caused by particles being removed from the oxide layer itself.

Regime IV symbolizes severe rapid wear. In addition to the high loads, the high velocities result in high frictional power and high temperatures which effectively melt the surfaces of the materials.

Regime V corresponds to mild wear. Although the sliding velocity is high, the load is low. The interface temperature is high but below melting point and results in rapid oxidation of the surface.

Regime VI represents mild wear. It operates in the transition zone between mild and severe wear. The increase in velocity results in a sporadic increase in temperature which results in random areas where oxidation occurs. Wear is generally due to the detachment of the oxide particles.

Regime VII represents severe wear and continues on from regime VI with wear in the form of detachment of metallic particles.

Regime VIII corresponds to mild wear. The increase in temperature and sudden cooling by the conduction of heat into the bulk material leads to the formation of martensite which provides mechanical support for the surface oxide film. Wear is in the form of detachment of the oxide particles.

Wear regime maps are generally constructed using a combination of finite element modelling and experimental testing and are useful tools for the assessment of wear properties within a system. However producing these maps can be time consuming. A simplified equation exists for calculating the wear rate due to sliding wear. This equation is referred to as the Archard wear equation and is described as follows [1, 3, 7]:

$$Q = KW/H \quad (2.2)$$

The quantity $Q$ is the volume of the material that has been worn per unit distance. This equation highlights the main contributing factors that affect the amount of wear that occurs. These factors are:

- $W$- the normal load;
- $K$- the dimensionless wear coefficient (which is less than unity) and
- $H$- the hardness of the softer surface.

The severity of the wear that has occurred is often indicated by the value of $K$ which may be used as a means for comparison. This equation is derived from the assumption that wear will occur between two surfaces where the asperities touch and that the true area of contact will be a summation of the individual asperities' areas [1,3]. An often more useful parameter to use for comparative purposes is the dimensional coefficient of wear, $k$, defined by $K/H$.

Tribological compatibility is usually a good indicator to whether high or low wear levels can be expected. Compatibility in this case refers to the resistance of the two opposing surfaces to form a strong interfacial bond. High levels of tribological compatibility are associated with low values of K and usually result between different non-metals or between non-metals and metals that have a low mutual solubility. Surface films such as oxide coatings influence the mutual solubility between materials with the absence of such coatings in noble metals resulting in low wear rates [1].

As mentioned earlier, the effects of sliding wear may initiate abrasive wear. This can have an effect on the overall wear resistance within the system. Materials with the same hardness under the same operating conditions could yield different results due to way in which they respond to the abrasive wear component. The ratio of E/H, where E is Young's modulus and H is the hardness, is generally used to explain such differences. When comparing materials of equal hardness, the material with the lower E/H ratio will yield a higher K value and thus have a higher wear rate [1].

### 2.3 Cemented carbides

Cemented carbides successfully combine the excellent properties of ceramics, such as hardness and heat resistance, with the excellent properties of metals, such as toughness and impact strength [3].

Cemented carbides, often referred to as hardmetals, are sintered materials comprising of carbide compounds of refractory metals, predominantly tungsten carbide (WC), cemented with a metallic binder [8-9]. Other carbides that may be added are nobium carbide (NbC), tantalum carbide (TaC), and titanium carbide (TiC) [3]. Possible binder phases are cobalt (Co), nickel (Ni) or combinations of these materials. Cemented carbides that have been bonded with nickel show inferior toughness properties compared to cemented carbides that have been bonded with cobalt [10]. This is due to the superior wetting properties of Co on the WC.  Therefore the most widely used cemented carbide is that based on the WC-Co system [9].

There is no internationally accepted naming system to classify cemented carbides. However the C-grade system is widely used and divides the carbides into four main categories. The first category (C1-C4) refers to cemented carbides consisting only of WC-Co. The grades from this category are used for machining cast irons, high temperature alloys and nonferrous metal such as titanium alloys. A second category (C5-8) refers to multi-carbide materials which contain different combinations of tungsten carbide, titanium carbide, tantalum carbide and niobium carbide bonded together by cobalt. This category is recommended when machining steels as they provide better crack resistance compared to the grades of category one. Contrary to categories one and two, categories three and four are not used for machining purposes. Category three (C9-C11) refers to cemented carbides used for wear resistance as its primary function and category four (C12-C14) for its impact resistance [8]. Generally the applications of cemented carbides broadly include that of machining [8].

*Production of cemented carbides*

Cemented carbides are produced by means of powder metallurgy techniques which mean that they are fabricated by using compaction and sintering techniques. The metal powders that form the final product undergo controlled carburisation which produces the various carbides. These carbide powders are then ball milled with the metal binder. Ball milling reduces the size of the carbide particles and ensures even coating by the metal binder particles. The carbide and cobalt powder mixture is then compacted into billets by hydrostatic means or they are press-compacted into components. Finally, the billets are generally vacuum or hydrogen hip-sintered to produce the final component form [3, 9].

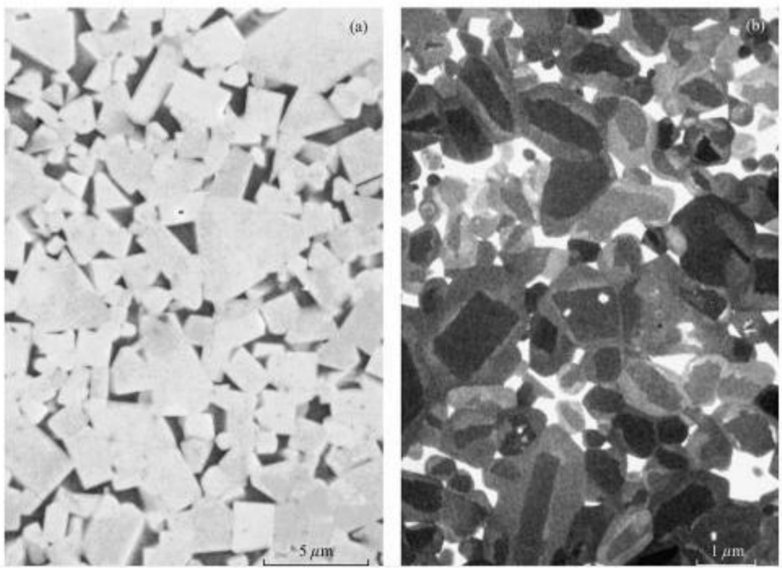


*Figure 2.7. Typical grain structure of a) WC-18vol% Co cemented carbide and b) TiCN-6.2vol% $Mo_2C$-6.3vol% Ni cermet [9].*

During the sintering process the microstructure is formed. The carbide phase partially dissolves within the binder and re-precipitates. This process results in the final shape and structure of the carbide grains. In cemented carbides, the solubility of the metallic elements within WC is very low and thus WC forms well defined single crystals, shown in Figure 2.7a [9].

Cemented carbides are manufactured into different grades by modifying the composition and weight percentage of the carbide/binder as well as the powder particle size [3]. The cobalt content is the most important variable when cemented carbides of varying properties are required; cobalt contents up to a maximum of 15-25% mass has the effect of increasing the transverse rupture strength of the cemented carbide significantly [10].

*Properties of cemented carbides*

Cemented carbides are known for their high hardness, which lends itself to high wear resistance [3]. The hardness of cemented carbides used for the machining of steel usually ranges between 1100HV to 1600HV, although it can be higher [8]. The hardness is influenced by the carbide as well as the binder content, together with the carbide grain size and chemical composition. Figure 2.8 demonstrates the influence that the binder content, in this case cobalt, has on the hardness of a specific cemented carbide [8].

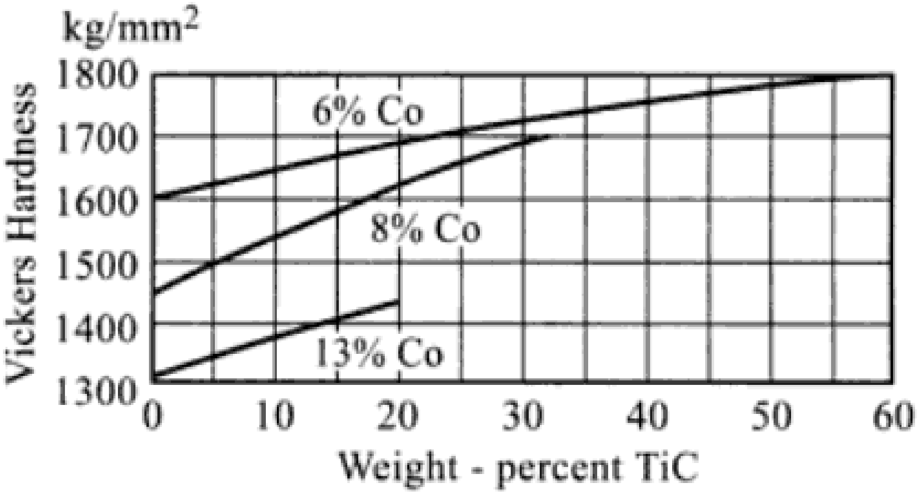


*Figure 2.8 Influence of Co and TiC content on the hardness of a WC-TiC-Co alloy [8].*

Cemented carbides are also known to have high hot-hardness qualities which are dependant on the carbide content. Figure 2.9 illustrates the high hot-hardness that WC-TiC-Co cemented carbide has in comparison to that of high speed steel. WC-TiC-Co cemented carbides still maintain a hardness of 850HV at a temperature of 1000°C [8]. At elevated temperatures however cermets portray higher hardness properties when compared to cemented carbides, thus allowing cermets to run at higher cutting speeds as they have good high temperature properties [11, 8]. The general properties of cermets are based on the titanium carbonitride phase.

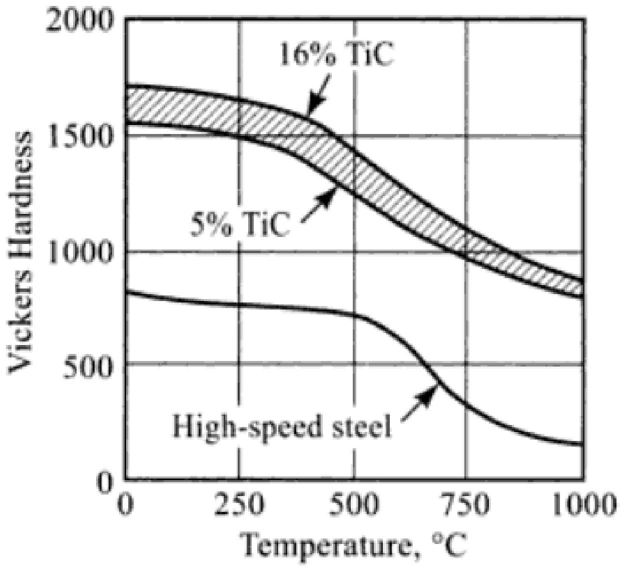


*Figure 2.9 Effect of TiC content on the hot-hardness of a WC-TiC-Co alloy [8].*

The compressive strength of cemented carbides is greater than that of most other materials and range between 3450MPa to 6900MPa. The compressive strength of WC-Co cemented carbides initially increases with an increase in the Co content and reaches a maximum at approximately 4wt%Co after which it decreases to a low at 27wt%Co. The addition of other carbides such as TiC can cause a decrease in the compressive strength as indicated in Figure 2.10 [8].

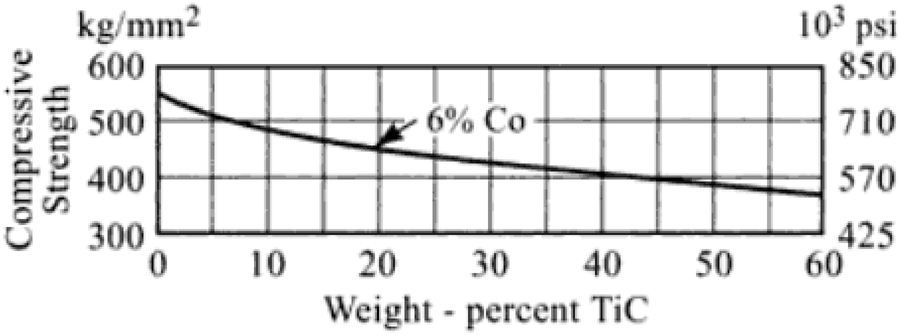


*Figure 2.10 The influence of TiC on the compressive strength of WC-TiC-Co cemented carbides at 6%Co content [8].*

Similarly to hardness, the compressive strength is influenced by the Co content as well as temperature, with an increase in either usually leading to a decrease in the compressive strength [8]. Cemented carbides under compression deform elastically rather than plastically. This has the consequence that the material fractures immediately when the elastic limit has been reached [8].

When considering the transverse rupture strength of a cemented carbide it has been found that the Co content and the carbide content both influence the transverse rupture strength but by opposite means. An increase in the Co content results in an increase in the transverse rupture strength whereas an increase in the carbide content has the reverse effect as shown in Figure 2.11.

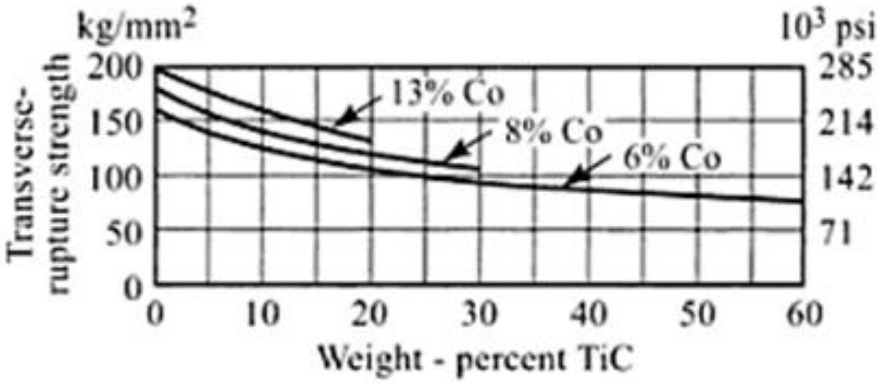


*Figure 2.11 Effect of Co and TiC content on transverse rupture strength of WC-TiC-Co cemented carbides [8].*

The overall wear resistance of cemented carbide is largely dependent on the carbide/binder ratio as well as the carbide grain size and bulk hardness of the particular carbide [7]. It has been observed that low Co binder concentrations and ultrafine (grain size less than 1µm) carbide grades improve wear resistance [3, 7, 12-13]. Figures 2.12 and 2.13 show the effect of grain size, binder content and hardness on the wear rate and wear resistance. Cermets exhibit similar behaviour as illustrated in Figure 2.12 although cemented carbides display superior performance [7].

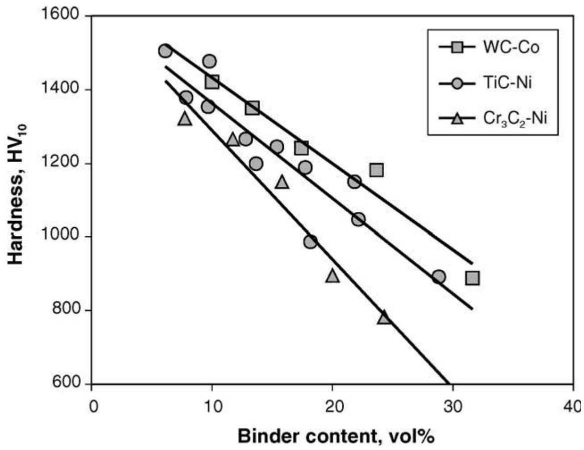


(a)

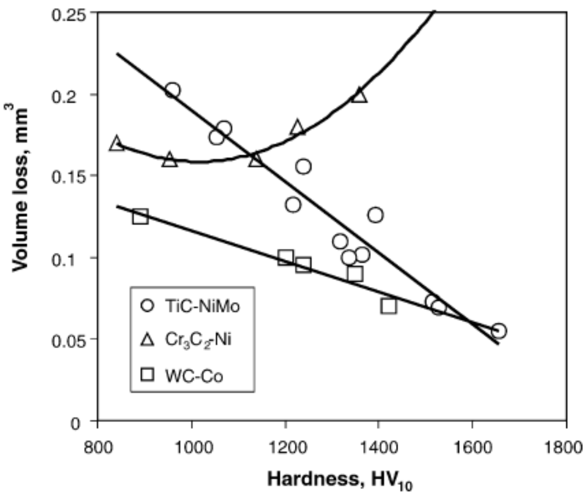


(b)

*Figure 2.12. Effect of (a) binder content on hardness and (b) hardness on the volume loss through dry sliding wear on a block-on-ring tester for cemented carbides and cermets [7].*

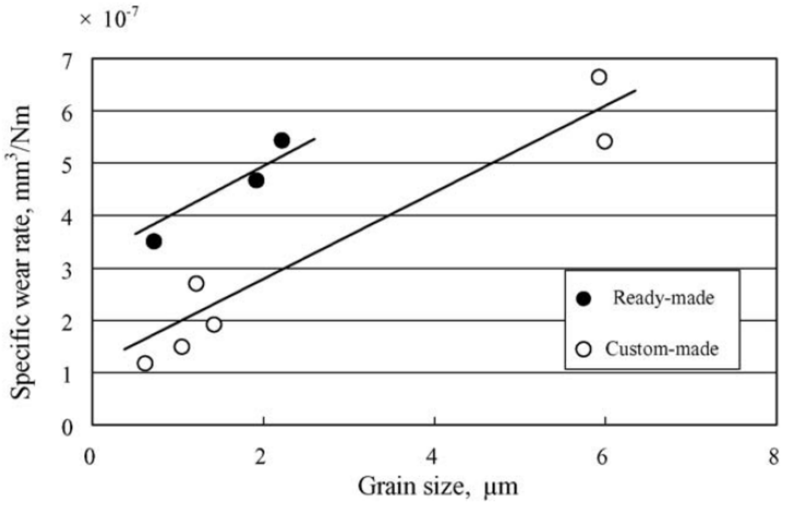


*Figure 2.13. Effect of grain size on the wear rate different types of WC-Co cemented carbides: ready-made industrially available grades and custom made grades designed on request to meet specific requirements [13].*

Although WC-Co is widely used for its high wear resistance it has been discovered that improved properties can be achieved when the carbides are alloyed with certain refractory carbides. Carbides of tantalum, columbium, molybdenum, cadmium, titanium vanadium and niobium are often used within cemented carbides with a Co binder [2-3]. From [2] it was seen that a smaller WC grain size results in a higher hardness which results in higher wear resistance. The addition of vanadium carbide, for example, to a cemented carbide results in a decreased carbide grain size as it acts as a grain growth inhibitor [12]. Similarly, the authors from [2] observed the effect of adding TiC, NbC, ZrC and TaC to WC-Co and found that all the carbides contributed to decreasing the WC grain size by inhibiting the grain growth. TiC served as the most effective singular grain growth inhibitor when added to the WC-Co powder. An interesting observation is that the combined addition of TiC and ZrC had the best effect overall [2]. TaC is found to be a very effective grain growth inhibitor when added in amounts of less than 2wt% [14]. In addition, TaC and NbC have been shown to increase the fracture toughness [10, 15-16] whereas TiC has the adverse effect on the room temperature transverse rupture strength [10]. Although some information is available on the effects that these additive carbides have on the performance of cemented carbides the effect that they might have when combined together within a cemented carbide still requires further investigation.

Titanium carbide is harder than tungsten carbide and thus cemented carbides with a high TiC content will be more abrasion resistant than a standard WC-Co alloy [3]. TiC is also known to reduce the tendency of welding between the tool tip and the machined chips [10]. Titanium has the added advantage of producing outstanding mechanical properties at temperatures ranging from room temperature up to 400°C which is beneficial for high temperature applications often experienced in industry [17].

As stated previously the wear rate increases when more Co binder is present in the material. This is due to the preferential wearing of the softer metallic binder phase. This is usually followed by fracturing of inter-granular boundaries and the fragmentation of the carbide grains [7]. The wear coefficient, K, is thus also dependant on the chemical composition of the alloys as this affects the carbide/binder ratio. An increase in binder content results in an increase in K, which usually indicates an increase in wear. Thus, when considering a WC-Co cemented carbide, the WC has a high hardness which correspondingly results in low values of K [7]. The same authors observed that the coefficient of friction increased slightly when the binder content was increased for cemented carbides.

Cemented carbides usually experience a run-in stage where the wear is relatively high before it decreases and settles into a linear pattern. This reduction is thought to be due to the formation of a tribofilm which consists of the extruded binder phase and some of the fractured carbide phase. The tribofilm serves to protect the surface from further damage [7].

In addition to material properties such as the carbide/binder ratio, grain size and bulk hardness of cemented carbide, other ways of controlling wear is by means of controlling the sliding wear system parameters. When studying the Archard equation, it can be see that the wear rate is largely dependent on the operating parameters of load and sliding velocity. Bonny *et al* [17] demonstrated that an increase in load caused increased wear and an increase in sliding velocity similarly, caused an increase in wear.

There are numerous processes by which cemented carbides experience wear. Wear mechanisms may vary throughout the sliding wear tests as the internal parameters such as friction and temperature change. The frictional forces experienced during the wearing process provide the energy that is required to remove the binder and cause micro-cracks [18]. It is believed that, although the exact process is unclear, friction is a result of three components; these components being adhesion, ploughing and asperity deformation [7]. Observations from test results [12] found that high tangential frictional forces were responsible for the smoothing of wear tracks during the running-in period. The high friction observed was identified when examining the specimen and observing deep, straight plough marks. These marks are indicative of the asperities that were present before being worn away. Where the friction coefficient begins to stabilise is when the smoothing mechanism has been completed. This illustrates the necessity for long test runs if accurate friction data is required. Variations in coefficient readings throughout a particular test are believed to be due to the breaking and reforming of new bonds between the particles [12].

Bonny *et al* [17] observed from the results from dry reciprocating sliding tests that were performed on WC-Co based cemented carbides that an increase in normal load corresponded to a decrease in friction. However an increase in sliding velocity corresponded to an increase in friction under the specific test conditions.

As described by Larson-Basse [18], there are several factors of a WC-Co alloy that contribute to its resistance to wear. These factors are described below:

- It is believed that inter-alloying between the WC and the Co occurs resulting in a strong inter-phase bond without any deterioration occurring.

- The WC grains are micro-sized and thus provide good resistance to micro-cracking.
- Upon cooling during the sintering process the binder cools down at a faster rate than the carbide thus cools under a tensile stress state simultaneously causing the carbide to cool under a compressive stress state; this provides the carbide with added resistance to brittle fracture.
- The tensile stress that the binder experiences during cooling acts as a pre-stressor. This pre-stressor sets a threshold which must first be overcome for wear to start.
- When Co cools down it undergoes a face centered cubic (f.c.c) - hexagonal close packed (h.c.p) transformation. This transformation does not occur in the thin binder regions of the WC-Co alloy however it can occur when these regions undergo deformation and possibly can improve the local ductility of the binder.

Larson-Basse [18] concluded that cobalt extraction plays a large role in the wear mechanisms of WC-Co alloys. It is thought that it occurs initially ahead and adjacent to the direct load that is applied and that the binder is squeezed out from between the WC grains which deforms very little and accumulates on the surface. The binder that accumulates on the surface is continuously smeared over the counterface causing deformation and in turn is smeared back onto the WC-Co alloy.

Under cyclic conditions the binder content decreases near the surface. This also relaxes the compressive stresses of the WC and the tensile stresses of the binder below. Further cyclic loading results in the fracturing of the more brittle carbide grains; this coincidently then provides new paths for further binder extrusion [18].

Eventually it is believed that the WC grains lose their compressive stressed state as the surrounding binder keeping it in that state has been removed plastically and it thus starts to fracture and is eventually removed. The edges of the surface grains which are next to a defect experience the highest loads and will fracture first and be removed. This continuously happens during repetitive loading and the damage from the deformation within the alloy will propagate very similarly to that of a pot hole [18]. The carbide grains that are removed as well as the smeared cobalt binder eventually leave the system as wear particles [18]. It is believed that cobalt however does act as a lubricant and assists in decreasing the wear after the run-in stage [18].

Results from Pirso *et al's* [7], sliding wear tests on WC-Co alloys against steel counterfaces indicate that plastic deformation of surface irregularities takes place first resulting in polished surfaces. This is followed by 'islands' forming on the surfaces of the WC-Co alloy as well as the steel surface from the resulting debris from the steel counterface. These islands break into either the steel or the WC-Co alloy and results in either material transfer between the two surfaces or the particles leave the system as wear debris. This process occurs after a certain period of time and then continues repeatedly during the duration of the tests.

Although the relationship between wear and friction is not defined, friction does play a major role in the wear mechanisms. Friction is accompanied by small changes in the frictional forces on the surface. These cyclic forces facilitate the development of fatigue cracks on and just below the surface. They usually follow the interface or inter-grain boundaries of the carbide grains. After numerous cycles, these cracks cause segments of the grain to detach leaving behind a cavity [7].

The complex dry sliding wear response of cemented carbides thus depends on numerous factors. Material properties including the carbide/binder ratio, grain size and bulk hardness plays a fundamental part in the wear response. System properties such as load and sliding velocity also contribute to the extent that wear is experienced. These inter-linked properties affect the frictional response which in turn often unpredictably influences the level of wear.

In conclusion, considering the design of components used in dry sliding wear conditions for industrial applications, it is important to consider the engineering material as well as the expected tribological constituents of friction and wear within the system as these factors influence the component's life span. Tungsten carbide-cobalt (WC-Co) is recognised in industry for its high hardness and excellent wear resistance. As discussed in this chapter, the wear resistance properties of WC-Co can be enhanced by adding refractory metals such as Ti, Ta and Nb [2]. Based on investigations it is noted that the combined effect of adding these refractories to WC-Co is not well researched, specifically when dry sliding wear is considered.

# Chapter 3

# Experimental Procedure

This chapter describes the experimental procedures that were followed to evaluate the friction and wear properties of three grades of cemented carbide buttons against two steel substrates. The resulting wear mechanisms were identified. The physical and mechanical properties of the buttons and substrates were determined.

## 3.1 Material characterization

### 3.1.1 Materials

The three grades of cemented carbides that were used constituted predominately of WC with the balance constituting of Co and mixed carbides as indicated in Table 3.1. The three grades of cemented carbides were similar in appearance exhibiting a dark grey metallic colour. All three grades were bullet shaped. Figure 3.1 illustrates button grade WC-A which represents the typical appearance of all three button grades.

Table 3.1 Button grade properties.

| **Button grade** | **Composition** | | | | **Diameter [mm]** | **Height [mm]** |
|---|---|---|---|---|---|---|
| | wt% Co | wt % TiC | wt % TaC | wt % NbC | | |
| WC-A | 6 | 0 | 0 | 0 | 9.2 | 13 |
| WC-B | 5.9 | 0 | 0.09 | 0.01 | | |
| WC-C | 6 | 2.83 | 3.47 | 0.39 | | |

*Figure 3.1. Shape of button grade WC-A; typical for all three WC grades.*

The two steel substrates used were commercial grades of 304 Stainless Steel and Bright Mild Steel (refer to Table 3.2). The steels were supplied in the form of 1m rods from which circular discs were cut to use in the tests.

Table 3.2. Substrate properties.

| **Substrate** | **Composition** | **Diameter [mm]** | **Height [mm]** |
| --- | --- | --- | --- |
| 304 Stainless Steel | Fe, 0.29Cr, 0.16Ni, 0.06C | 20 mm | ±4 mm |
| Bright Mild Steel | Fe, C, Mn, P, S | | |

### 3.1.2 Sample preparation

Prior to testing, cross sections of each button grade and substrate were mounted in PolyFast resin and then polished to a surface finish of 1 µm using a Leco Spectrum System 2000 automatic polishing machine. The polishing routine is described in Table 3.3. After each polishing step the samples were cleaned ultrasonically using an iS Integral Systems ultrasonic cleaner and water for a duration of 5 minutes.

Table 3.3 Automatic polishing routine

| Step | Time (min) | Speed (rpm) | Pressure (N) | Abrasive/ Polishing disc | Cooling/ abrasive aid |
|---|---|---|---|---|---|
| 1 | 5 | 300 | 25 | piano 220 | Water |
| 2 | 2 | 300 | 30 | piano 1200 | Water |
| 3 | 3 | 150 | 40 | 9 micron (Largo) | 9 µm Diamond suspension and diamond dispenser |
| 4 | 3 | 150 | 30 | 3 micron (DAC) | 3 µm Diamond suspension and diamond dispenser |
| 5 | 1 | 150 | 10 | 1 micron (Nap) | 1 µm Diamond suspension and diamond dispenser |

### 3.1.3 Microstructure

In order to characterize the microstructure of the materials the samples were etched using appropriate etching solutions. The etched surfaces were studied using a Zeiss Axiotech microscope at a magnification of 20x. Images were taken and any irregularities in the microstructure were noted.

*Bright mild steel*

The carbon steel sample was etched using a 3% Nital mixture (3 vol% $HNO_3$, 97 vol% Ethyl Alcohol) for 10 seconds. The sample was rinsed under running tap water followed by ethanol after which it was dried.

*304 Stainless steel*

The stainless steel was placed in an oversaturated solution of oxalic acid powder and water. The solution was then connected to a DC power source with the positive terminal touching the sample and the negative terminal placed in the solution. After 50 seconds the power source was removed and the sample was rinsed using water followed by ethanol and then dried.

*Cemented carbide buttons*

The cemented carbide buttons were etched using a fresh solution of Murakami's Reagent (10g KOH, 100ml Water, 10g $K_3Fe(CN)_6$). The buttons were submerged in the etchant for a duration of 90 seconds. The buttons were rinsed under running water and followed by ethanol and dried.

### 3.1.4 Vickers hardness and fracture toughness

Five polished samples representing each button grade and substrate type were used for hardness testing. Hardness was determined using a Leco V-100-A2 Vickers hardness machine. For the buttons an indenting load of 30kg was selected. For the substrates an indenting load of 20kg was selected. These loads were selected as they permit a sizeable indentation to be made which allows for easy measurement; a small indentation may lead to reduced precision and possible inaccuracy. The indenting loads were applied for a duration of 10 seconds. The hardness was calculated using Equation 3.1. The derivation of this equation can be found in Appendix A. Five indentations were made per sample from which the average hardness was calculated.

$$HV = \frac{1.854F}{d^2} \tag{3.1}$$

Where F = Indentation load [kg]

d = Average indentation diagonal [mm]

HV = Vickers hardness number [kg/(mm)$^2$]

The method used to obtain the fracture toughness for the button grades is the one developed by Shetty et al [19]. In this method the length of the cracks emanating from the corners of the Vickers hardness indentations are measured and the values inserted into Equation 3.2. These cracks, also known as Palmqvist cracks [19], were not generated on the substrate materials. This method of determining the fracture toughness of cemented carbides requires a test surface free of residual stresses [20]. Therefore the test surfaces required extended polishing times in order to eliminate these stresses.

The fracture toughness of the buttons was calculated using equation 3.2 [19].

$$K_{IC} = A_1 \sqrt{\frac{HV \times P}{\sum_1^4 a}} \quad [\text{MPa.m}^{1/2}] \tag{3.2}$$

Where $A_1$ = $887 \times 10^{-7}$
HV = Vickers hardness [MPa]
P = Indentation load [N]
a = Mean radial crack length [m]

### 3.1.5 Density and porosity

The density of the buttons and substrates was determined using the Archimedes principle. The specimens were first weighed in air, then again while suspended in water. The density was calculated using equation 3.3. Five density measurements were made per sample.

$$\rho_s = \rho_w \times \frac{M_a}{M_{wt} - M_w} \tag{3.3}$$

Where $\rho_s$ = density of the specimen
$\rho_w$ = density of water
$M_a$ = mass of specimen in air
$M_w$ = mass of specimen in water
$M_{wt}$ = wet mass of specimen

The % porosity for each button grade and substrate was calculated using equation 3.4.

$$Porosity = \frac{M_{wt} - M_a}{M_{wt} - M_w} \times 100 \tag{3.4}$$

3.1.6 XRD Analysis

XRD analysis was done on one polished sample of each button grade and substrate type using a BRUKER D2 machine (step size of 0.0200 °2Th, scan step time of 19.1 seconds, 30kV, 10mA). Peaks were identified using PANalytical X'pert High Score software. Where expected elements did not appear in the diffractograph the expected peaks were inserted in order to indicate where they should appear. The reason that some elements do not appear is due to the minor quantities in which they exist in the material and the limitations of the XRD.

3.1.7 Coercivity and magnetic saturation

The coercivity and magnetic saturation of the cemented carbide buttons were measured using a Dr. Foerster Koerzimat according to ISO3326. This machine provides the results for the coercivity and magnetic saturation in units of Oe and emu respectively. Equations 3.5 and 3.6 were used to convert these units to SI units.

$$1\ [Oe] = \frac{1000}{4 \times \pi}\ [A.m^{-1}] \tag{3.5}$$

$$1\ [emu] = 10^{-3}[Am^2] \tag{3.6}$$

Coercivity indicates the magnitude of the magnetic field required to demagnetize a fully magnetized cemented carbide specimen. Many factors such as composition and grain size may influence coercivity [21]. Coercivity decreases with an increase in cobalt content and with an increase in tungsten carbide grain size [22].

Magnetic saturation indicates the extent to which the hardmetal is saturated with carbon. Low levels of carbon indicate the presence of the undesirable carbon-deficient eta phase. High levels indicate the presence of free carbon in the material [21].

### 3.1.8 Young's modulus and Poisson's ratio

The Young's modulus of both the buttons and substrates was determined using speed of sound measurements. The density calculated in Section 3.1.5 was used in equations 3.7- 3.8 [23] and 3.9 to simultaneously calculate the Young's modulus as well as Poisson's ratio.

$$S_L = \sqrt{\frac{K + \frac{4}{3}G}{\rho}} \tag{3.7}$$

$$S_T = \sqrt{\frac{G}{\rho}} \tag{3.8}$$

$$E = 2 \times G \times (1 + \nu) = 3 \times K \times (1 - 2 \times \nu) \tag{3.9}$$

Where $S_L$ = Longitudinal speed of sound [$m.s^{-1}$]
$S_T$ = Transverse speed of sound [$m.s^{-1}$]
K = Bulk modulus [GPa]
G = Shear modulus [GPa]
E = Young's modulus [GPa]
$\rho$ = Sample density [$kg.m^{-3}$]
$\nu$ = Poisson's ratio

### 3.2 Sliding wear and friction tests

The sliding wear and friction tests were conducted using a CSM tribometer with a pin-on-disc configuration. In this work the button grades were the pins and the substrates the discs. The tribometer uses CSM software for online measurement. The tribometer has an elastic blade which serves as an arm which held the button with the aid of an adapter fixed in one position. Figure 3.2 illustrates the measurement head of the tribometer. There is a disc-holder mandrel to which the substrate is fixed. The substrate rotates at a speed which is set by the user on the tribometer's parameter input page in the software program. Test parameters that can be varied are the applied load on the button, the speed at which the substrate rotates, the wear track radius of the button on the substrate, and the total sliding distance for a specific test.

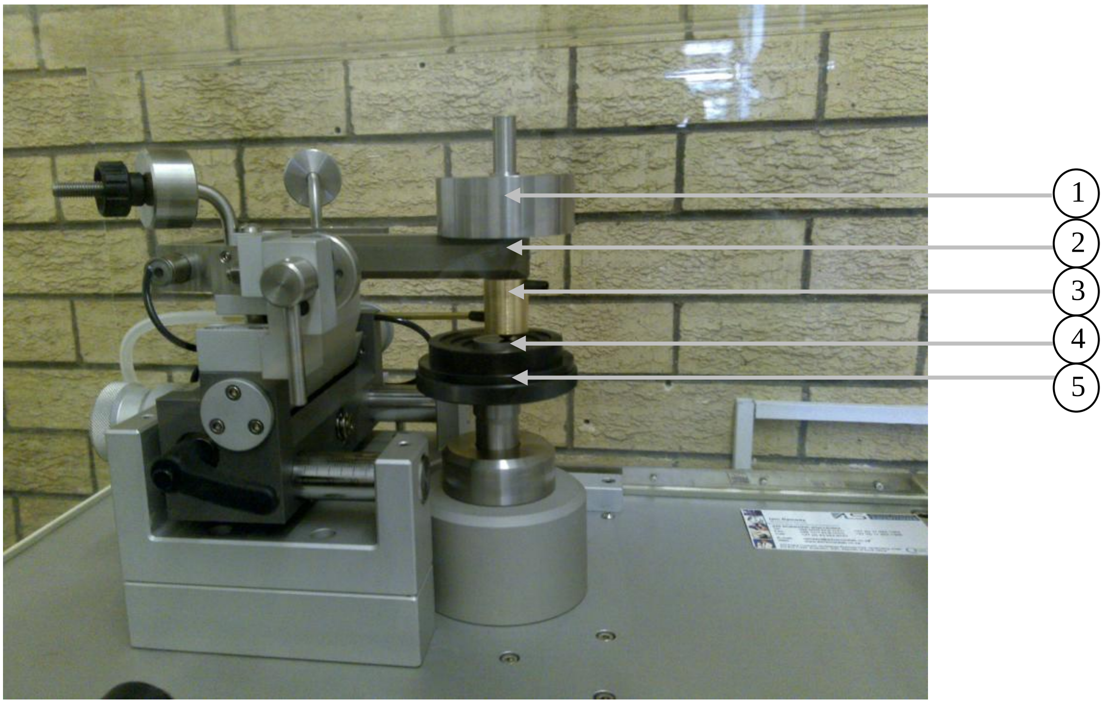


Description of elements:

1- Test Load
2- Elastic blade
3- Adapter
4- Substrate
5- Disc-holder mandrel

*Figure 3.2. Measurement head of the tribometer.*

Prior to each test the button and the substrate were each fitted into their correct positions in the tribometer. The substrate was placed on the disc-holder mandrel and tightened securely. The button was inserted into the adapter and tightened into position. The adapter in turn was fixed into position on the elastic blade of the tribometer. The height of the adapter was then adjusted accordingly into the correct position to accommodate the specific substrate height. The selected load is then applied to the button as indicated in Figure 3.2. Once this setup was completed the computer software was initiated to commence a test. The input parameters and the data sampling parameters were first verified in the input sheet. These factors were the frequency at which measurements would be taken, the linear speed, the sliding distance, the applied load and the wear track radius. Once these were confirmed the test was initiated.

During a test the tribometer software measures the static and dynamic friction coefficients as well as the penetration depth for the duration of the test. This data was used to draw conclusions on the friction response of the contact partners and to calculate the wear rates of the contact partners.

Initially various combinations of substrate and button pairs were tested under various applied load and speed parameters in order to establish a set of suitable testing conditions. These initial tests resulted in a speed limit of $0.2 m.s^{-1}$ under 5N as speeds higher than this yielded a tangential force overload error which acts as a safety mechanism for the tribometer against overloading the machine. However, the speed could be increased if the load was decreased to be within the limits of the allowed tangential force. It was also observed from analysis of the test results that a sliding distance of 300m is sufficient to obtain reproducible results.

Based on the preliminary tests the conditions selected for this project are shown in Table 3.4. These conditions will illustrate the effect load and speed on the wear and friction coefficients.

Table 3.4: Test conditions for the wear and friction tests.

| **Test Condition** | **Applied load (N)** | **Speed ($m.s^{-1}$)** | **Sliding distance (m)** | **Wear track radius (mm)** |
|---|---|---|---|---|
| 1 | 5 | 0.2 | 300 | 5 |
| 2 | 3 | 0.2 | 300 | 5 |
| 3 | 1 | 0.2 | 300 | 5 |
| 4 | 3 | 0.3 | 300 | 5 |
| 5 | 3 | 0.1 | 300 | 5 |

304 Stainless steel and bright mild steel discs, described in Table 3.2, were used for these tests. Prior to testing the substrate surfaces were polished to a 1 micron finish, cleaned ultrasonically for 5 minutes and the individual disc mass determined. The three button grades listed in Table 3.1 were used as the ‘pins’ in the tribometer and prior to testing the buttons were cleaned ultrasonically for 5 minutes and the individual button mass determined. Each button grade was tested against each steel disc according to the test conditions described in Table 3.4. Three tests per button-disc pair were conducted under each test condition. After each test the buttons and discs were cleaned ultrasonically and the individual masses determined. Each test result was analyzed to determine if the results were satisfactory. Unsatisfactory tests were repeated.

The button and the substrate were then examined using a Motic stereo microscope. The wear tracks on the substrate and the worn area on the button were examined and the approximate worn areas were measured. Figures 3.3 and 3.4 illustrate the typical images for the substrate and button respectively.

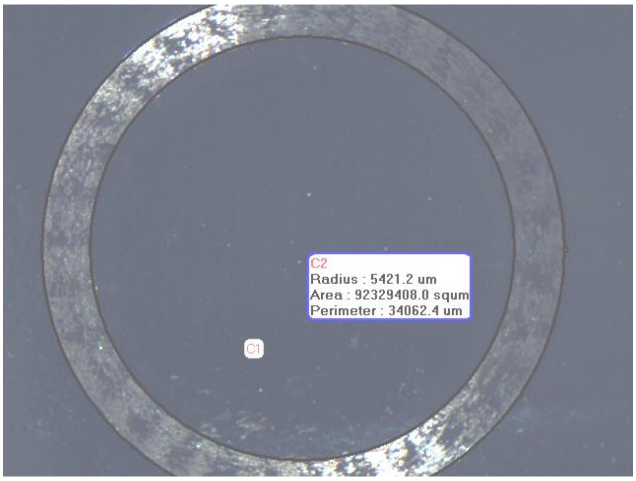


*Figure 3.3 Measurement of the outer radius, $R_o$, of a 304 stainless steel substrate wear track.*


*Figure 3.4 Measurement of the button wear area, $A_b$, of a WC-B button.*

Cross sections of the substrates were also examined under the microscope which provided information of the wear profile and whether the assumption of an elliptical wear track on the substrate was justified.

In order to obtain the worn volume of the substrate it was assumed that the wear track followed an elliptical shape due to the elliptical Hertzian pressure profile [5, 15] that the sphere shaped end of the button exerts onto the substrate. Important parameters when calculating the volume worn on the substrate were the width,

$D_M$, and the mean radius, $R_M$, of the wear track, obtained by measuring the outer and inner radius of the wear track. Thus the worn volume, $V_s$, for a given wear track of maximum penetration depth, $P_{dmax}$, is as follows:

$$V_s = \pi^2 \times \frac{D_M}{2} \times P_{dmax} \times R_M \qquad (3.10)$$

The derivation of equation (3.10) is shown in Appendix D.

In order to obtain the worn volume of the button, the wear area, $A_b$, had to be measured. Important parameters when calculating the volume worn on the button were the worn button height, h, and the button radius, $R_b$. The worn button height, h, is calculated using the worn area diameter, d, which is calculated from $A_b$. Thus the worn volume, $V_b$, for a given button is as follows:

$$V_b = \frac{1}{3} \times \pi \times h^2 \times (3 \times R_b - h) \qquad (3.11)$$

The derivation of equation (3.11) is shown in Appendix D.

The Archard equation (equation 2.2) was used to determine the wear rates of each substrate and button grade. When calculating the wear rate of the substrate $V_s$ is inserted into the equation. When calculating the wear rate of the button $V_b$ is inserted into the equation. The applied load and the sliding distance is identical in each case.

A FEI NOVANANO SEM200 scanning electron microscope (SEM) fitted with the Everhard-Thornley Detector (ETD) for secondary electron imaging was used to analyze each of the worn surfaces to determine the wear mechanisms. The wear scars were observed in planar view.

Energy Dispersive Spectroscopy (EDS) was also performed on selected areas to identify if there was any material transfer between the substrate and the button.

EDS was performed using an EDAX system for x-ray analysis together with a Backscattered Secondary Electron Detector (BSED) for backscattered SE imaging.

X-ray Photoelectron Spectroscopy (XPS) was performed on the wear tracks of selected substrates to verify the presence of oxides, if any. XPS was performed using a Physical Electronics Quantum2000 machine (X-rays: Al Kα (1486eV), 20W, beam diameter of 100μm, pass energy (wide) 117.4 eV, (narrow) 29.35 eV).

# Chapter 4

# Results

Results from the experimental tests performed on the cemented carbide button grades and the steel substrates are described in this chapter. The physical and mechanical properties of the buttons and the substrates as well as the friction and wear properties of the buttons against the steel substrates were determined.

## 4.1 Material characterization

### 4.1.1 Microstructure

*Bright mild steel*

Figure 4.1 illustrates the microstructure of the bright mild steel sample and the XRD pattern indicating the phases present.

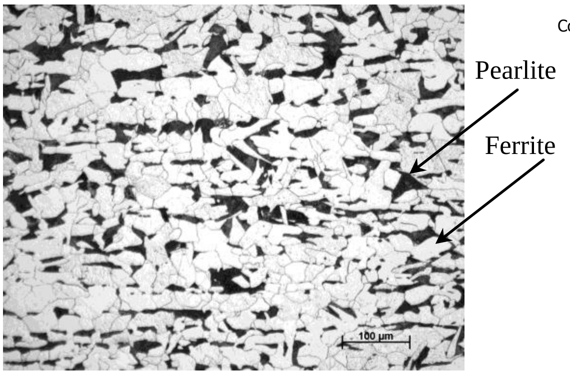


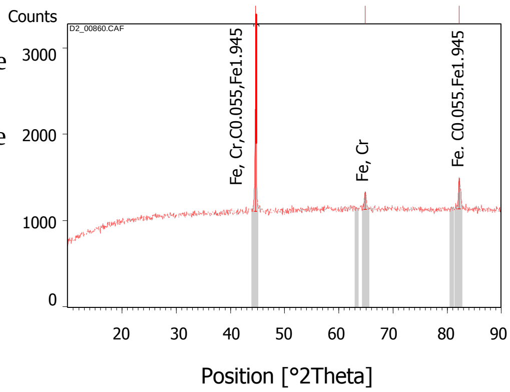


*(a)* *(b)*

*Figure 4.1 Bright Mild Steel. (a) Microstructure showing ferrite and pearlite phases (b) XRD pattern.*

The microstructure shown in Figure 4.1 is typical for carbon steel clearly indicating the lighter ferrite and darker pearlite grains. Banding is also noted which is a result of the manufacturing process. The XRD pattern highlights the presence of the main constituents of iron and carbon as expected. Small traces of chrome were also detected although no significant quantities of other elements were identified.

*304 Stainless steel*

Figure 4.2 illustrates the microstructure of the 304 stainless steel sample and its corresponding XRD pattern.

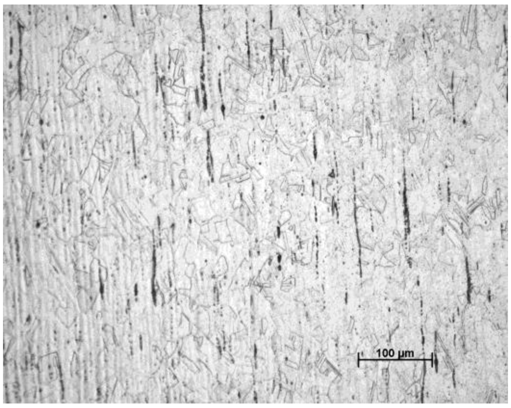


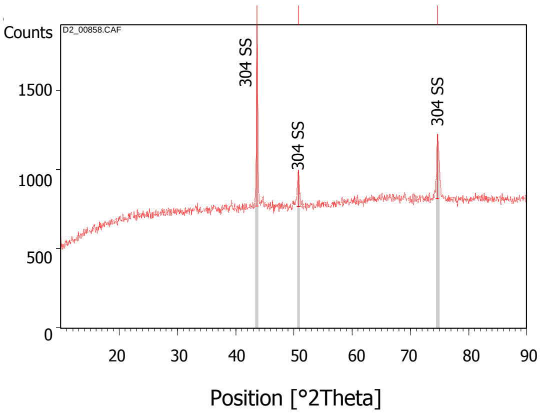


*(a)* *(b)*

*Figure 4.2 304 Stainless Steel (a) Microstructure showing austenitic grains structure (b) XRD pattern.*

Figure 4.2 illustrates the typical microstructure for an austenitic stainless steel. The vertical lines that can be seen are possibly due to rolling during the manufacturing process. The XRD results yielded a positive identification for the 304 stainless steel grade.

*Cemented carbide buttons*

*Grade WC-A*

Figure 4.3 illustrates the microstructure and XRD pattern of button grade WC-A. Studying the microstructure the angular carbide grain structure typical of cemented carbides is clearly visible. It is noted that the carbide grain size has a wide grain size distribution; from clearly defined large grains approximately 10µm in size down to grains 3µm in size. The XRD results confirm the presence of the typical WC phase. A peak identification line for the Co phase has been inserted on the XRD pattern where this phase would appear. No deleterious phases such as eta phase were detected.

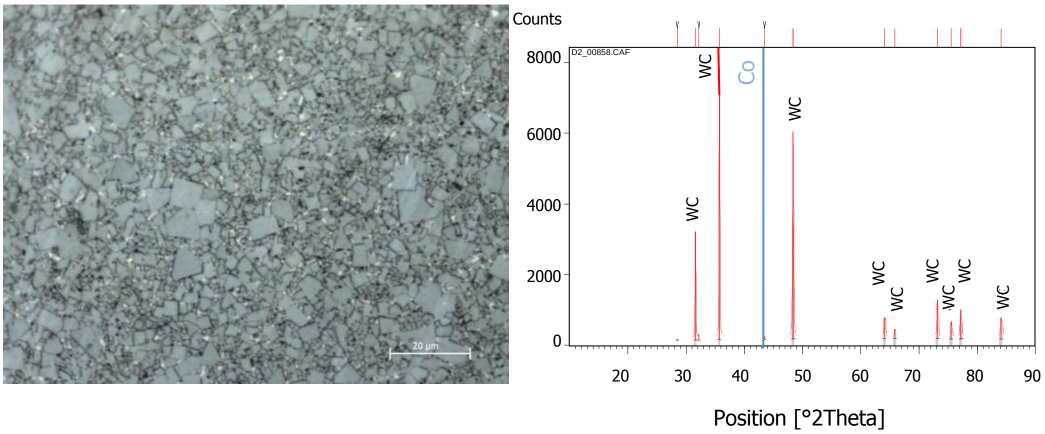


*(a)* *(b)*

*Figure 4.3 Button grade WC-A (a) Microstructure revealed using Murakami's Reagent (b) XRD pattern.*

*Button grade WC-B*

Figure 4.4 illustrates the microstructure and XRD pattern of button grade WC-B. This grade contained 0.09wt%TaC and 0.01wt%NbC. From the microstructure it can be seen that grade WC-B has very small carbide grain sizes, approximately 1 - 2µm. This grade has a finer microstructure than button grade WC-A. This is due to the TaC which acts as a WC grain growth inhibitor when added in amounts of less than 2wt%. The XRD pattern identified the WC phase but was unable to detect peaks for the TaC and NbC due to the small amounts added. Peak identification lines have been inserted on the XRD pattern where these phases would appear.

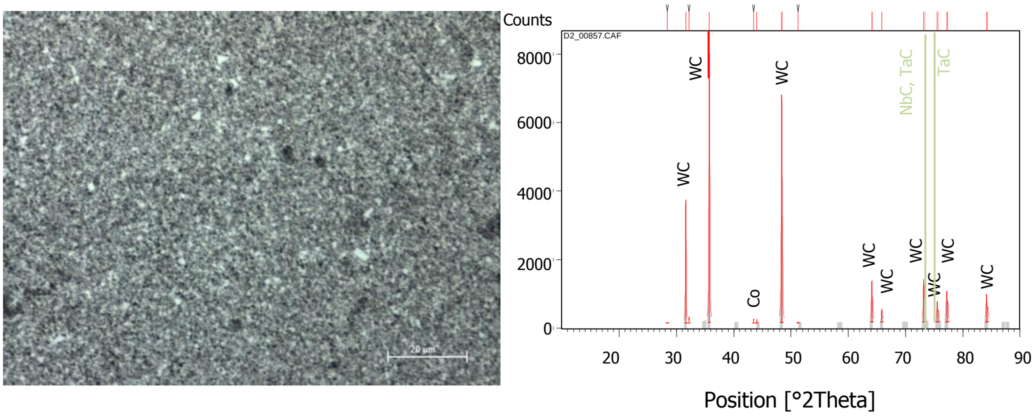


*(a)* *(b)*

*Figure 4.4 Button grade WC-B (a) Microstructure revealed using Murakami's Reagent (b) XRD pattern.*

*Button grade WC-C*

Figure 4.5 illustrates the microstructure and XRD pattern of button grade WC-C. This grade contained 2.83wt%TiC, 3.47wt%TaC and 0.39wt%NbC. The WC grains (grey phase) display the typical angular structure with a wide grain size distribution (3 – 8 µm). The mixed carbides (dark phases) have a typical globular structure. A few pure TiC grains are also visible as the bright (almost white) phase. XRD results identify the WC, TiC and TaC phases. Peak identification lines have been inserted on the XRD pattern where the Co and NbC phases would appear.

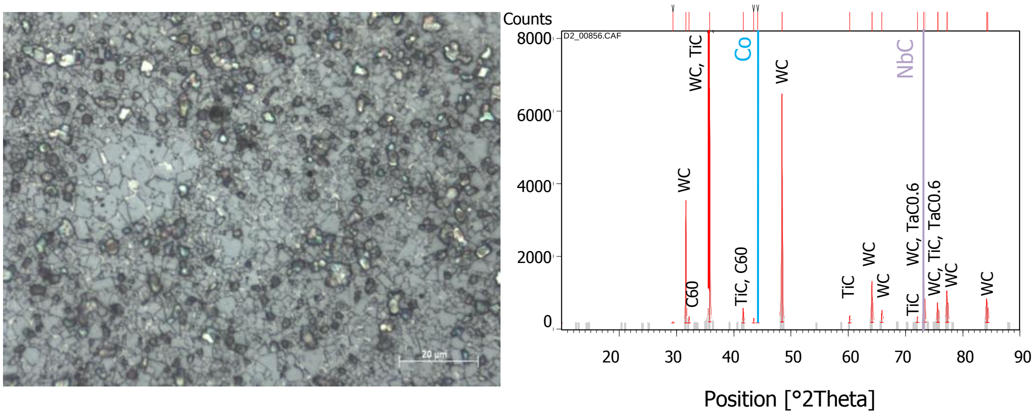


*(a)* *(b)*

*Figure 4.5 Button grade WC-C (a) Microstructure revealed using Murakami's Reagent (c) XRD pattern.*

4.1.2 Material properties

The physical and mechanical material properties of the cemented carbide button grades and steel substrates are listed in Tables 4.1, 4.2 and 4.3 respectively. Complete test data for the Vickers hardness, fracture toughness, density and porosity can be found in Appendices A to C.

Table 4.1. Physical material properties of the cemented carbide button grades.

| Material Grade | Density [$g/cm^3$] | Porosity (%) | Coercivity [kA/m] | Magnetic Saturation [$Am^2$] |
|---|---|---|---|---|
| WC-A | 14.87±0.046 | 0.0313 | 12.46 | 0.111 |
| WC-B | 14.97±0.037 | 0.0027 | 27.45 | 0.102 |
| WC-C | 14.18±0.030 | 0.0237 | 9.96 | 0.120 |

In Table 4.1, the calculated densities for the three button grades are within the typical range of 14.50 to 15.00 $g/cm^3$ for 6wt% Co cemented carbides. The porosity levels are low and similar for all three button grades. The coercivity of grade WC-B is more than double that of grade WC-A and almost triple that of grade WC-C. A high coercivity value generally indicates a very fine carbide grain size. Therefore grade WC-B should have the finest carbide grain size. This is confirmed when comparing the coercivity values to the microstructures shown in Figures 4.3 to 4.5. The fine grain size of grade WC-B can also be attributed to the addition of the TaC which as indicated earlier acts as a WC grain growth inhibitor. In some cases a very high coercivity value also indicates the presence of eta phase or high levels of porosity. However no eta phase was detected as reflected by the XRD patterns in Figures 4.3 to 4.5 and the porosity levels are low. The magnetic saturation results were found to be similar for all three grades and confirm the similarity in Co binder content for all three grades. The similarity in the saturation values further confirms that the high coercivity value for grade WC-B is due to a fine carbide grain size and not due to a lowering of the Co content by adverse microstructural effects such as eta phase.

Table 4.2. Mechanical properties of the cemented carbide button grades.

| Material Grade | Vickers Hardness $HV_{30}$ | Fracture Toughness $K_{IC}$ [$MPa.m^{1/2}$] | Young's Modulus [GPa] | Poisson's ratio | Speed of Sound $S_T$[1] [m/s] | Speed of Sound $S_L$[2] [m/s] |
|---|---|---|---|---|---|---|
| WC-A | 1420±11 | 18±1.6 | 649 | 0.23 | 4183 | 7062 |
| WC-B | 1915±64 | 10±0.2 | 644 | 0.23 | 4194 | 7074 |
| WC-C | 1604±12 | 16±3.0 | 604 | 0.23 | 4190 | 7053 |

[1]$S_T$ Transverse Speed of Sound
[2]$S_L$ Longitudinal Speed of Sound

From Table 4.2 it is noted that grade WC-B has the highest hardness and lowest fracture toughness. These results are aligned with the coercivity values and the microstructure images shown earlier. Grades WC-A and WC-C have similar fracture toughness values although grade WC-C has a higher hardness than grade WC-A. This is attributed to the presence of the TiC in grade WC-C. The Young's modulus was found to be within the expected range for 6wt% Co cemented carbides while Poisson's ratio was calculated to be the same for each grade. The speed of sound values were used to determine the Young's modulus and Poisson's ratio.

Table 4.3. Material properties of the steel substrates.

| Material Grade | Vickers Hardness $H_{V20}$ | Density [g/cm$^3$] | Porosity (%) | Young's Modulus [GPa] | Poisson's ratio |
|---|---|---|---|---|---|
| 304 Stainless steel | 262±6.8 | 7.86±0.030 | 0.0280 | 197 | 0.30 |
| Bright mild steel | 184±1.9 | 7.85±0.004 | 0.0335 | 213 | 0.29 |

The hardness results from Table 4.3 indicate that the stainless steel has a higher hardness than the mild steel. The calculated hardness for stainless steel is higher than the common value of 170HV for industrial grade 304 stainless steel. The increased hardness could be attributed to possible work hardening of the material during sample preparation. The mild steel's hardness is typical for that grade. The densities of both steels are close to their expected value of approximately 7.85 g/cm$^3$ for mild steel and 8.00 g/cm$^3$ for 304 stainless steel. Both steel grades showed similar levels of porosity with equal values for Poisson's ratio. The Young's modulus for the mild steel shows a slightly higher value than that of the stainless steel.

**4.2 Sliding wear and friction tests**

Figures 4.6 to 4.10 illustrate the friction behavior of each cemented carbide grade sliding against stainless steel and mild steel respectively for each test condition listed in Table 3.4 (Chapter 3). In the figures below T1, T2 and T3 represent the three tests done per button grade/steel pair, 'SS' indicates the 304 stainless steel and 'CS' the bright mild steel.

Figures 4.6 to 4.8 indicate the effect of decreasing applied load at a constant sliding velocity on the friction response of the sliding pairs. The highest friction values were recorded at the lowest load of 1N. Under all test conditions the friction values of stainless steel were higher than those of mild steel. In general the mild steel substrates have a fairly consistent and smooth friction response while the friction behavior of the stainless steel substrates is erratic. Each friction response is characterized by a running-in period as defined in Chapter 2, Section 2.1. This running-in period occurs during the first 50m of sliding. After this initial running-in period the friction behavior of the mild steel/button grade sliding pairs levels off to a constant value, while the stainless steel/button grade sliding pairs display inconsistent behavior.

The mild steel/button pairs for all three cemented carbide grades portray an initial peak during the running-in period after which it levels off at a lower value. This occurs for each operating condition regardless of the magnitude of the applied load. This friction response resembles that of pattern II from Figure 2.1. (Chapter 2).

All three button grades have very consistent and similar frictional behavior across all the loads. The only exceptions are those of grades WC-A and WC-C at the highest applied load of 5N where the results of the three tests for each button grade are not similar to each other such as those under lower applied loads.

The stainless steel/button pairs for all three cemented carbide grades shows an initial decrease in friction for a short duration during the running-in period. This is followed by a sharp increase in friction. Under a high load, the friction follows a decreasing exponential slope and is relatively smooth initially becoming more unstable towards the end of the test run. Under the lowest applied load however, the friction response becomes erratic very early on and the friction is remarkably high. These friction responses resemble patterns III and IV from Figure 2.1. (Chapter 2).

Grade WC-B's friction response pattern is the most consistent across all the applied loads. Grade WC-A has the most erratic friction response pattern regardless of the applied load.

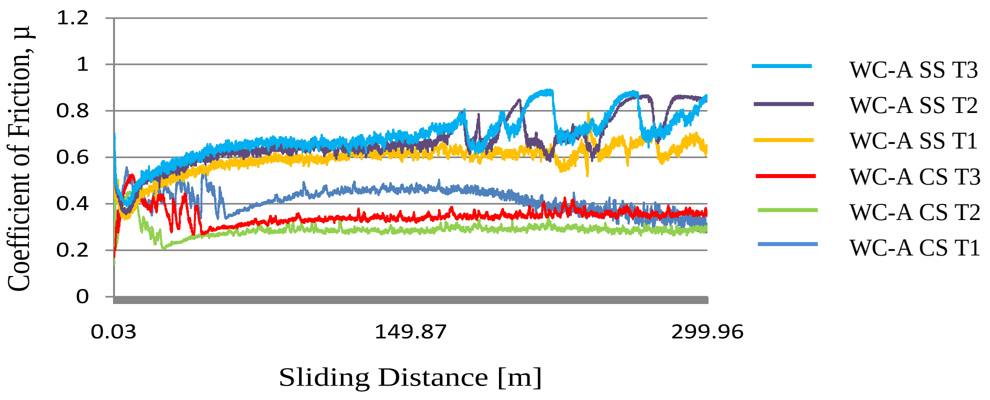


(a)

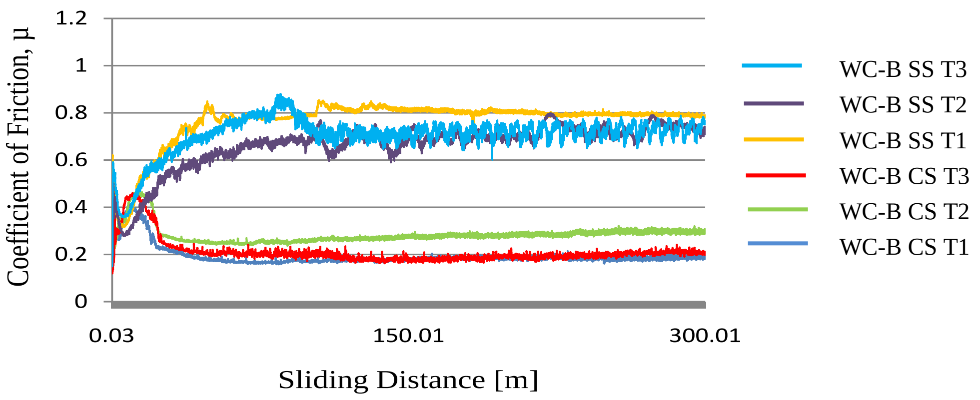


(b)

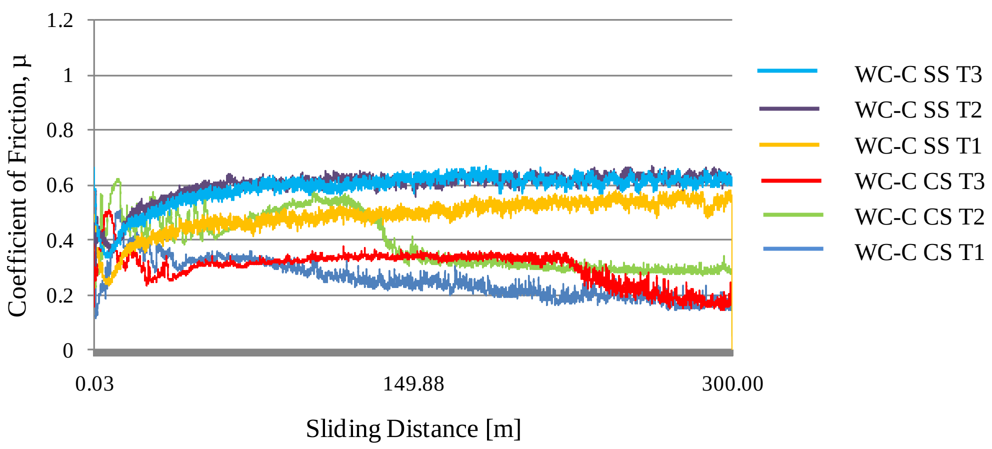


(c)

*Figure 4.6. Friction response of buttons (a) WC-A, (b), WC-B and (c) WC-C sliding against 304 stainless steel and bright mild steel under test condition 1 parameters (Load: 5N, Sliding velocity 0.2m.s$^{-1}$).*

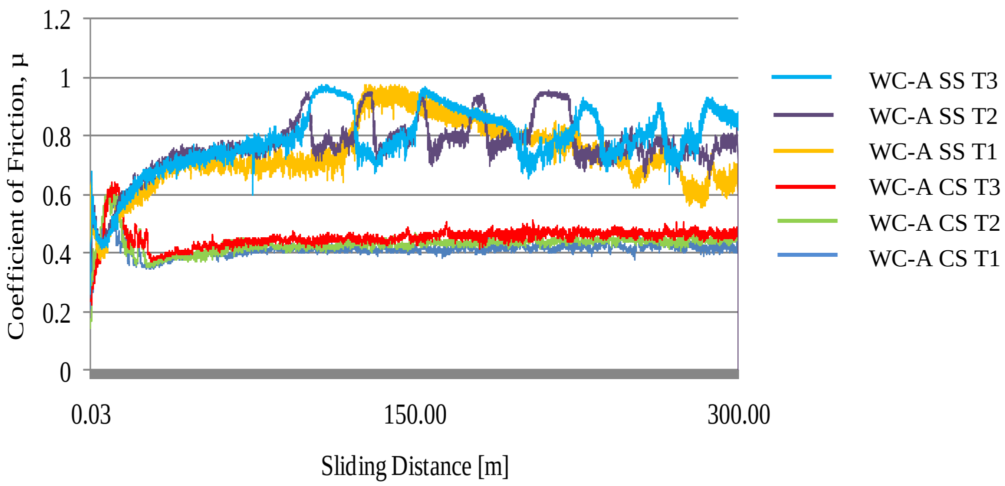


(a)

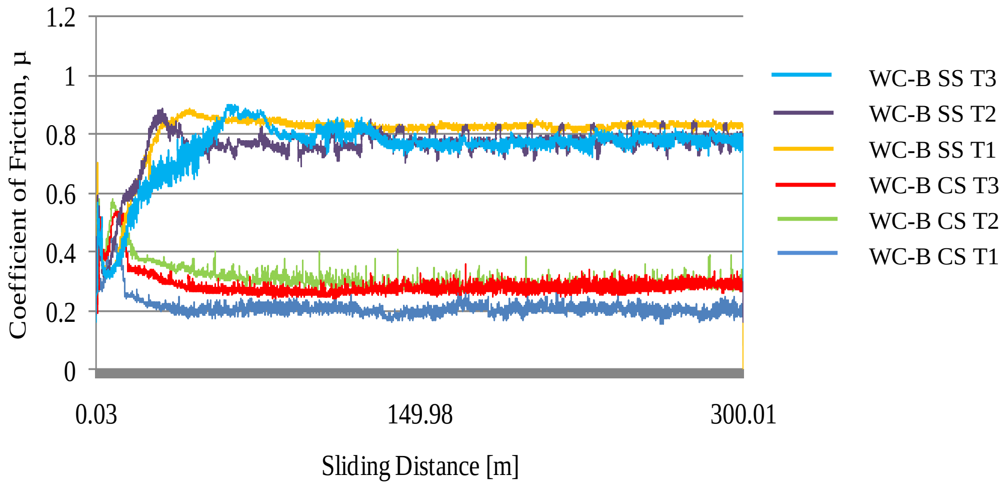


(b)

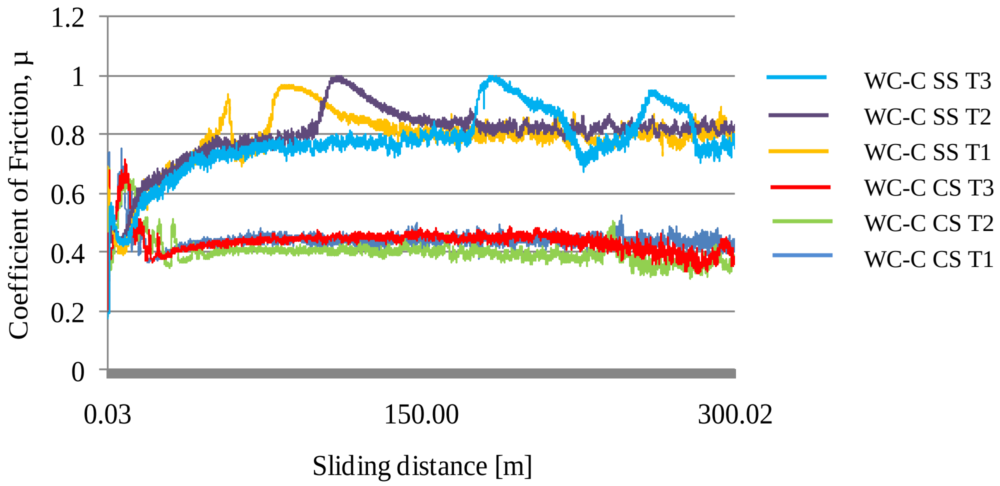


(c)

*Figure 4.7. Friction response of buttons (a) WC-A, (b), WC-B and (c) WC-C sliding against 304 stainless steel and bright mild steel under test condition 2 parameters (Load: 3N, Sliding velocity 0.2m.s$^{-1}$).*

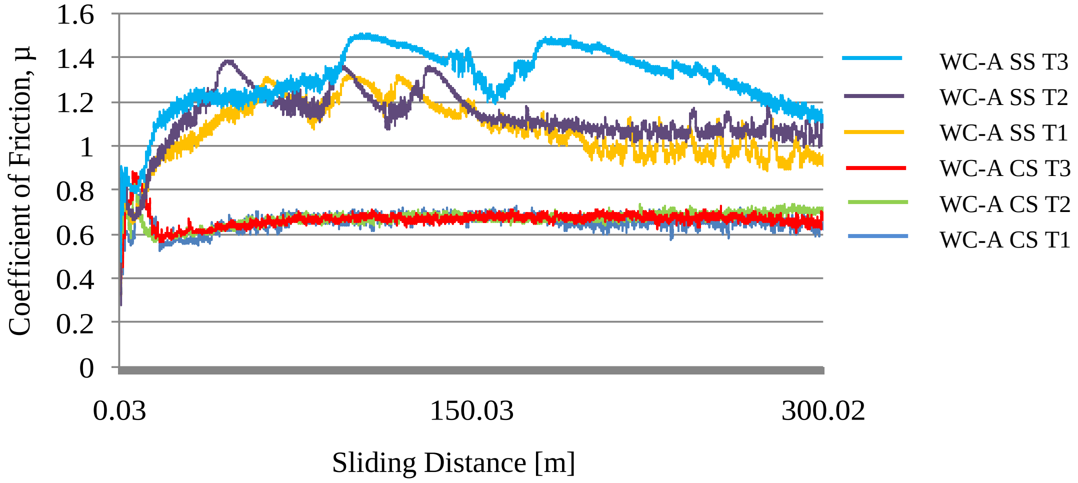


(a)

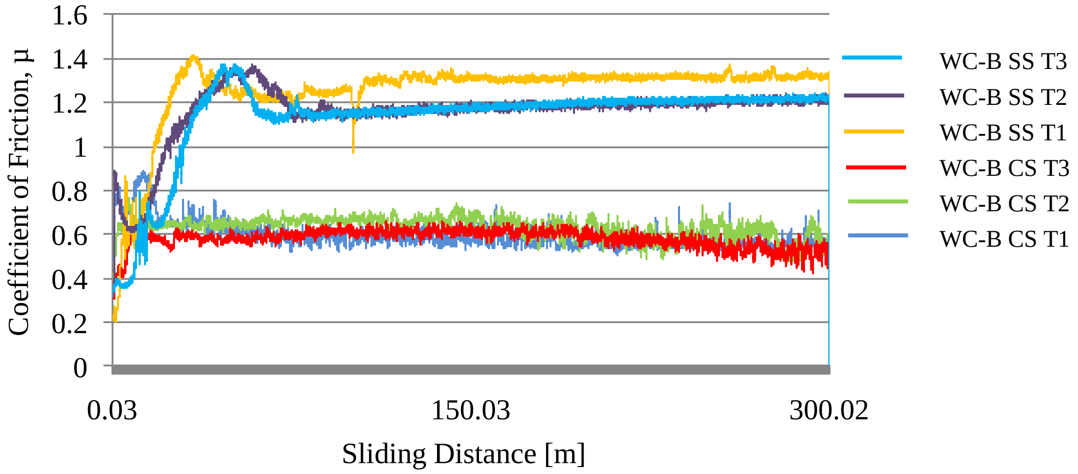


(b)

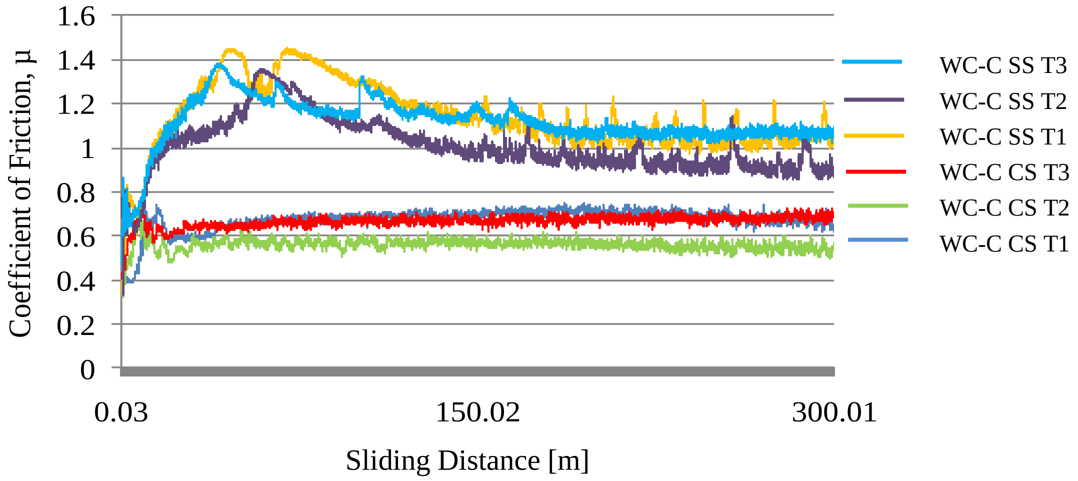


(c)

*Figure 4.8. Friction response of buttons (a) WC-A, (b), WC-B and (c) WC-C sliding against 304 stainless steel and bright mild steel under test condition 3 parameters (Load: 1N, Sliding velocity 0.2m.s$^{-1}$).*

Figures 4.9 and 4.10 indicate the effect of decreasing sliding velocity under a constant applied load of 3N on the friction response of the sliding pairs. The friction values were very similar across all sliding velocities. The friction values of stainless steel were higher than those of mild steel under all test conditions. The mild steel substrates in general have a fairly consistent and smooth friction response while the friction behavior of the stainless steel substrates is unpredictable. Similar to the applied load results, each friction response is characterized by a running-in period as defined in Chapter 2, Section 2.1. This running-in period occurs during the first 75m of sliding. After this initial running-in period the friction behavior of the mild steel/button grade sliding pairs levels off to a constant value, while the stainless steel/button grade sliding pairs display inconsistent behavior.

The mild steel paired button grades follow a similar pattern to the first three test conditions where load was varied. During the run-in period the friction increases to a distinctive peak after which it decreases and levels off at a lower level. This resembles friction response pattern II from Section 2.1.

The friction responses for the three grades paired with a mild steel substrate are very similar across all sliding velocities. There is one exception which occurs at the highest sliding velocity of $0.3m.s^{-1}$ for grades WC-A and WC-C where the results of the three tests for each button grade take longer to level off and are not similar to each other as is the case with the other sliding velocities.

Similar to the first three test conditions, the stainless steel paired buttons showed an initial decrease in friction followed by a sharp increase after which it either remains at that level or decreases and then levels off. At the highest sliding velocity, the friction response for all three button grades is initially smooth, increasing at a decreasing exponential rate during the running-in period and then becoming irregular towards the end of the test. At the lowest sliding velocity however, the three buttons have distinctly different responses to each other and to that experienced at the higher sliding velocities.

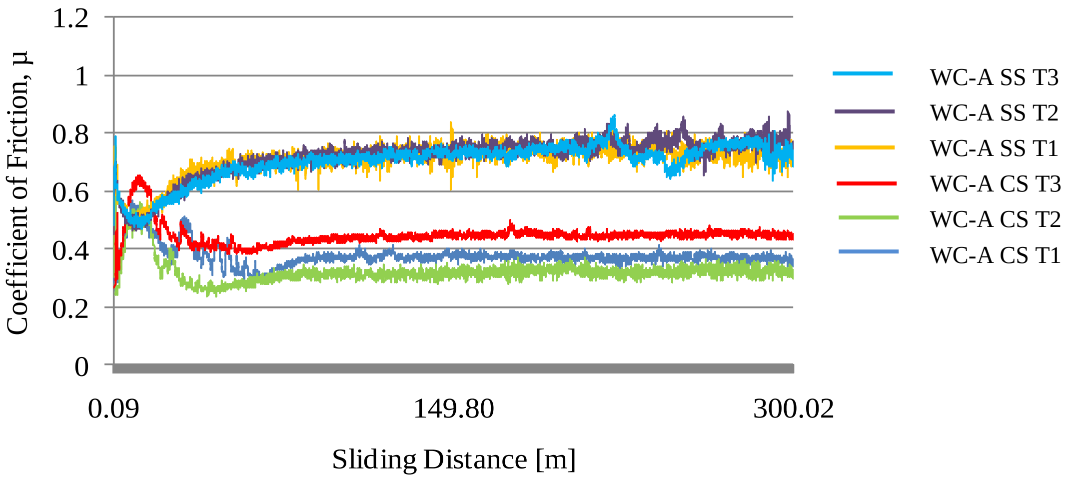


(a)

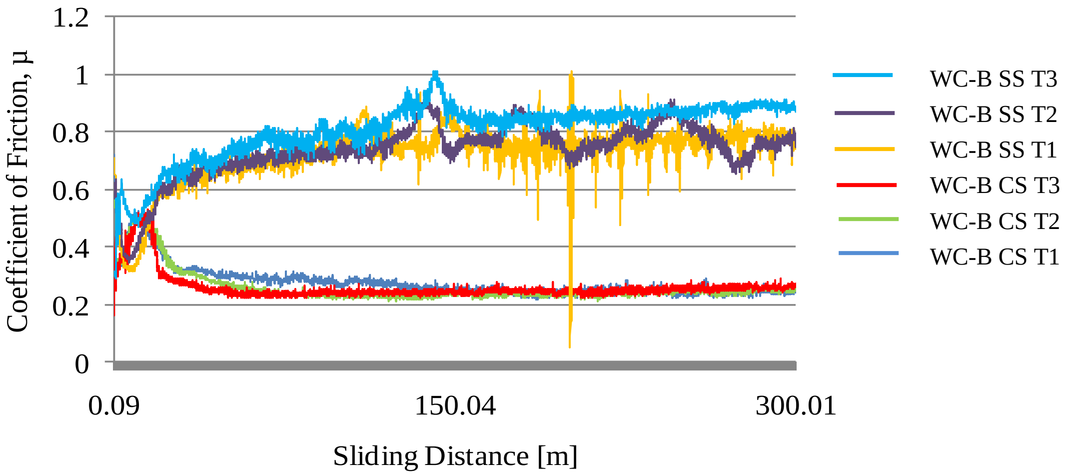


(b)

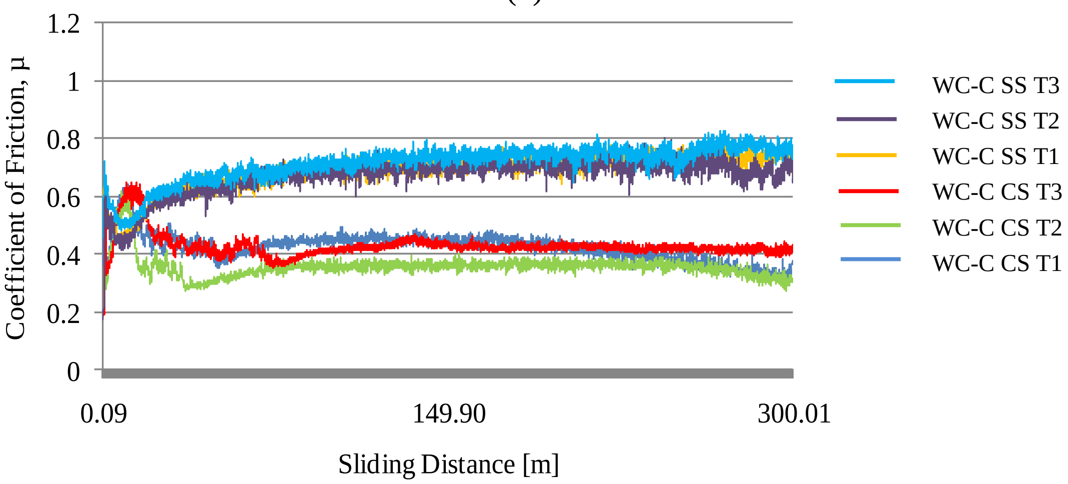


(c)

*Figure 4.9. Friction response of buttons (a) WC-A, (b), WC-B and (c) WC-C sliding against 304 stainless steel and bright mild steel under test condition 4 parameters (Load: 3N, Sliding velocity 0.3m.s$^{-1}$).*

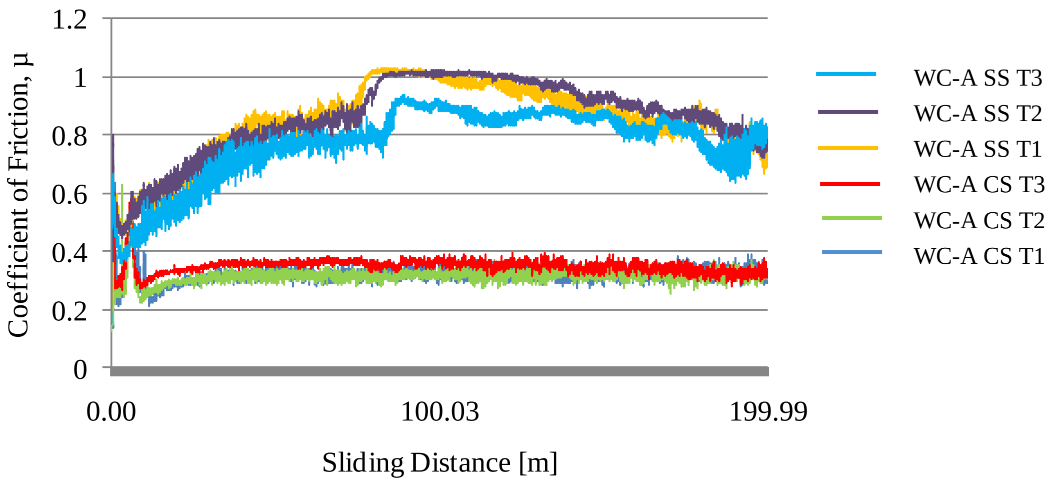


*(a)*

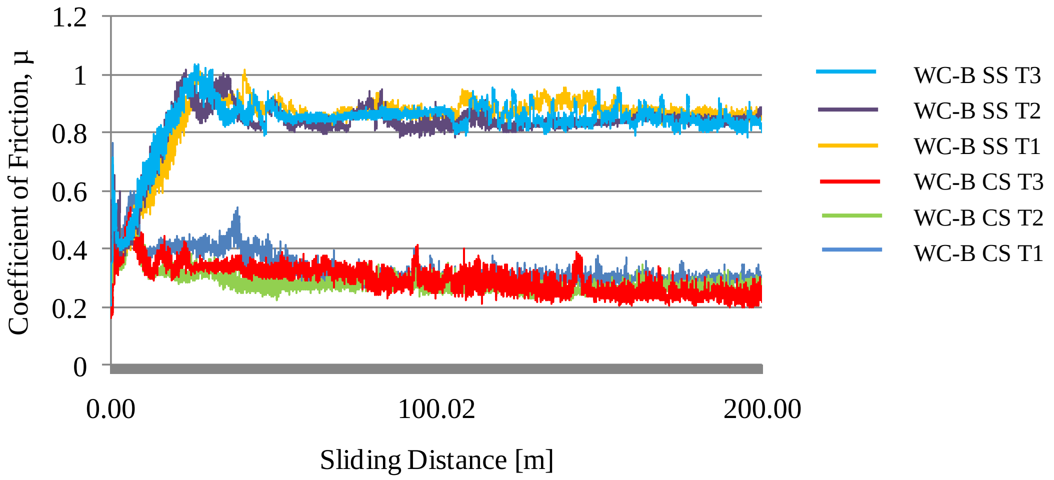


*(b)*

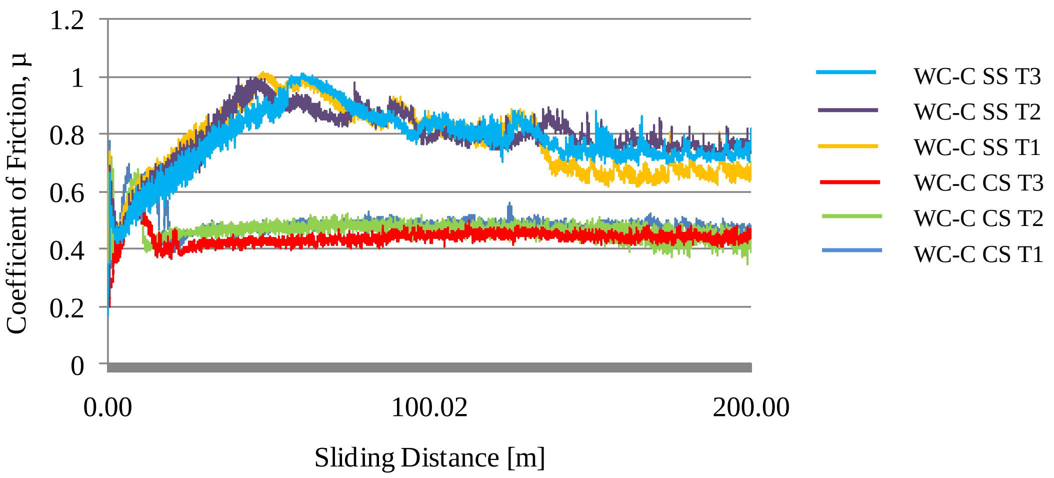


*(c)*

*Figure 4.10. Friction response of buttons (a) WC-A, (b), WC-B and (c) WC-C sliding against 304 stainless steel and bright mild steel under test condition 5 parameters (Load: 3N, Sliding velocity 0.1m.s$^{-1}$).*

Figure 4.11 illustrates the maximum penetration depths on the steel substrates by the button grades during wear testing for each of the test conditions listed in Table 3.4 (Chapter 3). In the figure 'OP' signifies 'operating parameter'; e.g. 'OP1' defines test condition number 1. From Figure 4.11 it can be seen that the maximum penetration depths for the different button grade/steel pairs under the different test conditions are generally similar and average between 1.6µm and 1.9µm with the exception of isolated cases. The sliding pair of button grade WC-C against stainless steel under test condition 1 (i.e. highest load) showed the greatest penetration depth of 2.7µm. Under the same test condition all the other sliding pairs showed an average penetration depth of 1.7 to 1.8 µm. Under test condition 4 (i.e. highest load/speed combination) button grade WC-B had high penetration depths against both steel substrates.

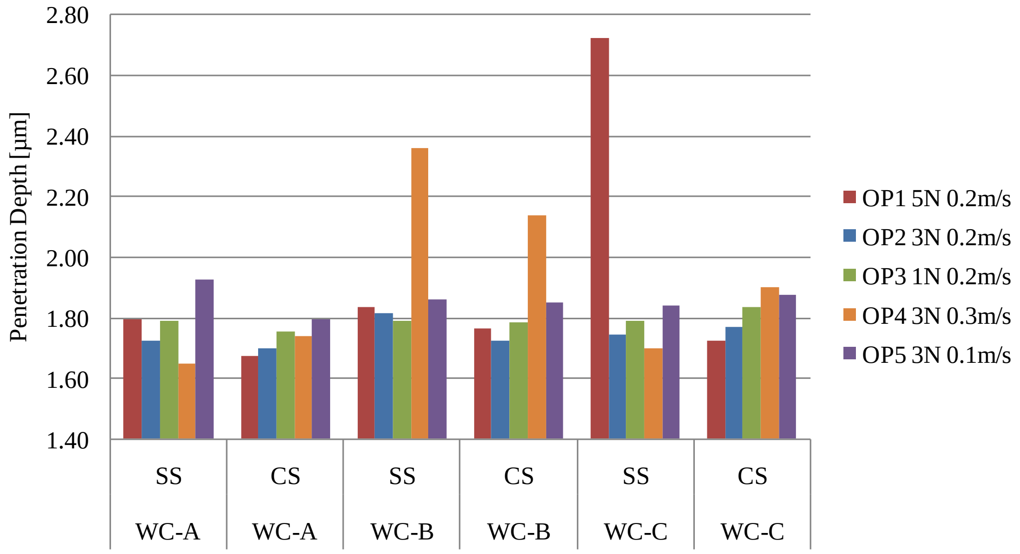


*Figure 4.11. Comparison of the maximum penetration depths for the different button/steel pairs for the five operating conditions.*

Figure 4.12 illustrates the width of the wear tracks on the steel substrates for each sliding pair under each test condition. A distinct trend is noted. The test conditions can be ranked in terms of which condition provides the widest track width. Therefore from widest to narrowest the test conditions may be ranked as, OP1, OP4, OP2, OP5, OP3, in which the highest applied load has produced the widest wear track width and the lowest applied load the narrowest width. In certain cases there are minor differences in the ranking order, e.g. the sliding pair of button grade WC-B against mild steel yields almost similar results for all test conditions. Button grades WC-A and WC-C display fairly similar values against both steel substrates and is consistently higher than the widths achieved by the button grade WC-B/steel sliding pairs.

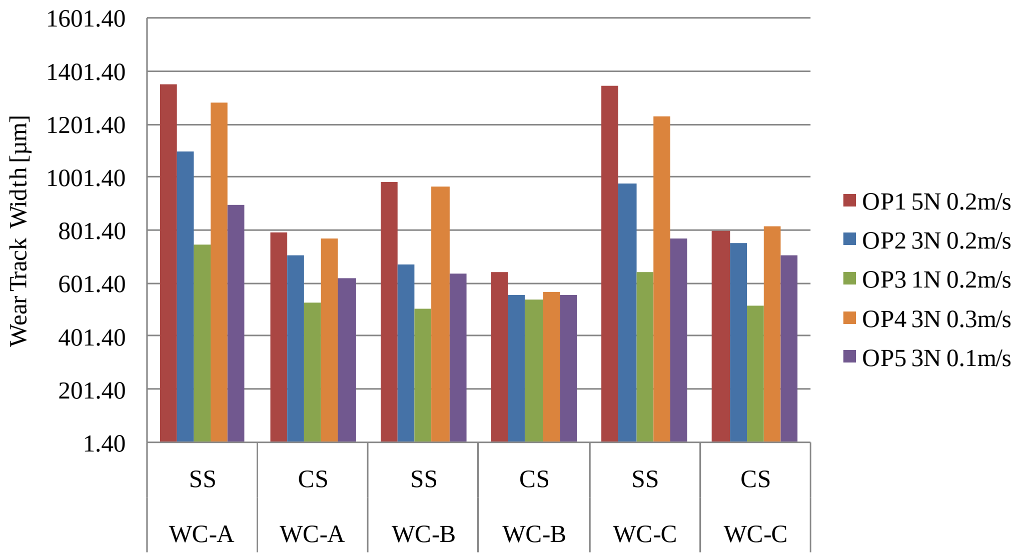


*Figure 4.12. Comparison of the wear track width for the different button/steel pairs for the five operating conditions.*

Figure 4.13 graphically compares the static and kinetic coefficients of friction of each button grade and steel sliding pair across the different test conditions. The complete set of data, including the standard deviations, is tabulated in Appendix D. In general stainless steel experienced higher friction (static and kinetic) compared to mild steel under all test conditions except in two instances, both related to button grade WC-C for test conditions 2 (OP2) and 3 (OP3) where the static friction coefficients for mild steel were higher than those for stainless steel. The highest friction values, often surpassing the $\mu=1$ mark, were recorded under test condition 3 (OP3 – lowest load)) for all three button grades sliding against stainless steel. The lowest kinetic friction values were recorded for button grade WC-B sliding against mild steel under all 5 test conditions. In line with friction theory, the static friction values are higher than the kinetic friction values under all test conditions for all button/steel sliding pairs except in three instances. In two instances, both for button grade WC-C sliding against stainless steel (OP2) and mild steel (OP3) respectively, the difference is less than 10%. In the third case, for button grade WC-B sliding against stainless steel (OP3) the difference is less than 30%. As described in Section 2.1, the static coefficient of friction is usually larger that the kinetic coefficient [1, 4] but this is not necessarily always the case. The cause for the increase in kinetic friction to be greater than the original static friction is possibly due to the changes in the surface conditions between the two materials during the running of the test.

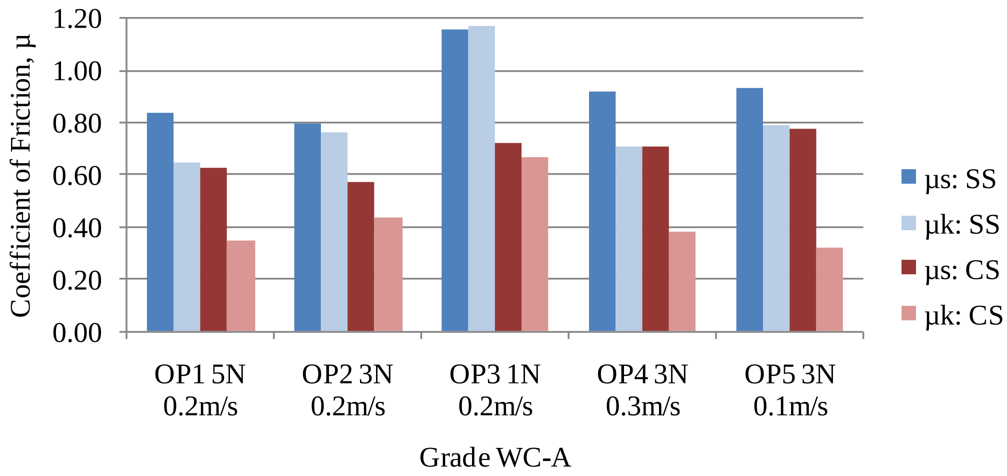


(a)

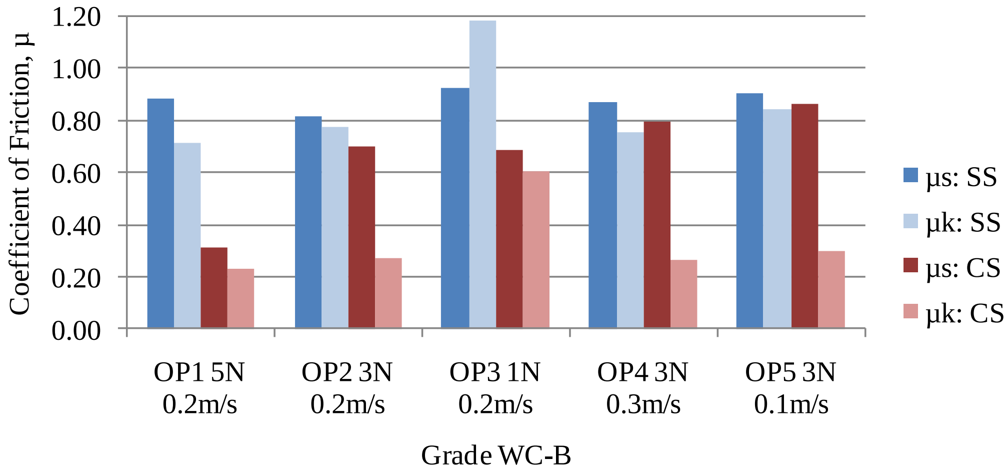


(b)

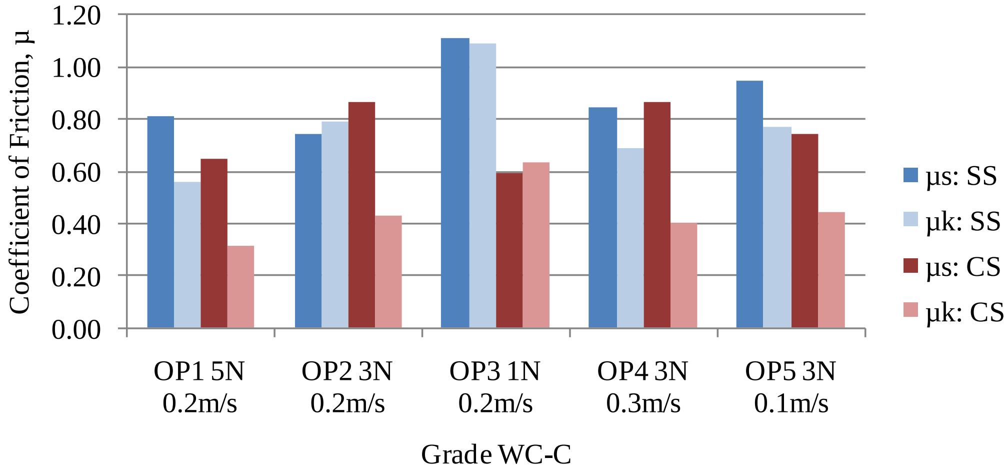


(c)

*Figure 4.13. Comparison of the static and dynamic coefficient of friction for the various (a) WC-A, (b) WC-B, (c), WC-C button/steel pairs for the five test conditions.*

The averaged sliding wear and friction test results for each button-substrate pair for each test condition, during which the load and sliding velocity was varied, is summarized in Table 4.4. The individual test results can be found in Appendix D. Figures 4.14 to 4.17 graphically represent the data listed in Table 4.4.

Table 4.4. Averaged sliding wear and friction test results[1].

| Sample pairs | | | μ | $V_S$ ($x10^4$) | $k_s$ ($x10^{-6}$) | $V_B$ ($x10^4$) | $k_B$ ($x10^{-6}$) |
|---|---|---|---|---|---|---|---|
| Test Condition 1 | WC-A | SS | 0.65 | 5882.83 | 39.22 | 360.88 | 2.41 |
| | WC-A | CS | 0.35 | 3205.50 | 21.37 | 61.22 | 0.41 |
| | WC-B | SS | 0.71 | 4347.40 | 28.98 | 140.30 | 0.94 |
| | WC-B | CS | 0.23 | 2673.91 | 17.83 | 32.22 | 0.21 |
| | WC-C | SS | 0.56 | 8753.46 | 58.36 | 398.89 | 2.66 |
| | WC-C | CS | 0.31 | 3305.74 | 22.04 | 64.74 | 0.43 |
| Test Condition 2 | WC-A | SS | 0.76 | 4593.43 | 51.04 | 136.69 | 1.52 |
| | WC-A | CS | 0.43 | 2877.20 | 31.97 | 31.59 | 0.35 |
| | WC-B | SS | 0.77 | 2976.29 | 33.07 | 51.96 | 0.58 |
| | WC-B | CS | 0.27 | 2286.70 | 25.41 | 23.52 | 0.26 |
| | WC-C | SS | 0.79 | 4131.14 | 45.90 | 117.50 | 1.31 |
| | WC-C | CS | 0.43 | 3165.40 | 35.17 | 58.76 | 0.65 |
| Test Condition 3 | WC-A | SS | 1.17 | 3065.90 | 102.20 | 66.00 | 2.20 |
| | WC-A | CS | 0.66 | 2207.84 | 73.59 | 17.15 | 0.57 |
| | WC-B | SS | 1.18 | 2166.06 | 72.20 | 28.77 | 0.96 |
| | WC-B | CS | 0.60 | 2266.45 | 75.55 | 17.55 | 0.58 |
| | WC-C | SS | 1.09 | 2710.01 | 90.33 | 41.41 | 1.38 |
| | WC-C | CS | 0.63 | 2232.08 | 74.40 | 22.71 | 0.76 |

Table 4.4 Averaged sliding wear and friction test results[1] continued.

| Sample pairs | | | μ | $V_S$ ($x10^4$) | $k_s$ ($x10^{-6}$) | $V_B$ ($x10^4$) | $k_B$ ($x10^{-6}$) |
|---|---|---|---|---|---|---|---|
| Test Condition 4 | WC-A | SS | 0.71 | 5129.18 | 56.99 | 149.68 | 1.66 |
| | WC-A | CS | 0.38 | 3173.71 | 35.26 | 27.36 | 0.30 |
| | WC-B | SS | 0.75 | 5464.83 | 60.72 | 75.57 | 0.84 |
| | WC-B | CS | 0.27 | 2934.92 | 32.61 | 17.01 | 0.19 |
| | WC-C | SS | 0.69 | 5076.80 | 56.41 | 138.19 | 1.54 |
| | WC-C | CS | 0.40 | 3632.63 | 40.36 | 32.80 | 0.36 |
| Test Condition 5 | WC-A | SS | 0.79 | 4191.27 | 46.57 | 46.66 | 0.52 |
| | WC-A | CS | 0.32 | 2594.30 | 28.83 | 8.57 | 0.10 |
| | WC-B | SS | 0.85 | 2906.43 | 32.29 | 20.35 | 0.23 |
| | WC-B | CS | 0.30 | 2482.06 | 27.58 | 13.82 | 0.15 |
| | WC-C | SS | 0.77 | 3404.18 | 37.82 | 32.57 | 0.36 |
| | WC-C | CS | 0.45 | 3133.57 | 34.82 | 14.41 | 0.16 |

[1] Definitions for sliding wear and friction parameters within Table 4. 4 are as follows:

μ Kinetic coefficient of friction.

$V_S$ Total worn volume of substrate [$\mu m^3$]

$k_S$ Dimensional substrate wear coefficient [$mm^3/Nm$]

$V_B$ Total worn volume of button [$\mu m^3$]

$k_B$ Dimensional button wear coefficient [$mm^3/Nm$]

Figure 4.14, which illustrates the effect of load on the coefficient of friction at a constant sliding velocity, clearly depicts that an increase in load causes a non-linear decrease in friction. The friction response of the mild steel is at least 50% lower than that of the stainless steel at all loads tested. Within experimental error the friction response of the button grades is similar for each steel at each load.

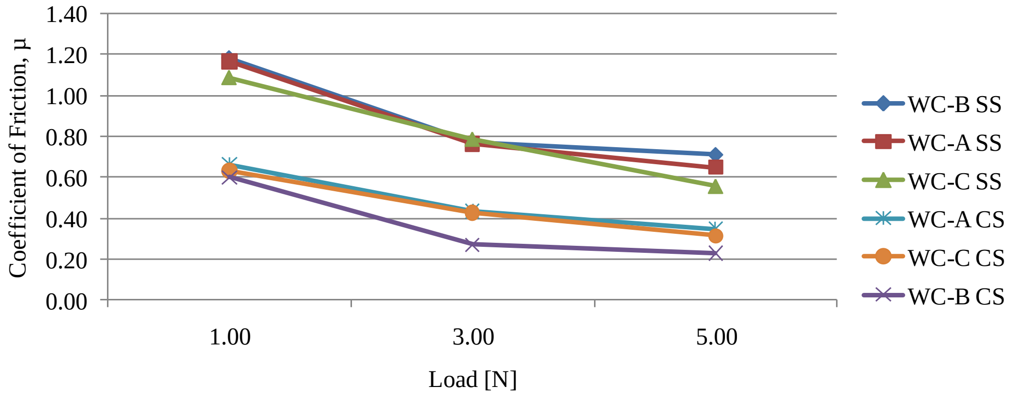


*Figure 4.14 Effect of applied load on friction for 304 stainless stee,(SS) and bright mild steel (CS) substrates at a sliding velocity of 0.2m.s$^{-1}$.*

With respect to Figure 4.15 which demonstrates the effect that sliding velocity has on friction under a constant load it is observed that within experimental error the coefficient of friction remains relatively constant for each sliding pair. This aligns with one of the laws of friction generally applied to metals which states that friction is independent of sliding velocity. The friction response of the mild steel is at least 50% lower than that of the stainless steel at all speeds tested; similar to the trend observed in Figure 4.14 with respect to the effect of load on friction.

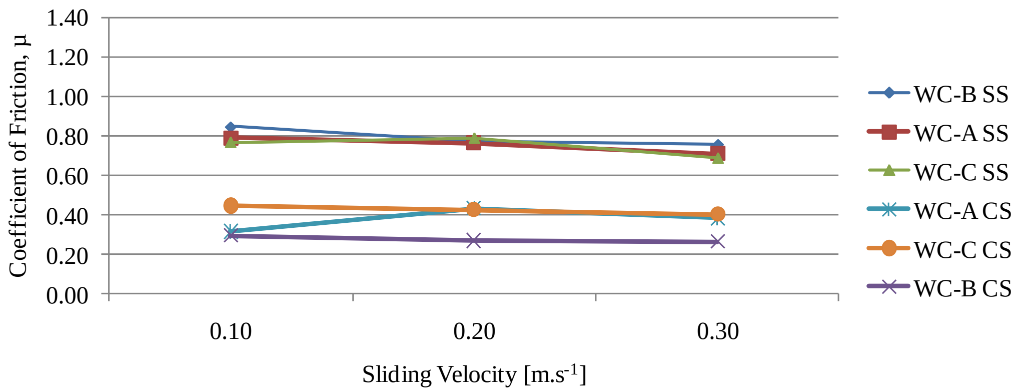


*Figure 4.15. Effect of sliding velocity on friction for 304 stainless steel ( SS) and bright mild steel (CS) substrates at a load of 3N.*

The dimensional wear coefficient, k, is used to characterise the wear response of a material. The wear coefficient and the factors which influence it were reviewed in Chapter 2, Section 2.2. The volume of material lost during wear is used to calculate the wear coefficient. Table 4.4 lists the calculated wear coefficients for each of the sliding pairs under each test condition as well as the total volume loss of the button grades and steel substrates. Figure 4.16 compares the volume of material lost by the three different button grades against the respective steel substrates under the five operating conditions. This graph clearly illustrates the different responses of the three grades of cemented carbides to the differences in applied load and in sliding velocity. Generally all three button grades have low volume losses against mild steel with grade WC-B having the lowest wear volume overall. This aligns with the friction data presented earlier.

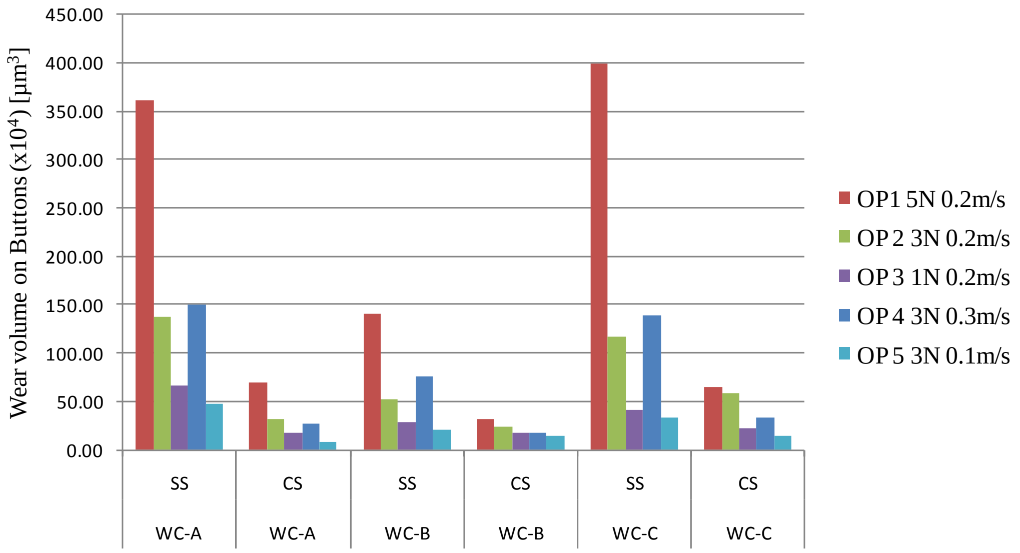


*Figure 4.16 Comparison of wear volumes between the three button grades for all test conditions.*

Figure 4.17 shows the influence of the applied load on the dimensional wear coefficient, k, when the sliding velocity is held constant. Figure 4.18 illustrates the effect of sliding velocity on the dimensional wear coefficient, k, when the applied load is held constant. The trends shown in these figures appear to follow the trends observed with respect to the friction response of the materials shown in earlier figures. Sliding pairs which displayed high friction values have high wear coefficients which translate into high wear rates. With respect to applied load the wear coefficients show a minimum at a load of 3N for all the stainless steel sliding pairs and the WC-A/mild steel sliding pair. However the WC-B/mild steel and WC-C/mild steel sliding pairs show a decrease in wear as the load is increased. With respect to sliding velocity there appears to be a general trend of a sharp increase in wear when the velocity is increased from 0.1 to 0.2 m/s after which the wear levels off as the velocity is increased to 0.3 m/s. There are two exceptions to this trend. The WC-C/mild steel sliding pair shows a decrease in wear as the speed is increased from 0.2 to 0.3 m/s. The stainless steel/WC-B sliding pair shows an increase in wear as the velocity increases from 0.1 to 0.3 m/s. In general the WC-B button grades have the lowest wear rates against both steels tested. The trends observed in these figures will be discussed in detail in Chapter 5.

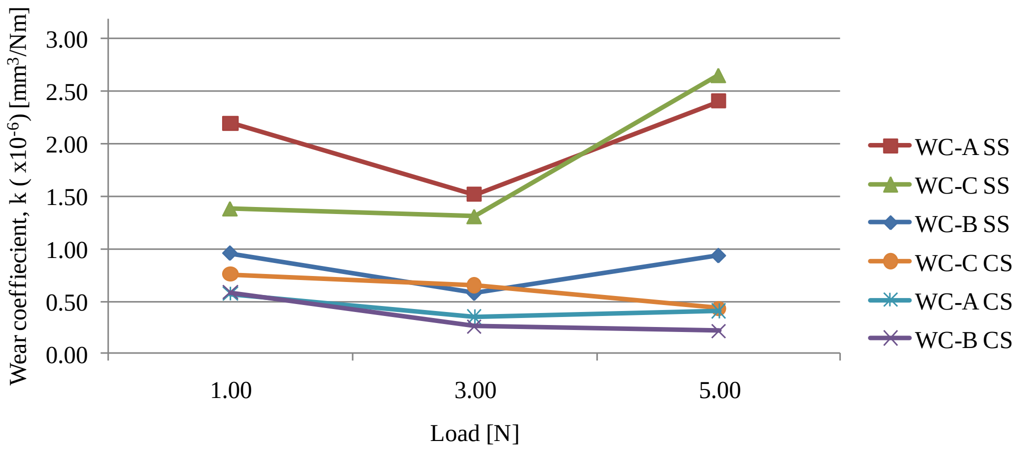


*Figure 4.17. Effect of applied load on the dimensional wear coefficient, k, for 304 stainless steel (SS) and bright mild steel (CS) substrates at a sliding velocity of 0.2m.s$^{-1}$.*

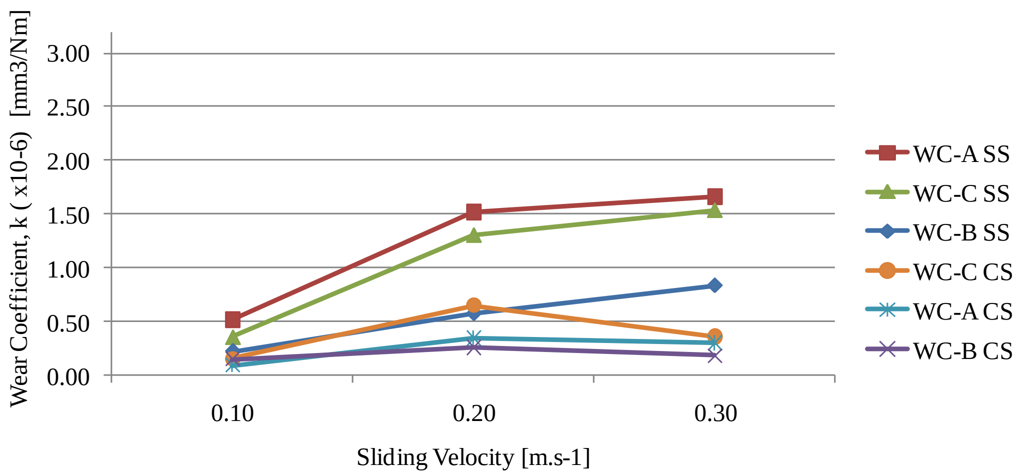


*Figure 4.18. Effect of sliding velocity on the dimensional wear coefficient, k, using 304 stainless steel, SS, and bright mild steel, CS, substrates at a load of 3N.*

### 4.3 Wear scar analyses

The wear scars were examined using SEM, XPS and EDS. A complete set of SEM images detailing the wear scars of the steel substrates and the cemented carbide buttons under the different test conditions can be found in Appendix E. In this section selected SEM images are presented to provide a summary of the wear mechanisms observed. In many instances similar wear mechasnisms were observed under the different test conditions.

Figure 4.19. illsutrates the typical wear tracks on the steel substrates under various test conditions. These images provide a general impression of the variation in wear track widths achieved by the different button grades which are also depended on the operating conditions. Figures 4.20 and 4.21 provide high magnification images of these wear tracks on the stainless steel and mild steel subsrates respectively.

Figure 4.22. illustrates the typical wear scars on the cemented carbide button grades used to produce the wear tracks on the steels shown in Figure 4.19. Thus Figure 4.22.(a) is the button grade used to produce the wear track shown in Figure 4.19.(a). Figures 4.23 and 4.24 provide high magnification images of the wear scars on the button grades used to produce wear tracks on the stainless steel and mild steel substrates respcetively.

The wear mechanisms for the 304 stainless steel and bright mild steel substrates were found to be very similar. Severe plastic deformation is evident. Large amounts of wear debris can be seen together with roughened surfaces. The ploughing of wear particles is clearly evident and contributed to groove formation and smearing. Figures 4.20 and 4.21 clearly illustrate large amounts of wear debris on the roughened surfaces of the steel substrates, grooving and the smearing of the displaced material. The grooving, as well as cutting, can be seen to be parallel with the sliding direction. Figure 4.19(d) shows extensive smearing occurred, particularly between the grade WC-B/stainless steel sliding pair.

The bright mild steel substrates show less wear debris on their surfaces compared to those of the 304 stainless steel substrates which correlates with the decreased wear that the mild steel substrates experienced. Figures 4.19 (a) and (b) shows this difference as well as the differences in the wear track widths. The stainless steel substrates, usually exhibiting the higher wear rate generally has a wider wear track than its mild steel counterparts.

The wear mechanisms for the three cemented carbide grades were generally found to be the same portraying severe plastic deformation. Preferential binder removal is clearly evident. It is believed that the binder removal occurs first, followed by subsequent carbide grain cracking and carbide grain pull-out, highly distinguishable in Figure 4.24(d). Often visible is the presence of the occasional tribofilm which formed during wear. These mechanisms were identified to be the main causes of wear across all the test conditions and are clearly illustrated in Figures 4.23 and 4.24. Figure 4.22 shows the extent of the transferred material on the various buttons.

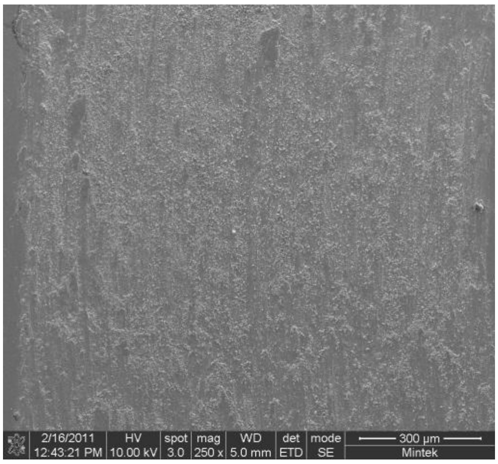


*(a)*

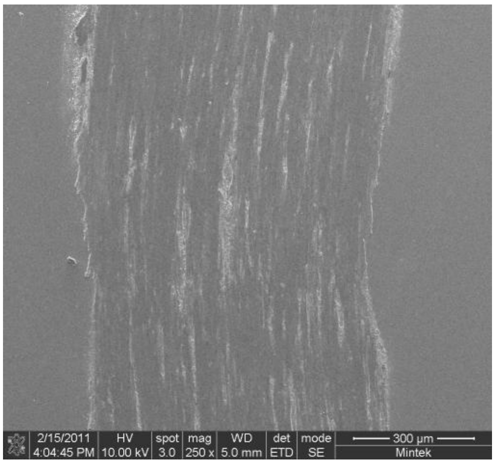


*(b)*

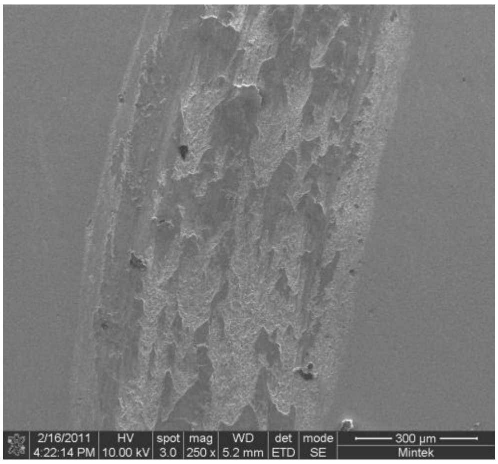


*(c)*

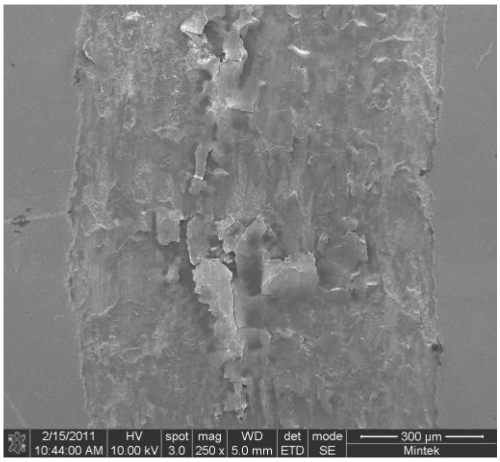


*(d)*

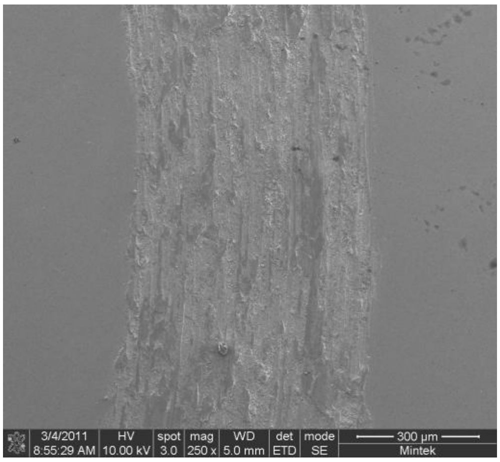


*(e)*

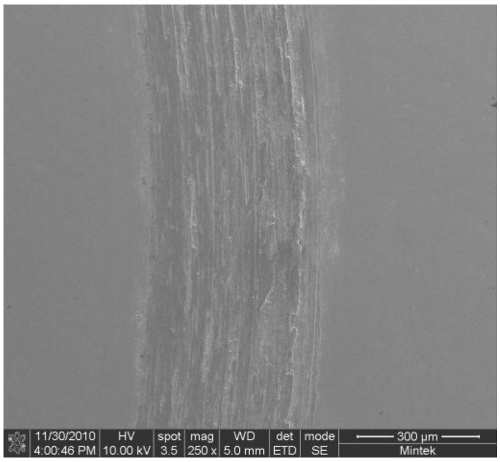


*(f)*

*Figure 4.19. SEM images of the wear tracks on the steel substrates under various test conditions. (a) WC-A/SS OP4 (3N, 0.3m.s$^{-1}$) (b) WC-A/CS OP4 (3N, 0.3m.s$^{-1}$) (c) WC-B/SS OP5 (3N, 0.1m.s$^{-1}$) (d) WC-B/SS, OP1 (5N, 0.2m.s$^{-1}$) (e) WC-C/SS OP3 (1N, 0.2m.s$^{-1}$) (f) WC-B/CS OP3 (2N, 0.2m.s$^{-1}$).*

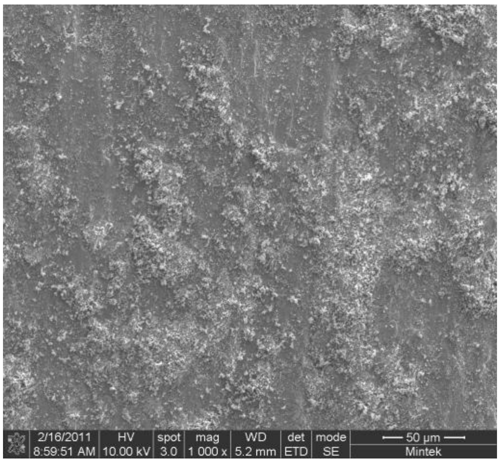


*(a)*

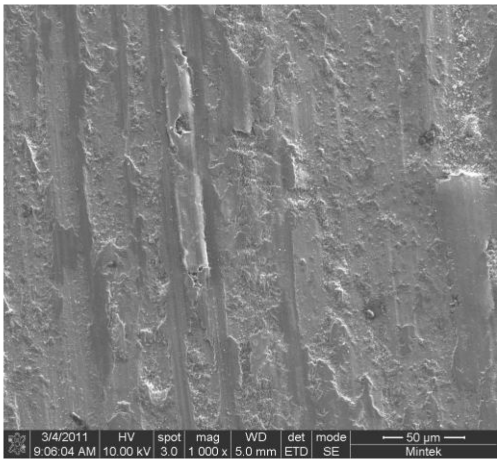


*(b)*

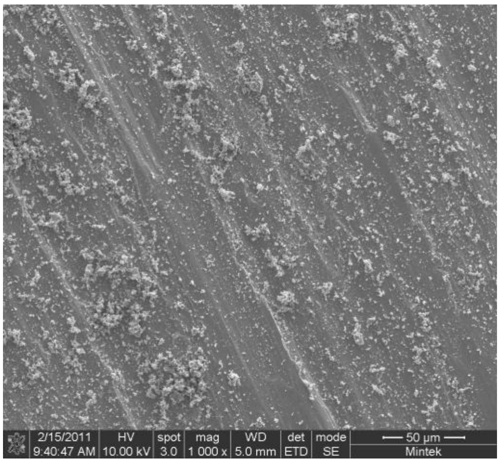


*(c)*

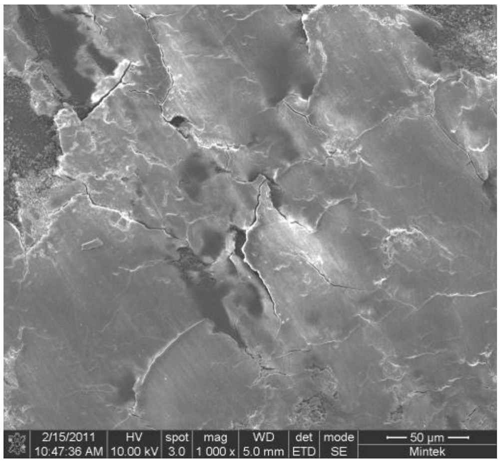


*(d)*

*Figure 4.20. SEM imags of the wear scars of the stainless steel substrates tested under various conditions by different button grades. (a) WC-A/SS OP1 (5N, 0.2m.s$^{-1}$) (b) WC-C/SS OP3 (1N, 0.2m.s$^{-1}$) (c) WC-C/SS OP1 (5N, 0.2m.s$^{-1}$) (d) WC-B/SS OP1 (5N, 0.2m.s$^{-1}$).*

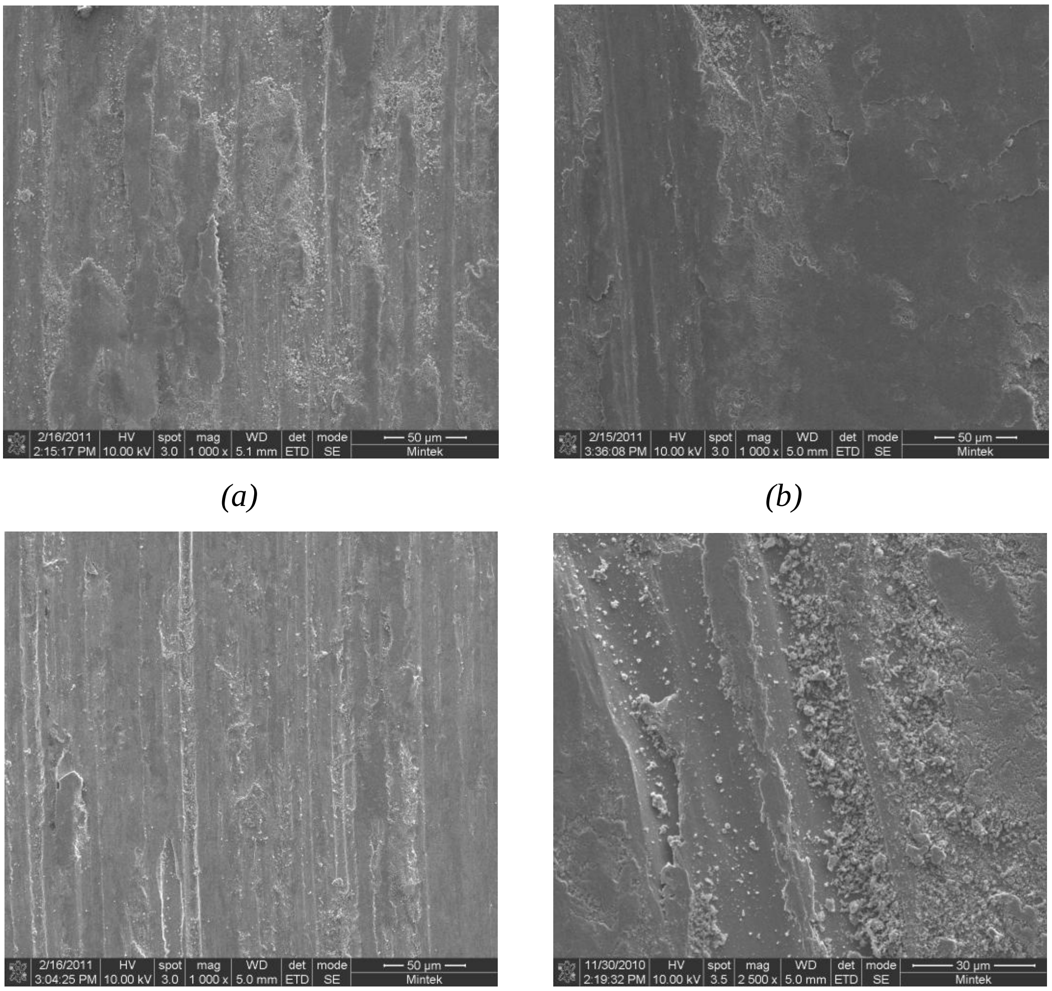


*(a)* *(b)* *(c)* *(d)*

*Figure 4.21. SEM imags of the wear scars of the mild steel substrates tested under various conditions by different button grades. (a) WC-C/CS OP5 (3N, 0.1m.s$^{-1}$) (b) WC-B/CS OP4 (3N, 0.3m.s$^{-1}$) (c) WC-A/CS OP5 (3N, 0.1m.s$^{-1}$) (d)4 WC-B/CS OP1 (5N, 0.2m.s$^{-1}$).*

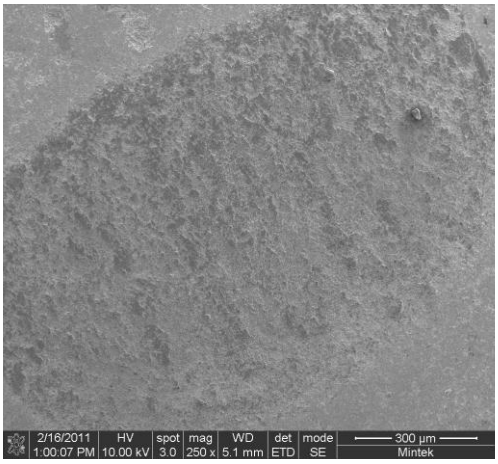


*(a)*

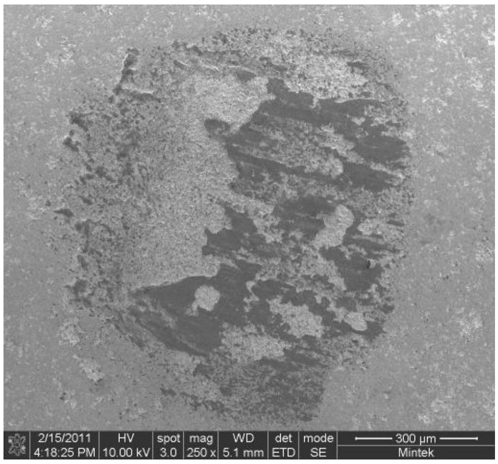


*(b)*

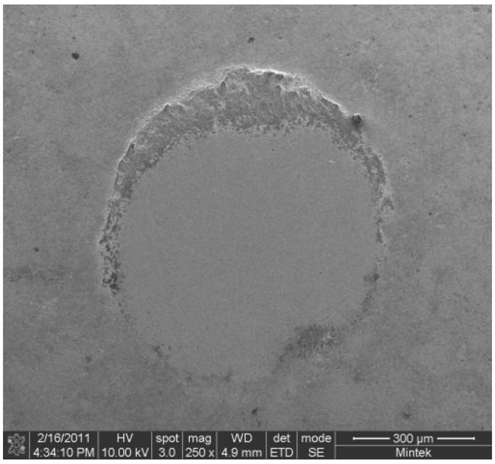


*(c)*

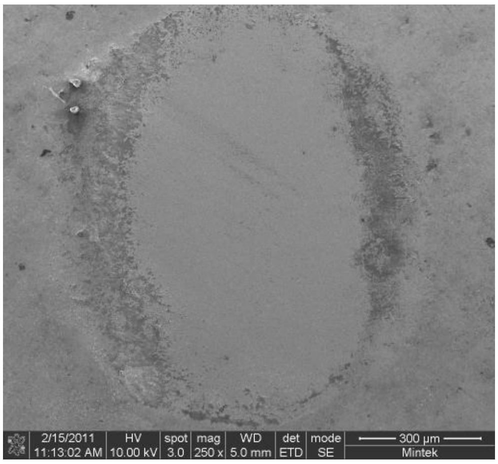


*(d)*

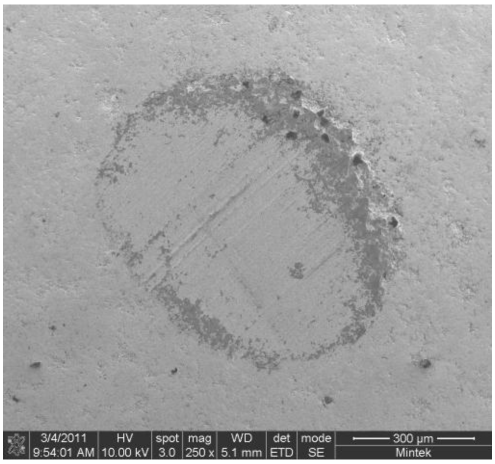


*(e)*

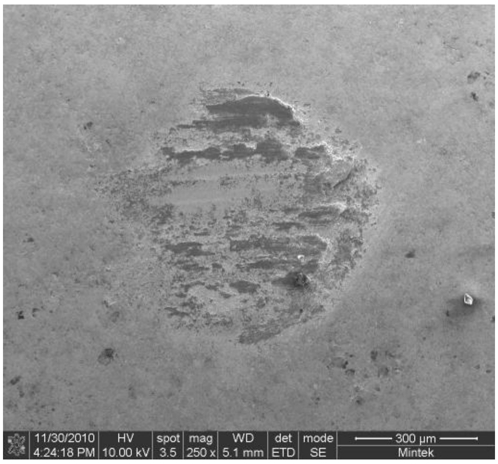


*(f)*

*Figure 4.22. SEM images of the wear scars on the button grades used to produce the wear tracks shown in Figure 4.19. (a) WC-A/SS OP4 (3N, 0.3m.s$^{-1}$) (b) WC-A/CS OP4 (3N, 0.3m.s$^{-1}$) (c) WC-B/SS OP5 (3N, 0.1m.s$^{-1}$) (d) WC-B/SS OP1 (5N, 0.2m.s$^{-1}$) (e) WC-C/SS OP3 (1N, 0.2m.s$^{-1}$) (f) WC-B/CS OP3 (1N, 0.2m.s$^{-1}$).*

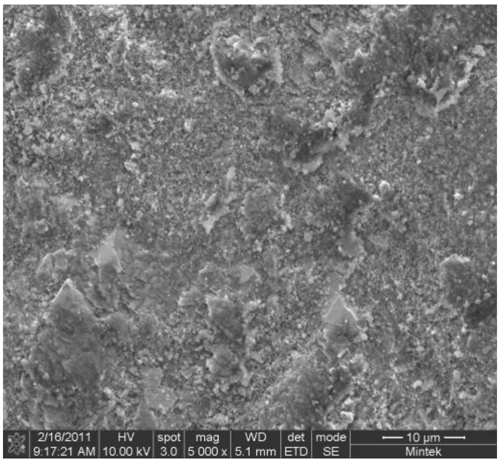


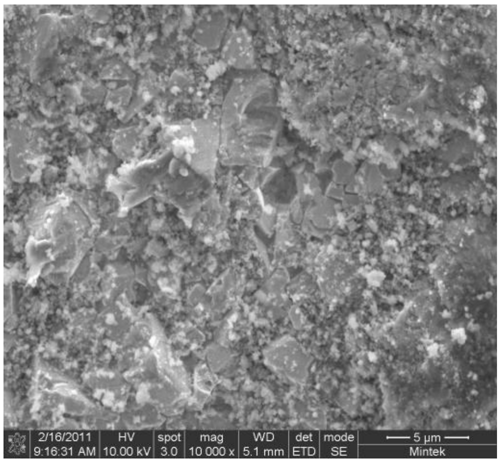


*(a)* *(b)*

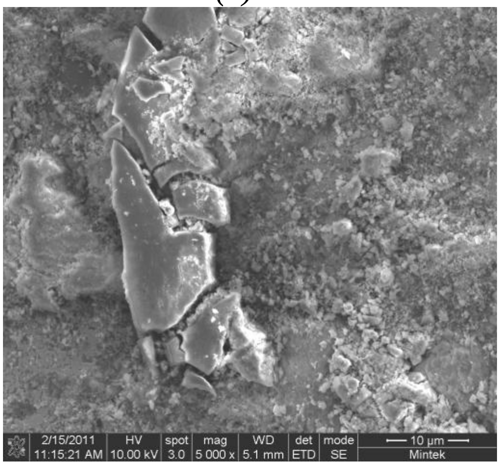


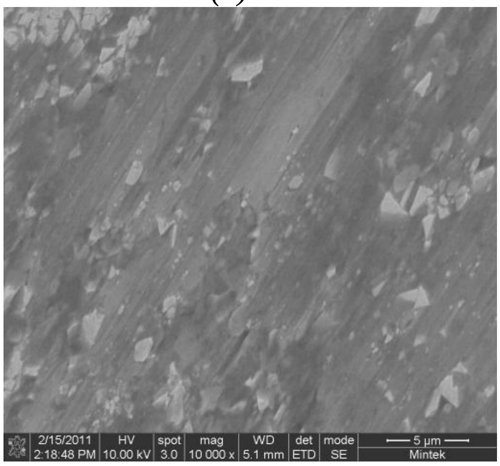


*(c)* *(d)*

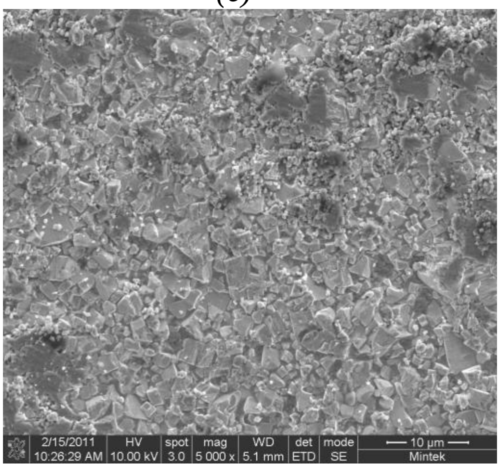


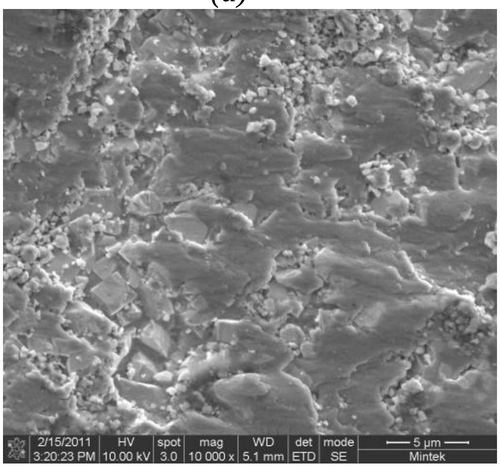


*(e)* *(f)*

*Figure 4.23. SEM images of the wear scars on the button grades used to produce the wear tracks on the stainless steel substrates. (a) WC-A/SS OP1 (5N, 0.2m.s$^{-1}$) (b) WC-A/SS OP1(5N, 0.2m.s$^{-1}$) (c) WC-B/SS OP1 (5N, 0.2m.s$^{-1}$) (d) WC-B/SS OP3 (1N, 0.2m.s$^{-1}$) (e) WC-C/SS OP1(5N, 0.2m.s$^{-1}$) (f) WC-C/SS OP4 (5N, 0.2m.s$^{-1}$).*

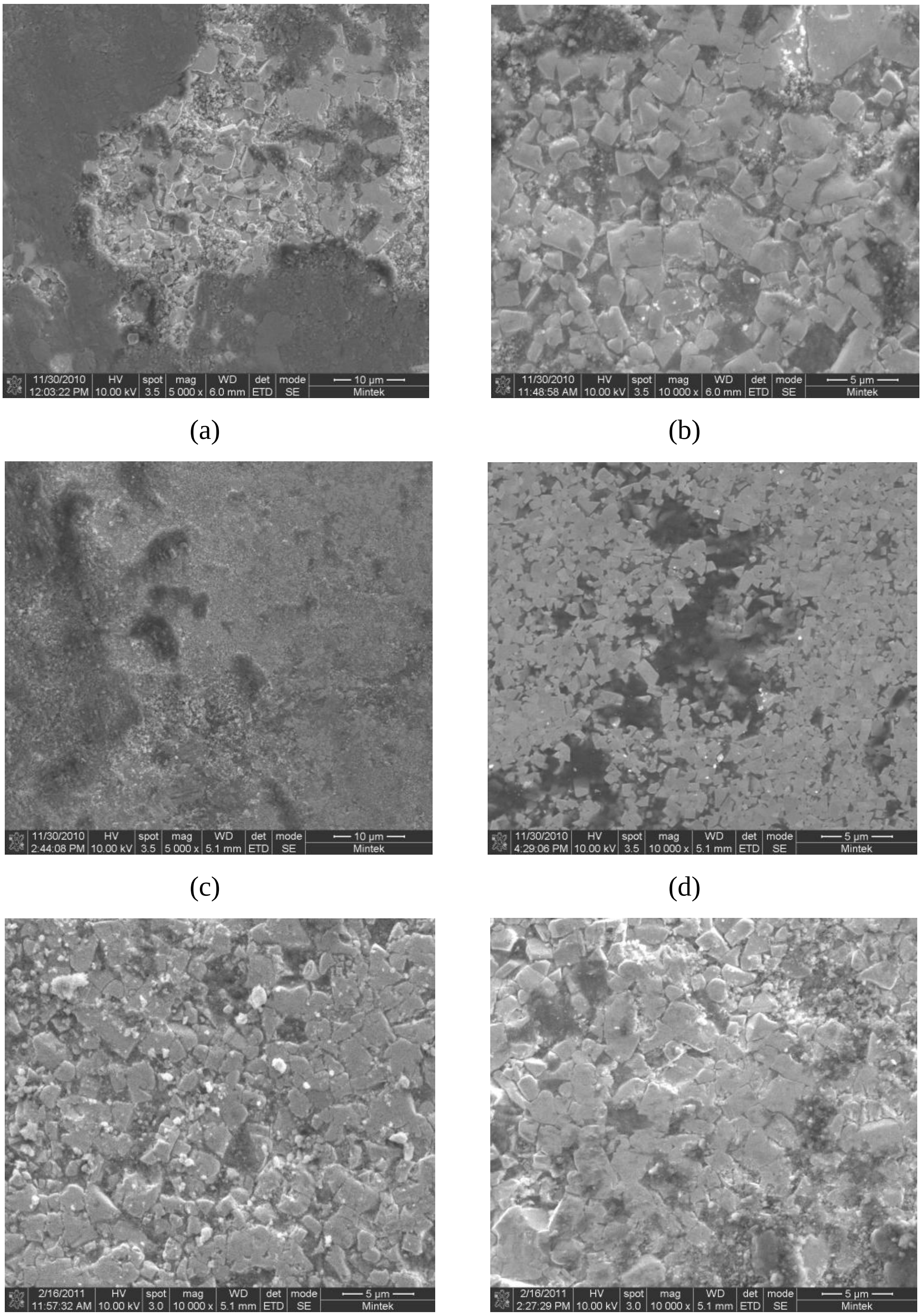


*Figure 4.24. SEM images of the wear scars on the button grades used to produce the wear tracks on the mild steel substrates. (a) WC-A/CS OP1 (5N, 0.2m.s$^{-1}$) (b) WC-A/CS OP1 (5N, 0.2m.s$^{-1}$) (c) WC-B/CS OP1 (5N, 0.2m.s$^{-1}$) (d) WC-B/CS OP3 (1N, 0.2m.s$^{-1}$) (e) WC-C/CS OP3 (1N, 0.2m.s$^{-1}$) (f) WC-C/CS OP5 (3N, 0.1m.s$^{-1}$).*

*XPS Results*

The XPS results are tabulated in Table 4.5 and the complete set of XPS data can be found in Appendix F.

Table 4.5. XPS results for the steel substrates under the two most stringent test conditions.

| | Sample | Possible Compounds Formed |
|---|---|---|
| | Bright Mild Steel | Fe |
| | Stainless Steel | Fe, Cr, Ni |
| Test Condition 1 | WC-A/CS | Fe, FeO |
| | WC-A/SS | Fe, FeO, Cr, $Cr_2O_3$, $CrO_2$, Ni |
| | WC-B/CS | Fe |
| | WC-B/SS | Fe, FeO, $Cr_2O_3$, $CrO_2$, Ni, $WO_3$ |
| | WC-C/CS | Fe, FeO |
| | WC-C/SS | Fe, FeO, Cr, $Cr_2O_3$, $CrO_2$, Ni |
| Test Condition 4 | WC-A/CS | Fe |
| | WC-A/SS | Fe, Cr, $Cr_2O_3$, $CrO_2$, Ni |
| | WC-B/CS | Fe, FeO, $WO_3$ |
| | WC-B/SS | Fe, FeO, $Cr_2O_3$, $CrO_2$, Ni, $WO_3$ |
| | WC-C/CS | Fe |
| | WC-C/SS | Fe, Cr, $Cr_2O_3$, $CrO_2$, Ni |

The compounds present on the surfaces of the bright mild steel and 304 stainless steel substrates were found to be very similar across the different sliding pairs and test conditions. Iron oxide tends to be more prevalent under test condition 1 than test condition 4. The compound $WO_3$ is observed to be present on the substrate surface for three cases; grade WC-B/SS under test condition 1 and grades WC-B/SS and WC-B/CS under test condition 4. The presence of $WO_3$ indicates material transfer has taken place from the button to the substrate.

*EDS Results*

EDS results for button grade WC-B, tested under test condition 1, is presented in Figure 4.25. The presence of Fe and Cr confirms the transfer of material from the steel substrate to the button during wear.

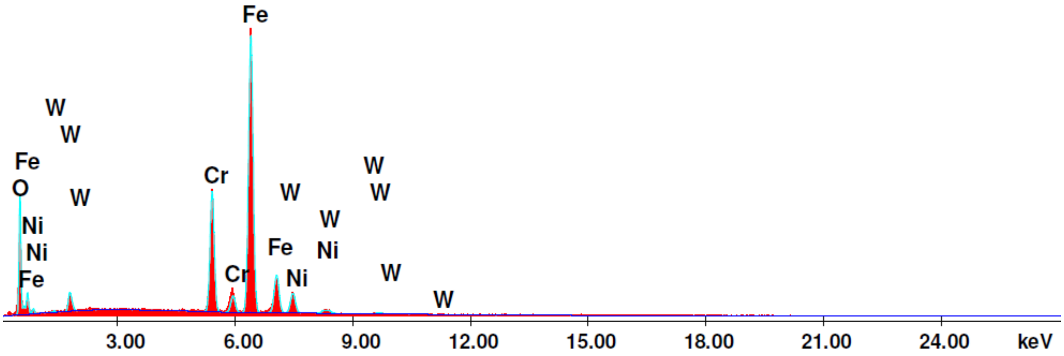


*(a)*

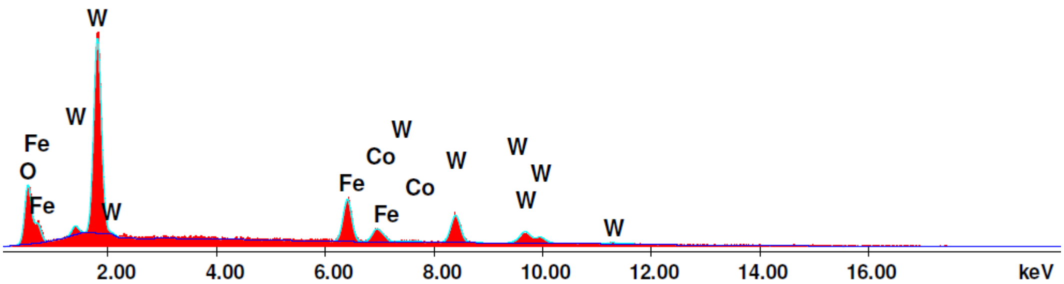


*(b)*

*Figure 4.25. EDS results for (a) WC-B/Stainless steel and (b) WC-B/Mild steel sliding pairs under test condition 1 (5N, 0.2m.s$^{-1}$).*

# Chapter 5

# Discussion

The focus of this project was to systematically investigate the friction and sliding wear characteristics of three grades of WC-Co alloys to which refractory carbides TiC, TaC and NbC were added. The wear behaviour was characterized by sliding the carbide alloys against two grades of steel in a pin-on-disc configuration and determining the associated wear mechanisms. The influence of applied load and sliding velocity on the friction and wear response was also analyzed. In this chapter the results of these characterization tests and analyses are discussed.

### 5.1 Friction response of the cemented carbides

Friction is not a material property but rather a system response [1]. It is influenced by properties of the materials in contact as well as the operating environment. Friction in a sliding system is generally described in terms of the static and kinetic coefficients of friction and it is known that $\mu_s$ is usually higher than $\mu_k$ as the force required to initiate motion is usually larger than the force required to maintain motion [1,4]. In the current project this trend was observed for all the cemented carbide-steel sliding pairs under five different test conditions with three minor exceptions.

The influence of three different applied loads and three different sliding velocities on friction was investigated. According to the Laws of Friction, the frictional forces are proportional to applied load and independent of sliding velocity [1,3,5]. In the investigated sliding systems an increase in load caused a non-linear decrease in friction while an increase in sliding velocity did not have a significant effect. The friction response of the mild steel was at least 50% lower than that of the stainless steel at all loads and speeds tested. Within experimental error the friction response of the button grades was similar for each steel at each load.

Sliding velocity affects the frictional energy dissipation which in turn affects the temperature at the sliding interface [1]. The friction tests were conducted at sliding velocities of 0.1 to 0.3 $m.s^{-1}$. These velocities are considered to be too low to cause a significant increase in the interface temperature. At this speed any heat generated at the interface is expected to be rapidly conducted away. Temperature measurements taken during random tests confirm that the test area remained at room temperature. Although the friction tests were conducted at room temperature, oxides were detected on several steel surfaces using XPS. It is possible that flash temperatures occurred at the higher applied load and speed combinations leading to the formation of the $WO_3$ oxide detected on the 304 stainless steel and occasionally the bright mild steel when sliding against cemented carbide WC-B. The occurrence of hot spots during sliding wear is well known [1]. Unfortunately it is not possible to measure these flash temperatures in the current test system.

The friction response of the cemented carbide/steel sliding pairs under each of the five test conditions can be aligned with one or more of the four hypothetical S-shaped patterns defined by [5] and reviewed in Chapter 2, Section 2.1. Table 5.1 indicates the pattern followed by each of the investigated sliding systems.

Table 5.1. Hypothetical friction patterns [5] followed for each sliding system under each test condition.

| | OP1 (5N, 0.2m.s$^{-1}$) | OP2 (3N, 0.2m.s$^{-1}$) | OP3 (1N, 0.2m.s$^{-1}$) | OP4 (3N, 0.3m.s$^{-1}$) | OP5 (3N, 0.1m.s$^{-1}$) |
|---|---|---|---|---|---|
| WC-A/CS | II | II | II | II | II |
| WC-A/SS | III | III/IV | III/IV | I | II/III |
| WC-B/CS | II | II | II | II | II |
| WC-B/SS | II | III | II | I | II |
| WC-C/CS | II | II | II | II | II |
| WC-C/SS | I | III | II/III | I | II |

Table 5.1 shows that regardless of the button grade, the mild steel paired buttons consistently followed pattern II. Pattern II involves smoothing of the contact surfaces due to plastic deformation which results in a decrease in the contribution of the ploughing component to friction. Any wear debris present on the surface leads to a decrease in the real contact area. The mild steel has a much lower hardness than the cemented carbides and thus easily plastically deforms under the harder material resulting in a lower wear rate for the cemented carbide buttons. The low friction levels and wear rates of the mild steel paired buttons are clearly highlighted in Figures 4.14 to 4.15 and Figures 4.17 to 4.18 respectively.

The stainless steel paired buttons do not follow a specific friction pattern. All except one of the grade WC-A-sliding systems displayed pattern III behavior, while the WC-B grades tended towards pattern II behavior and grade WC-C showed a combination of patterns I, II and III. This extreme variation in friction responses makes the stainless steel sliding systems unpredictable. Patterns III and IV are associated with the constant formation and subsequent expulsion of wear particles during sliding consequently leading to high wear rates. Figures 4.14 to 4.15 and Figures 4.17-4.18 show the distinct increase in friction and wear rates of the stainless steel paired buttons compared to that of the mild steel paired buttons.

With respect to operating conditions, test condition 4 (OP4) showed the mildest friction response and typically followed the more stable I or II friction patterns for all sliding systems. It is believed that these conditions provide enough energy for the initial smoothing, associated with these patterns, to occur thus providing a more stable pattern. Comparing Figure 4.9 to Figure 4.7 clearly illustrates this.

In general the mild steel substrates had a fairly consistent and smooth friction response while the friction behavior of the stainless steel substrates was erratic. The highest friction values, often surpassing the $\mu=1$ mark, were recorded under test condition 3 (OP3 – lowest load) for all three button grades sliding against stainless steel. The lowest kinetic friction values were recorded for button grade WC-B sliding against mild steel under all five test conditions.

### 5.2 Wear response of the cemented carbides

The overall wear resistance of WC-Co alloys is largely dependent on the carbide/binder ratio, the carbide grain size and bulk hardness of the particular carbide [7]. Generally low Co binder concentrations, ultrafine grain sizes (less than 1µm) and a high hardness leads to superior wear resistance [3, 7, 12-13]. It has been shown that the properties of WC-Co can be improved when the hardmetals are alloyed with refractory carbides such as tantalum, columbium, molybdenum, cadmium, titanium vanadium and niobium [2-3]. In the current project three grades of cemented carbides were studied, namely WC-A (WC-6wt%Co), WC-B (WC-5.9wt%Co-0.09wt%TaC-0.01wt%NbC) and WC-C (WC-6wt%Co-2.83wt%TiC-3.47wt%TaC-0.39wt%NbC).

Grade WC-B had the highest hardness which was due to the TaC which acts as a WC grain growth inhibitor when added in amounts of less than 2wt% [14]. Although the carbide grain size was not measured, the high coercivity of this grade as well as visual examination of the microstructure confirms the fineness of the carbide grain size. The straight WC-Co alloy (Grade WC-A) had the lowest hardness as expected. Although Grade WC-C had TaC and TiC its hardness was intermediate between that of grades WC-A and WC-B. In this grade more than 2wt%TaC was added which decreased its effectiveness as a grain growth inhibitor. TiC is harder than WC therefore its addition should have improved the hardness. However the grain size distribution in this grade was wide, possibly due to insufficient milling and hence this grade's hardness was lower than expected. Based on hardness alone Grade WC-B was expected to possess the best wear resistance.

None of the carbide grades contained any deleterious phases such as eta phase as confirmed by XRD and microscopic analysis. The magnetic saturation results were found to be similar for all three grades and confirm the similarity in Co binder content for all three grades. The density for grades WC-A and WC-B were found to be similar to one another and far higher than the high-TiC grade, grade WC-C. The similarity in the saturation values further confirms that the high coercivity value for grade WC-B is due to a fine carbide grain size and not due to a lowering of the Co content by adverse microstructural effects such as eta phase. On this basis the friction and wear properties of the three cemented carbides could be compared objectively.

In the sliding system tested, the cemented carbide buttons were pressed against the steel substrates under an applied load. This configuration places the carbide buttons under a state of compression. It is well established that cemented carbides under compression deform elastically rather than plastically [8]. This has the consequence that the material fractures immediately when the elastic limit has been reached. The loads applied in this project are too low to cause the carbides to reach their elastic limit therefore carbide grain deformation is considered to be predominantly elastic. Fracture of the carbide grains will generally only occur after the cobalt binder is selectively removed during wear. This point is explained further under Section 5.3 where the mechanisms of material removal are discussed. The addition of TiC is known to cause a decrease in the compressive strength of WC-Co alloys as indicated in Figure 2.10 [8]. Hence the level of elastic deformation experienced by grade WC-A is expected to be greater than that of Grade WC-C.

This elastic nature of the cemented carbides as well as alloy hardness under this compressive type of sliding wear configuration influences the depth to which the buttons will indent and wear the steel surfaces. Naturally the hardness of the steels and their elastic/plastic properties play a complimentary role in the material removal process. The role of these properties can be assessed in terms of two ratios defined by Hutchings [1] namely the material's E/H ratio where E is the modulus of elasticity and H is the hardness and the Hwc/Hs ratio where Hwc is the hardness of the button grade and Hs the hardness of the steel surface. Low E/H ratios indicate that materials will tend to wear by the cutting mode of material removal whereas high E/H ratios indicate that wear will proceed predominantly by ploughing of the material. The cutting mode typically causes higher material removal rates than the ploughing mode as plastic deformation is greater under ploughing conditions. The higher the Hwc/Hs ratio, the higher the degree of indentation, which generally leads to higher wear rates. Typically a Hwc/Hs ratio of 1.2 signifies the boundary condition between mild and severe wear as defined by Hutchings [1]. Tables 5.2 and 5.3 lists the respective ratios for each of the materials and sliding pairs.

Table 5.2. E/H ratios for the experimental materials.

| Sample | Young's Modulus [GPa] | Hardness [$HV_{30}$] | E/H |
|---|---|---|---|
| WC-A | 649 | 1420 | 0.46 |
| WC-B | 644 | 1915 | 0.34 |
| WC-C | 604 | 1604 | 0.38 |
| 304 Stainless Steel | 197 | 262 | 0.75 |
| Bright Mild Steel | 213 | 184 | 1.16 |

Table 5.3. Vickers Hardness (Hwc/Hs) ratios for the investigated sliding pairs.

| WC-A/SS | WC-A/CS | WC-B/SS | WC-B/CS | WC-C/SS | WC-C/CS |
|---|---|---|---|---|---|
| 5.4 | 7.7 | 7.3 | 10.4 | 6.1 | 8.7 |

Based on the E/H ratios it is expected that the stainless steel substrates should experience more cutting than ploughing compared to the mild steel substrates and hence have higher wear rates than the mild steel substrates. However based on the Hwc/Hs ratios the mild steel should experience more severe wear than the stainless steel. The Hwc/Hs ratios far exceed the 1.2 boundary condition defined earlier and therefore all the investigated sliding systems should be termed 'severe wear' systems.

In the current project the maximum penetration depths (refer to Figure 4.11) for the different button grade/steel pairs under the different test conditions were generally similar and averaged between 1.6μm and 1.9μm with the exception of isolated cases even though the Hwc/Hs ratios were very different for each sliding pair. However the stainless steels generally had wider wear track widths compared to those on the mild steels as evidenced by the SEM images shown in Chapter 4 and in Appendix E. The variation in applied load and sliding velocity also influenced the wear track widths of the steels. The five test conditions in which the applied load and sliding velocity were varied could be ranked in terms of which condition provided the widest track width. Despite minor differences in the ranking order it was found that the highest applied load produced the widest wear track width and the lowest applied load the narrowest width.

Based on this experimental evidence it is clear that the E/H ratios are more accurate in predicting the wear response of the steel substrates in the investigated sliding systems. The role of the Hwc/Hs ratios cannot be discredited as these ratios did predict severe wear damage to the surfaces and this is confirmed by the SEM analysis. The E/H ratios of the cemented carbides indicate that the WC-B grades which have the lowest E/H ratio should have more cutting than ploughing wear mechanisms than the other two button grades, while grade WC-A which has the highest E/H ratio should show more ploughing than cutting. From the SEM analysis (refer to Appendix E) this was found to be true in the investigated sliding systems. Smearing indicative of ploughing and cracks/grooves indicative of cutting are visible on the wear scars of the buttons. Based on these E/H ratios alone it is expected that grade WC-B would have the highest wear rate and grade WC-A the lowest. However experimental evidence showed that button grade WC-B has the lowest wear rate while the wear rates for grades WC-A and WC-C are similar. Grade WC-B has the highest hardness and it appears that this property plays a more significant role in predicting the wear response of the carbide buttons in the investigated system than the E/H ratios.

The wear rates of the materials were defined by the dimensional wear coefficient, k, which is based on the volume of material lost during wear, the applied load and the material hardness. Sliding pairs which displayed high friction values were found to have high wear coefficients which translated into high wear rates. With respect to applied load the wear coefficients showed a minimum at a load of 3N for all the stainless steel sliding pairs and the WC-A/mild steel sliding pair. However the WC-B/mild steel and WC-C/mild steel sliding pairs showed a decrease in wear rate as the load was increased. The applied load directly influences the stress experienced by the steel. For each sliding pair under each test condition the applied stress was calculated using the applied force and the geometry of the wear scar generated on the button grade and the results are listed in Table 5.4.

Table 5.4. Applied stress [MPa] experienced during wear by each sliding pair.

| | OP1 (5N, 0.2m.s$^{-1}$) | OP2 (3N, 0.2m.s$^{-1}$) | OP3 (1N, 0.2m.s$^{-1}$) | OP4 (3N, 0.3m.s$^{-1}$) | OP5 (3N, 0.1m.s$^{-1}$) |
|---|---|---|---|---|---|
| WC-A/CS | 7.61 | 5.56 | 2.54 | 4.22 | 7.61 |
| WC-A/SS | 4.16 | 3.46 | 1.67 | 2.51 | 3.92 |
| WC-B/CS | 9.23 | 8.45 | 2.53 | 5.37 | 5.94 |
| WC-B/SS | 5.32 | 4.41 | 2.01 | 2.51 | 5.50 |
| WC-C/CS | 6.40 | 4.09 | 2.33 | 3.87 | 5.90 |
| WC-C/SS | 3.57 | 3.56 | 1.94 | 2.56 | 4.56 |

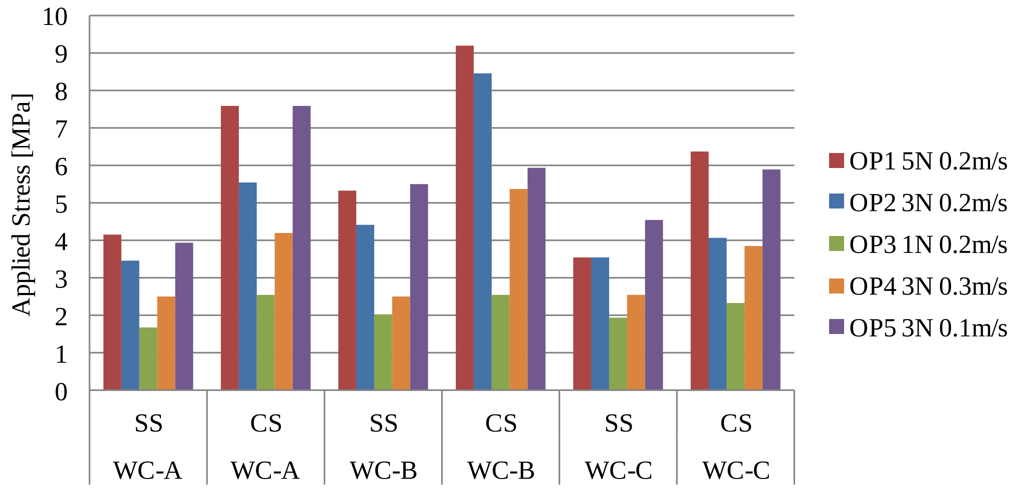


*Figure 5.1. Applied stress [MPa] experienced during wear by each sliding pair.*

The applied stress data follows the logical trend of increasing stress associated with an increase in applied load, except for sliding system WC-C/SS where the stress is similar at 5N and 3N. With this trend it is expected that the highest stress should cause the most mechanical damage to the surface leading to high wear rates. However based on the data for the wear coefficients this trend was generally not followed indicating that the role of the applied load in determining the wear rates is not significant for the investigated system. This is further evidenced by the fact that the stainless steels had higher wear rates than the mild steels yet the applied stress experienced by the stainless steels is far lower than that experienced by the mild steel. From SEM analysis (refer to Appendix E) the stainless steels had wider wear track widths than the mild steels leading to a greater surface area for the distribution of the applied load and hence the lower stress values.

With respect to sliding velocity there appeared to be a general trend of a sharp increase in wear when the velocity was increased from 0.1 to 0.2 $m.s^{-1}$ after which the wear levelled off as the velocity was increased to 0.3 $m.s^{-1}$. There were two exceptions to this trend. The WC-C-mild steel sliding pair showed a decrease in wear as the speed increased from 0.2 to 0.3 $m.s^{-1}$. The stainless steel-WC-B sliding pair showed an increase in wear as the velocity increased from 0.1 to 0.3 $m.s^{-1}$. When considering the stress experienced at the various sliding speeds a general trend of decreasing stress with an increase in speed was observed. These results are in accordance with the wear track widths which increased in width as the speed increased. The wider tracks led to increased material removal as confirmed by the calculated wear coefficients.

In general the WC-B button grades have the lowest wear rates against both steels tested which aligns with its high hardness.  These results illustrate the extrinsic nature of wear described in Chapter 2. The wear behaviour of a material is very dependent on the operating conditions as well the material properties of the surfaces in dynamic contact. The interaction between these parameters will determine the wear characteristics of the system.

### 5.3 Mechanisms of wear

Several mechanisms have been proposed to explain how sliding wear operates. Although the specific details of material removal differ for each sliding system, plastic deformation has been shown to be the main mechanism of wear [1]. Shearing of the asperities on the interfaces and possible subsequent adhesion of these fragments onto one or both of the surfaces as well as ploughing and smearing of the interfaces are primary mechanisms by which plastic deformation occurs during sliding wear [1,7]. Combinations of these mechanisms were observed for all the sliding pairs under all test conditions.

The wear mechanisms of the cemented carbide and steel substrates are largely attributed to a combination of adhesive and abrasive forces. The extent of damage was found to depend on the interaction between the inherent properties (e.g. hardness) of the materials in contact, the level of mechanical stress exerted under the applied load, the sliding velocity and oxide formation. These factors are interrelated and are influenced by changes in the sliding condition parameters such as the normal load, sliding velocity and often the sliding time or distance [1].

The wear mechanisms for the 304 stainless steel and bright mild steel substrates were predominantly smearing and groove formation caused by ploughing of the wear particles. Grooving is initially caused by the initial deformation of asperities on the contact surfaces. Subsequent grooving is caused by abrasive wear by particles of wear debris. Low magnification SEM images of the wear tracks revealed rough surfaces which had significant amounts of loose and adhered wear debris as well as scratches and grooves parallel to the sliding direction. Extensive plastic deformation was particularly prevalent on the 304 stainless steel substrate when paired with the hardest cemented carbide, WC-B. SEM images of this wear track indicated severe smearing with ribbon-like fragments of steel peeling off. This severe plastic deformation is characteristic of sliding wear [1]. The XPS results indicated that the 304 stainless steel substrates had approximately 30% more oxides present on their worn surfaces than the mild steel substrates at the highest test load. At the highest sliding velocity the level of oxides present were approximately 60% higher. The oxides provide low shear strength at the sliding interface thereby reducing friction due to limited metallic contact consequently reducing wear.

The predominant wear mechanisms for the cemented carbides were preferential binder removal, followed by carbide grain cracking and carbide grain pull-out, similar to that found by other authors [7, 18]. The initial increase in the friction which was observed in all the wear tests provides the energy required to initiate the binder removal and micro-cracking [18]. Occasional grooving of the cemented carbide matrix was also observed. This is believed to be caused by hard carbide grains which have been extracted from the matrix and subsequently act as abrasive particles as sliding continues. The presence of Fe and Cr on the carbide wear scars confirm that transfer of material from the steel substrate to the button occurred during wear. The level of material transfer was generally higher along the outer edges of the wear scar with limited material transfer in the central region of the wear scar. The high amount of transferred material at the edges was likely wear debris that has been ploughed to the edges as sliding proceeded. This indicates that the adhesive forces between the steel substrates and the carbides are low.

WC grains are generally resistant to brittle fracture due to the inherent compressive stress state which arises during the cooling down period after sintering. Upon cooling the binder cools down at a faster rate than the carbide thus causing the binder to be under a tensile stress state and the carbide to go into compression. During wear the WC grains eventually lose this compressive stressed state as the surrounding binder keeping it in that state is removed plastically. This initiates fracture within the carbide grains due to stress relief and facilitates the carbide grain removal [18]. The carbide grains that are removed as well as the smeared cobalt binder eventually leave the system as wear particles.

SEM images of several worn button surfaces indicated the presence of tribofilms. A tribofilm typically consists of the extruded binder phase and some of the fractured carbide phase.  Larson-Basse [18] concluded that cobalt extraction occurs initially ahead and adjacent to the direct load that is applied and that the binder is squeezed out from between the WC grains which deforms very little and accumulates on the surface. This accumulated binder is continuously smeared between the interfaces along with fragmented carbide grains. In some cases the tribofilm has been shown to protect the surface from further damage [7] and in the present work the presence of these tribofilms may account for the low wear rates achieved.

### 5.4. Tribometer set-up and experimental error

The tribometer is extremely sensitive to the contact surface gradient that exists between the pin and the disk. This gradient is required to be 0% and the slightest deviation will negatively influence the test data. This criterion posed a challenge in the current work as the steel substrates used as the disk in the system needed to be polished to a 1 micron surface finish and with the available polishing systems it was often difficult to maintain a level test surface. This may have caused slight fluctuations in the friction data shown in Figures 4.6 to 4.10.

An area which is prone to error is that of the measurement of the wear track and wear scar on the substrate and button respectively. This was done with the aid of a high magnification microscope used to capture images of the worn surfaces followed by manually measuring the required dimensions. This type of measurement is subject to human error in terms of deciding where the edges of the features were. Small measurement errors here could pose difficulties in highlighting differences between materials displaying similar friction and wear properties.

# Chapter 6

# Conclusions

The friction and sliding wear characteristics of three WC-Co alloys to which refractory metals, TiC, TaC and NbC have been added was systematically investigated. The influence of applied load and sliding velocity on wear and friction was also analyzed.

With increasing sliding distance the mild steel substrates had a fairly consistent and smooth friction response while the friction behavior of the stainless steel substrates was erratic. An increase in load caused a non-linear decrease in friction while an increase in sliding velocity did not have a significant effect. The friction response of the three alloys were found to be similar with the most significant conclusion being that the stainless steel sliding pairs experienced 50% more friction than the bright mild steel sliding pairs under both increasing applied load and sliding velocity.

Sliding pairs which displayed high friction values were found to have high wear coefficients which translated into high wear rates. The WC-Co alloy to which small amounts of TaC and NbC were added, i.e. grade WC-B, was found to be the most effective in increasing the sliding wear resistance of the alloys under all the operating conditions tested. This aligns with its high hardness. The wear response of grades WC-A and WC-C were found to be comparable.

The wear mechanisms for the 304 stainless steel and bright mild steel substrates were predominantly smearing and groove formation caused by ploughing of the wear particles. The predominant wear mechanisms for the cemented carbides were preferential binder removal, followed by carbide grain cracking and carbide grain pull-out with the occasional tribofilm.

## 6.1 Recommendations

### 6.1.1 Application

Cemented carbides such as that of Grade WC-B would be best applied to sliding wear applications where the corresponding sliding surface is carbon steel. This will minimise tool wear and increase tool life. Grade WC-B operates favourably over a range of applied loads and sliding speeds however low load and low sliding speed applications would contribute to even lower wear being experienced.

### 6.1.2 Future Research

- The cemented carbide grades that were tested showed a much higher sliding wear resistance when matched with carbon steel than that of stainless steel. It would be of interest to see what refractory metals, if any, could be added to WC-Co to improve the cemented carbide's sliding wear resistance when matched with stainless steel. Would it ever be improved to a level that equally matches that of carbon steel?

- Limited information is available on the effect that adding various refractory metals simultaneously to a cemented carbide has on the wear resistance of cemented carbides. Testing different combinations of refractory metals and different compositions would broaden the current knowledge base. To what degree can refractory metals enhance sliding wear properties of cemented carbides?

# References


1. I.M. Hutchings, *Tribology: Friction and Wear of Engineering Materials*, Edward Arnold, 1992, London.
2. J. Weidow, J. Zackrisson, B. Jansson, H-O. Andren, *Characterization of WC-Co with cubic carbide additions*, Int. Journal of Refractory Metals & Hard Materials, 2009, 27: 244-248.
3. K.G. Budinski, M.K. Budinski, *Engineering Materials, Properties and Selection*, 7$^{th}$ Edition, Prentice Hall, 2002, Upper Saddle River, New Jersey Columbus, Ohio.
4. H.D. Young, R.A. Freedman, T.R. Sandin, A. Lewis Ford, Sears *and Zemansky's University Physics*, 10$^{th}$ Edition, Addison Wesley Longman Inc. , 2000, San Francisco.
5. B. Bhushan, *Introduction to Tribology*, John Wiley & Sons Inc., 2002, New York.
6. E. Rabinowicz, *The effect of size on the looseness of wear fragments*, Wear, 1958/59, 2, 4-8.
7. Jüri Pirso, Mart Viljus, Sergei Letunovitš, *Friction and dry sliding wear behaviour of cermets*, Wear, 2006, 260: 815–824.
8. E. Isakov, *Cutting data for turning of steel*, Industrial Press Inc., 2009, New York, USA.
9. A. Mortensen, *Concise encyclopedia of composite materials- Second Edition*, Elsevier, 2007, Oxford, UK.
10. G.S. Upadhyaya, *Materials science of cemented carbides - an overview*, Materials and Design, 2001, 22: 483 – 489.

11. George S Brady, Henry R Clauser, John A Vaccari, Materials Handbook 15th Edition, McGraw-Hill, 2002, New York.
12. K. Bonny, P. De Baets, J. Vleugels, S. Huang, O. Van der Biest, B. Lauwers, *Impact of Cr3C2/VC addition on the dry sliding friction and wear response of WC–Co cemented carbides*, Wear, 2009, 267: 1642–1652.
13. Hiroyuki Saito, Akira Iwabuchi, Tomoharu Shimizu, *Effects of Co content and WC grain size on wear of WC cemented carbide,* Wear, 2006, 261: 126–132.
14. KJA Brookes, *Hardmetals and other hard materials*, 3rd Edition, International Carbide Data, BPC Digital Information Limited, 1998, Exeter, UK.
15. M. Mahmoodan, H. Aliakbarzadeh, R. Gholamipour, *Microstructural and mechanical characterization of high energy ball milled and sintered WC–10 wt%Co–xTaC nano powders,* International Journal of Refractory Metals and Hard Materials, 2009, 27: 801-805.
16. D. Xiao, Y. He, W. Luo, M. Son, *Effect of VC and NbC additions on microstructure and properties of ultrafine WC-10Co cemented carbides,* Transactions of Nonferrous Metals Society of China, 2009, 19: 1520-1525.
17. K. Bonny, P. De Baets, Y. Perez, J. Vleugels, B. Lauwers, *Friction and wear characteristics of WC-Co cemented carbides in dry reciprocating sliding contact*, Wear, 2010, 268: 1504–1517.
18. Jorn Larsen-Basse, *Binder extrusion in sliding wear of WC-Co alloys*, Wear, 1985, 105: 247 – 256.
19. D.K. Shetty, I.G. Wright, P.N. Mincer, A.H. Clauer, *Indentation fracture of WC-Co cermets*, Journal of Materials Science, 1985, 20: 1873-1882.
20. H. E. Exner, *The influence of Sample Preparation on Palmqvist's Method for Toughness Testing of Cemented Carbides,* Transactions of the Metallurgical Society of AIME, 1969, 245:677.

21. Tungsten carbide and tungsten carbide components by Federal Carbide Company. INTERNET.
http://www.federalcarbide.com/cemented_tungsten_carbide.html.
Cited 26 March 2011.
22. Gopal S. Upadyaya, *Cemented Tungsten Carbides Production, Properties and Testing*, Noyes Publications, 1998, Westwood, New Jersey, USA.
23. L. E. Kinsler, A.R. Frey, A.B. Coppens, J. V. Saunders, *Fundamentals of acoustics*, 4th Edition, John Wiley and sons Inc., 2000, New York, USA.

# Appendix A

## Hardness Test Data

A.1

The Vickers hardness was calculated using equation A.1.

$$HV = \frac{F}{A}$$

$$HV = \frac{2 \times F \times (\sin\theta)}{d^2}$$

$$HV = \frac{1.854F}{d^2} \qquad [\text{kg/(mm)}^2] \qquad (A.1)$$

A.2

The tabulated individual results for the first set of Vickers hardness testing on the bright mild steel and the 304 stainless steel is given in Tables A.1 and A.2 respectively. These tests were performed using a load of 20kg.

Table A.1. Vickers hardness tests results for bright mild steel.

| Test # | $d_1$ [µm] | $d_2$ [µm] | d [µm] | HV |
|---|---|---|---|---|
| 1 | 448 | 449 | 448.5 | 184.34 |
| 2 | 446 | 445 | 445.5 | 186.83 |
| 3 | 454 | 448 | 451 | 182.30 |
| Average | | | | 184 |
| Standard Deviation | | | | ±1.92 |

Table A.2. Vickers hardness tests results for 304 stainless steel.

| Test # | $d_1$ [µm] | $d_2$ [µm] | d [µm] | HV |
|---|---|---|---|---|
| 1 | 386 | 386 | 386 | 248.87 |
| 2 | 378 | 375 | 376.5 | 261.58 |
| 3 | 377 | 372 | 374.5 | 264.38 |
| Average | | | | 258 |
| Standard Deviation | | | | ±6.75 |

The individual results for the Vickers hardness testing on the carbide buttons are provided in Tables A.3 to A.5. The average values of these tests were used to determine the average Vickers hardness of the buttons reflected in Table 4.1. These tests were performed using a load of 30kg.

Table A.3. Vickers hardness tests results for button grade WC-A.

| Test # | $d_1$ [µm] | $d_2$ [µm] | d [µm] | HV |
|---|---|---|---|---|
| 1 | 199 | 198 | 198.5 | 1411.59 |
| 2 | 196 | 199 | 197.5 | 1425.93 |
| 3 | 197.5 | 201 | 199.25 | 1400.99 |
| 4 | 197 | 198 | 197.5 | 1425.96 |
| 5 | 196 | 198 | 197 | 1433.17 |
| Average | | | | 1420 |
| Standard Deviation | | | | ±11.01 |

Table A.4. Vickers hardness tests results for button grade WC-B.

| Test # | $d_1$ [µm] | $d_2$ [µm] | d [µm] | HV |
|---|---|---|---|---|
| 1 | 166 | 164 | 165 | 2042.98 |
| 2 | 172 | 172 | 172 | 1880.07 |
| 3 | 170 | 173 | 171.5 | 1891.05 |
| 4 | 171 | 173 | 172 | 1880.07 |
| 5 | 170 | 174 | 172 | 1880.07 |
| Average | | | | 1915 |
| Standard Deviation | | | | ±64.2 |

Table A.5. Vickers hardness tests results for button grade WC-C.

| Test # | $d_1$ [µm] | $d_2$ [µm] | d [µm] | HV |
|---|---|---|---|---|
| 1 | 183 | 187 | 185 | 1625.13 |
| 2 | 185 | 187 | 186 | 1607.70 |
| 3 | 184 | 189 | 186.5 | 1599.09 |
| 4 | 184 | 190 | 187 | 1590.55 |
| 5 | 183 | 190 | 186.5 | 1599.09 |
| Average | | | | 1604 |
| Standard Deviation | | | | ±11.7 |

# Appendix B

## Fracture Toughness Data

B.1

As stated in Section 3.1.4, equation 3.2 was used to calculate the fracture toughness, $K_{IC}$, of the carbide buttons.

$$K_{IC} = A_1 \sqrt{\frac{HV \times P}{\sum_1^4 a}} \tag{3.2}$$

Where $A_1 = 887 \times 10^{-7}$

HV = Vickers Hardness [MPa]

P = Indentation Load [N]

a = Mean radial crack length [m], defined by equation B.1

$$a = \frac{C_{av} - d}{2} \times 10^{-6} \tag{B.1}$$

Where $C_{av}$ = Averaged crack length [µm].

d = averaged Vickers indentation diagonal length [µm].

B.2

Palmqvist cracks were observed after the buttons had undergone sufficient polishing to relieve the surface residual stresses. Five indentations were made per button grade from which the average was calculated. The indentation load used for the buttons was 30kg (294 N). Tables B1 to B3 provide the measured data. The averaged results are shown in Table 4.2.

Table B.1. Fracture toughness data: Grade WC-A.

| | d [μm] | $C_1$ [μm] | $C_2$ [μm] | $C_{av}$ [μm] | a [μm] | HV [MPa] | HV [GPa] | $K_{IC}$ [MPa.m$^{0.5}$] |
|---|---|---|---|---|---|---|---|---|
| 1 | 202.50 | 249.00 | 259.00 | 254.00 | 25.75 | 13302.00 | 13.30 | 17.29 |
| 2 | 200.00 | 238.00 | 232.00 | 235.00 | 17.50 | 13636.63 | 13.64 | 21.24 |
| 3 | 200.00 | 236.00 | 267.00 | 251.50 | 25.75 | 13636.63 | 13.64 | 17.51 |
| 4 | 201.00 | 246.00 | 248.00 | 247.00 | 23.00 | 13501.28 | 13.50 | 18.43 |
| 5 | 200.50 | 251.00 | 261.00 | 256.00 | 27.75 | 13568.71 | 13.57 | 16.82 |
| Average | | | | | | | | 18.26 |
| Standard Deviation | | | | | | | | ±1.58 |

Table B.2. Fracture toughness data: Grade WC-B.

| | d [μm] | $C_1$ [μm] | $C_2$ [μm] | $C_{av}$ [μm] | a [μm] | HV [MPa] | HV [GPa] | $K_{IC}$ [MPa.m$^{0.5}$] |
|---|---|---|---|---|---|---|---|---|
| 1 | 179.00 | 394.00 | 380.00 | 387.00 | 104.00 | 17023.98 | 17.02 | 9.73 |
| 2 | 177.00 | 390.00 | 363.00 | 376.50 | 99.75 | 17410.88 | 17.41 | 10.05 |
| 3 | 177.00 | 358.00 | 366.00 | 362.00 | 92.50 | 17410.88 | 17.41 | 10.44 |
| 4 | 177.00 | 365.00 | 388.00 | 376.50 | 99.75 | 17410.88 | 17.41 | 10.05 |
| 5 | 176.50 | 390.00 | 354.00 | 372.00 | 97.75 | 17509.61 | 17.51 | 10.18 |
| Average | | | | | | | | 10.09 |
| Standard Deviation | | | | | | | | ±0.23 |

Table B.3. Fracture toughness data: Grade WC-C.

| | d [μm] | $C_1$ [μm] | $C_2$ [μm] | $C_{av}$ [μm] | a [μm] | HV [MPa] | HV [GPa] | $K_{IC}$ [MPa.m$^{0.5}$] |
|---|---|---|---|---|---|---|---|---|
| 1 | 191.50 | 338.00 | 303.00 | 320.50 | 64.50 | 14874.06 | 14.87 | 11.55 |
| 2 | 153.00 | 226.00 | 214.00 | 220.00 | 33.50 | 23301.52 | 23.30 | 20.06 |
| 3 | 172.50 | 261.00 | 261.00 | 261.00 | 44.25 | 18331.12 | 18.33 | 15.48 |
| 4 | 161.50 | 258.00 | 263.00 | 260.50 | 49.50 | 20913.28 | 20.91 | 15.64 |
| 5 | 154.00 | 228.00 | 228.00 | 228.00 | 37.00 | 22999.89 | 23.00 | 18.97 |
| Average | | | | | | | | 16.34 |
| Standard Deviation | | | | | | | | ±3.00 |

# Appendix C

## Density and Porosity Data

C.1

The density of the steels and the button grades were calculated using equation 3.3 from Section 3.1.5 according to Archimedes principle.

$$\rho_s = \rho_w \times \frac{M_a}{M_{wt} - M_w} \qquad (3.3)$$

Where: $\rho_s$ = density of the specimen

$\rho_w$ = density of water

$M_a$ = mass of specimen in air

$M_w$ = mass of specimen in water

$M_{wt}$ = wet mass of specimen

As indicated in Section 3.1.5, the porosity of the steels and the button grades were calculated using equation 3.4.

$$Porosity = \frac{M_{wt} - M_a}{M_{wt} - M_w} \times 100 \qquad (3.4)$$

C.2

The raw data used to calculate the density and porosity for both the steels and the button grades are listed in Tables C.1 to C.5.

Table C.1. Data used to calculate density of Bright Mild Steel.

| Measurements | Mass of specimen in water (g) | Wet mass of specimen (g) | Mass of specimen in air (g) | Density [g/cm$^3$] | Porosity % |
|---|---|---|---|---|---|
| 1 | 11.0386 | 12.6497 | | | |
| 2 | 11.0365 | 12.6496 | | | |
| 3 | 11.0378 | 12.6494 | | | |
| 4 | 11.0375 | 12.6492 | | | |
| 5 | 11.0363 | 12.6493 | | | |
| Average | 11.03734 | 12.64944 | 12.6489 | 7.8462 | 0.0335 |

Table C.2. Data used to calculate density of 304 Stainless Steel.

| Measurements | Mass of specimen in water (g) | Wet mass of specimen (g) | Mass of specimen in air (g) | Density [g/cm$^3$] | Porosity % |
|---|---|---|---|---|---|
| 1 | 11.2862 | 12.9316 | | | |
| 2 | 11.2911 | 12.9314 | | | |
| 3 | 11.289 | 12.9314 | | | |
| 4 | 11.2754 | 12.9315 | | | |
| 5 | 11.2934 | 12.9314 | | | |
| Average | 11.28702 | 12.93146 | 12.931 | 7.8635 | 0.0280 |

Table C.3. Data used to calculate density of button grade WC-A.

| Measurements | Mass of specimen in water (g) | Wet mass of specimen (g) | Mass of specimen in air (g) | Density [g/cm$^3$] | Porosity % |
|---|---|---|---|---|---|
| 1 | 10.6238 | 11.3889 | | | |
| 2 | 10.6259 | 11.3886 | | | |
| 3 | 10.6191 | 11.3884 | | | |
| 4 | 10.6228 | 11.3880 | | | |
| 5 | 10.6200 | 11.3883 | | | |
| Average | 10.62232 | 11.38844 | 11.3882 | 14.8648 | 0.0313 |

Table C.4. Data used to calculate density of button grade WC-B.

| Measurements | Mass of specimen in water (g) | Wet mass of specimen (g) | Mass of specimen in air (g) | Density [g/cm$^3$] | Porosity % |
|---|---|---|---|---|---|
| 1 | 10.5105 | 11.2618 | | | |
| 2 | 10.5121 | 11.2614 | | | |
| 3 | 10.5075 | 11.2617 | | | |
| 4 | 10.5078 | 11.2619 | | | |
| 5 | 10.5091 | 11.2618 | | | |
| Average | 10.5094 | 11.26172 | 11.2617 | 14.9693 | 0.0027 |

Table C.5. Data used to calculate density of button grade WC-C.

| Measurements | Mass of specimen in water (g) | Wet mass of specimen (g) | Mass of specimen in air (g) | Density [g/cm$^3$] | Porosity % |
|---|---|---|---|---|---|
| 1 | 9.9964 | 10.754 | | | |
| 2 | 9.9965 | 10.7535 | | | |
| 3 | 9.9944 | 10.7538 | | | |
| 4 | 9.9922 | 10.7535 | | | |
| 5 | 9.9963 | 10.7536 | | | |
| Average | 9.99516 | 10.75368 | 10.7535 | 14.1770 | 0.0237 |

# Appendix D

## Sliding Wear and Friction Test Data

D.1

The derivations of the equations used to determine the worn substrate and button volumes used in calculating the wear rates given in Section 3.2 by equations 3.10 and 3.11 respectively are given below.

*Wear volume of substrate, $V_S$*

$$V_s = \frac{Area\ of\ Ellipse}{2} \times Circumference\ of\ Wear\ Track \qquad (D.1)$$

Where

$$Area\ of\ Ellipse = \frac{Major\ Axis\ \times Minor\ Axis \times \pi}{2} \qquad (D.2)$$

$$= \frac{\frac{D_M}{2} \times P_d \times \pi}{2} \qquad (D.3)$$

And

$$Circumference\ of\ Wear\ Track = 2 \times \pi \times R_M \qquad (D.4)$$

Thus,

$$V_s = \pi^2 \times \frac{D_M}{2} \times P_{dmax} \times R_M \qquad (3.10)$$

*Wear volume of button, $V_b$*

Mathematically the volume of a spherical segment is given as follows:

$$V_{Spherical\ Segment} = \frac{1}{6} \times \pi \times h \times (3 \times a^2 + 3 \times b^2 + h^2) \qquad (D.5)$$

Where a, b, and h are the lower base radius, the upper base radius and the segment height respectively, as shown in Figure D.1.

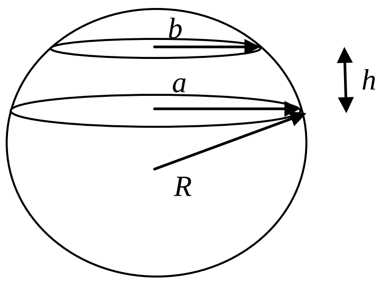


*Figure D.1. Sketch showing parameters, a, b, h and R of a spherical segment.*

For a spherical cap, $b = 0$

Thus,

$$V_{Cap} = \frac{1}{6} \times \pi \times h \times (3 \times a^2 + h^2) \quad \text{(D.6)}$$

From Pythagoras's Theorem:

$$R^2 = a^2 + (R - h)^2 \quad \text{(D.7)}$$

Rearranging:

$$a^2 = 2Rh - h^2 \quad \text{(D.8)}$$

Substituting this into formula D.6 yields:

$$V_{Cap} = \frac{1}{6} \times \pi \times h \times (6Rh - 2h^2) \quad \text{(D.9)}$$

$$= \pi \times Rh^2 - \frac{1}{3} \times \pi \times h^3 \quad \text{(D.10)}$$

$$= \frac{1}{3} \times \pi \times h^2 \,(3R - h^2) \quad \text{(D.11)}$$

For the current project R = $R_b$:

$$V_b = \frac{1}{3} \times \pi \times h^2 \times (3 \times R_b - h) \quad \text{(3.11)}$$

D.2

The complete sliding wear and friction test data for all the button-substrate pairs under the five operating conditions are given in Tables D.1 to D.5.

Table D.1. Sliding wear and friction test results for Test Condition 1[1].

| Sample pairs | | | μ | $D_M$ | $P_d$ | $A_S$ | $V_S$ ($x10^4$) | **$k_s$ ($x10^{-6}$)** | $A_B$ | $D_B$ | h | $V_B$ ($x10^4$) | **$k_B$ ($x10^{-6}$)** |
|---|---|---|---|---|---|---|---|---|---|---|---|---|---|
| **Test 1** | WC-A | SS | 0.69 | 1345.10 | 2.06 | 2178.26 | 6750.21 | 45.00 | 1158750.00 | 754.10 | 15.48 | 345.86 | 2.31 |
| | WC-A | CS | 0.42 | 835.60 | 1.77 | 1164.78 | 3542.45 | 23.62 | 685071.90 | 509.50 | 7.06 | 71.98 | 0.48 |
| | WC-B | SS | 0.77 | 815.20 | 1.69 | 1080.47 | 3279.13 | 21.86 | 751621.70 | 489.10 | 6.51 | 61.12 | 0.41 |
| | WC-B | CS | 0.19 | 652.10 | 1.76 | 899.81 | 2684.73 | 17.90 | 471068.40 | 387.20 | 4.08 | 24.00 | 0.16 |
| | WC-C | SS | 0.49 | 1324.70 | 1.84 | 1918.09 | 5710.65 | 38.07 | 1437998.40 | 774.50 | 16.33 | 384.88 | 2.57 |
| | WC-C | CS | 0.26 | 774.50 | 1.64 | 997.22 | 2988.15 | 19.92 | 751621.70 | 489.10 | 6.51 | 61.12 | 0.41 |
| **Test 2** | WC-A | SS | 0.59 | 1426.60 | 1.91 | 2137.12 | 6540.61 | 43.60 | 1323167.40 | 794.80 | 17.20 | 426.90 | 2.85 |
| | WC-A | CS | 0.29 | 774.40 | 1.59 | 966.73 | 2971.04 | 19.81 | 540228.10 | 468.80 | 5.98 | 51.59 | 0.34 |
| | WC-B | SS | 0.71 | 937.50 | 1.85 | 1359.34 | 4160.27 | 27.74 | 913429.10 | 570.70 | 8.86 | 113.34 | 0.76 |
| | WC-B | CS | 0.28 | 591.00 | 1.85 | 858.01 | 2587.48 | 17.25 | 631571.00 | 448.40 | 5.47 | 43.17 | 0.29 |
| | WC-C | SS | 0.60 | 1365.50 | 2.64 | 2826.94 | 8633.77 | 57.56 | 1424949.40 | 794.80 | 17.20 | 426.90 | 2.85 |
| | WC-C | CS | 0.30 | 733.70 | 1.73 | 999.07 | 3108.83 | 20.73 | 751621.70 | 489.10 | 6.51 | 61.12 | 0.41 |
| **Test 3** | WC-A | SS | 0.67 | 1283.90 | 1.42 | 1432.84 | 4357.66 | 29.05 | 1127432.50 | 733.70 | 14.65 | 309.89 | 2.07 |
| | WC-A | CS | 0.35 | 774.40 | 1.65 | 1005.48 | 3103.02 | 20.69 | 746402.10 | 487.00 | 6.45 | 60.08 | 0.40 |
| | WC-B | SS | 0.66 | 1202.40 | 1.97 | 1857.89 | 5602.80 | 37.35 | 1153530.50 | 692.90 | 13.07 | 246.44 | 1.64 |
| | WC-B | CS | 0.21 | 692.90 | 1.69 | 921.52 | 2749.51 | 18.33 | 521959.50 | 407.60 | 4.52 | 29.47 | 0.20 |
| | WC-C | SS | 0.59 | 1345.10 | 3.69 | 3893.46 | 11915.98 | 79.44 | 1338826.10 | 774.50 | 16.33 | 384.88 | 2.57 |
| | WC-C | CS | 0.39 | 896.90 | 1.79 | 1264.10 | 3820.24 | 25.47 | 815561.70 | 509.50 | 7.06 | 71.98 | 0.48 |

Table D.2. Sliding wear and friction test results for Test Condition 2[1].

| Sample pairs | | | μ | $D_M$ | $P_d$ | $A_S$ | $V_S$ ($x10^4$) | **$k_s$ ($x10^{-6}$)** | $A_B$ | $D_B$ | h | $V_B$ ($x10^4$) | **$k_B$ ($x10^{-6}$)** |
|---|---|---|---|---|---|---|---|---|---|---|---|---|---|
| **Test 1** | WC-A | SS | 0.74 | 978.20 | 1.70 | 1308.80 | 4022.32 | 44.69 | 794683.40 | 591.00 | 9.50 | 130.36 | 1.45 |
| | WC-A | CS | 0.43 | 652.20 | 1.61 | 827.22 | 2563.48 | 28.48 | 521959.50 | 407.60 | 4.52 | 29.47 | 0.33 |
| | WC-B | SS | 0.81 | 652.20 | 1.89 | 966.42 | 2970.10 | 33.00 | 690291.40 | 468.80 | 5.98 | 51.59 | 0.57 |
| | WC-B | CS | 0.31 | 570.60 | 1.71 | 767.57 | 2368.81 | 26.32 | 493251.70 | 428.00 | 4.98 | 35.83 | 0.40 |
| | WC-C | SS | 0.79 | 855.90 | 1.61 | 1080.43 | 3292.81 | 36.59 | 712474.80 | 529.90 | 7.64 | 84.23 | 0.94 |
| | WC-C | CS | 0.44 | 733.70 | 1.74 | 1003.72 | 3059.02 | 33.99 | 631571.00 | 448.40 | 5.47 | 43.17 | 0.48 |
| **Test 2** | WC-A | SS | 0.79 | 1141.30 | 1.69 | 1510.45 | 4680.72 | 52.01 | 870367.50 | 591.00 | 9.50 | 130.36 | 1.45 |
| | WC-A | CS | 0.45 | 693.00 | 1.71 | 932.70 | 2866.45 | 31.85 | 521959.50 | 407.60 | 4.52 | 29.47 | 0.33 |
| | WC-B | SS | 0.76 | 733.70 | 1.72 | 990.31 | 3094.25 | 34.38 | 720304.10 | 489.10 | 6.51 | 61.12 | 0.68 |
| | WC-B | CS | 0.29 | 489.20 | 1.85 | 710.85 | 2230.17 | 24.78 | 375810.80 | 366.80 | 3.66 | 19.33 | 0.21 |
| | WC-C | SS | 0.80 | 937.50 | 1.83 | 1348.77 | 4024.27 | 44.71 | 845574.40 | 550.30 | 8.24 | 97.98 | 1.09 |
| | WC-C | CS | 0.40 | 774.50 | 1.83 | 1112.00 | 3332.10 | 37.02 | 751621.70 | 489.10 | 6.51 | 61.12 | 0.68 |
| **Test 3** | WC-A | SS | 0.77 | 1182.10 | 1.78 | 1652.08 | 5077.26 | 56.41 | 939527.10 | 611.40 | 10.17 | 149.33 | 1.66 |
| | WC-A | CS | 0.42 | 774.50 | 1.76 | 1073.07 | 3201.67 | 35.57 | 575460.40 | 428.00 | 4.98 | 35.83 | 0.40 |
| | WC-B | SS | 0.76 | 631.80 | 1.84 | 914.92 | 2864.52 | 31.83 | 631571.00 | 448.40 | 5.47 | 43.17 | 0.48 |
| | WC-B | CS | 0.21 | 611.40 | 1.61 | 771.07 | 2261.12 | 25.12 | 377115.70 | 346.50 | 3.26 | 15.39 | 0.17 |
| | WC-C | SS | 0.77 | 1141.30 | 1.79 | 1604.95 | 5076.34 | 56.40 | 970844.70 | 631.80 | 10.86 | 170.30 | 1.89 |
| | WC-C | CS | 0.44 | 754.10 | 1.75 | 1034.02 | 3105.06 | 34.50 | 815561.70 | 509.50 | 7.06 | 71.98 | 0.80 |

Table D.3. Sliding wear and friction test results for Test Condition 3[1].

| Sample pairs | | | μ | $D_M$ | $P_d$ | $A_S$ | $V_S$ ($x10^4$) | **$k_s$ ($x10^{-6}$)** | $A_B$ | $D_B$ | h | $V_B$ ($x10^4$) | **$k_B$ ($x10^{-6}$)** |
|---|---|---|---|---|---|---|---|---|---|---|---|---|---|
| **Test 1** | WC-A | SS | 1.07 | 733.70 | 1.80 | 1036.98 | 2854.96 | 95.17 | 540228.10 | 468.80 | 5.98 | 51.59 | 1.72 |
| | WC-A | CS | 0.66 | 529.90 | 1.75 | 727.98 | 2162.72 | 72.09 | 471068.40 | 387.20 | 4.08 | 24.00 | 0.80 |
| | WC-B | SS | 1.25 | 448.30 | 1.80 | 634.17 | 1924.63 | 64.15 | 377115.70 | 346.50 | 3.26 | 15.39 | 0.51 |
| | WC-B | CS | 0.59 | 509.50 | 1.76 | 704.17 | 2123.53 | 70.78 | 293602.20 | 305.70 | 2.54 | 9.32 | 0.31 |
| | WC-C | SS | 1.14 | 652.20 | 1.79 | 915.58 | 2778.70 | 92.62 | 510215.40 | 468.80 | 5.98 | 51.59 | 1.72 |
| | WC-C | CS | 0.67 | 468.80 | 1.81 | 667.74 | 2013.68 | 67.12 | 422787.20 | 366.80 | 3.66 | 19.33 | 0.64 |
| **Test 2** | WC-A | SS | 1.13 | 692.90 | 1.82 | 989.86 | 3004.08 | 100.14 | 544189.00 | 491.20 | 6.56 | 62.18 | 2.07 |
| | WC-A | CS | 0.67 | 529.90 | 1.80 | 748.72 | 2281.88 | 76.06 | 334054.10 | 326.10 | 2.89 | 12.07 | 0.40 |
| | WC-B | SS | 1.16 | 570.60 | 1.78 | 797.18 | 2449.98 | 81.67 | 690291.40 | 468.80 | 5.98 | 51.59 | 1.72 |
| | WC-B | CS | 0.63 | 529.90 | 1.86 | 774.30 | 2359.81 | 78.66 | 422787.20 | 366.80 | 3.66 | 19.33 | 0.64 |
| | WC-C | SS | 1.01 | 672.50 | 1.85 | 975.55 | 2904.46 | 96.82 | 516739.90 | 448.40 | 5.47 | 43.17 | 1.44 |
| | WC-C | CS | 0.56 | 529.90 | 1.82 | 757.50 | 2250.41 | 75.01 | 422787.20 | 366.80 | 3.66 | 19.33 | 0.64 |
| **Test 3** | WC-A | SS | 1.30 | 815.20 | 1.76 | 1123.80 | 3338.67 | 111.29 | 712474.80 | 529.90 | 7.64 | 84.23 | 2.81 |
| | WC-A | CS | 0.67 | 529.90 | 1.72 | 714.94 | 2178.91 | 72.63 | 377115.70 | 346.50 | 3.26 | 15.39 | 0.51 |
| | WC-B | SS | 1.13 | 489.20 | 1.79 | 688.10 | 2123.56 | 70.79 | 422787.00 | 366.80 | 3.66 | 19.33 | 0.64 |
| | WC-B | CS | 0.58 | 570.70 | 1.73 | 776.23 | 2316.00 | 77.20 | 471068.40 | 387.20 | 4.08 | 24.00 | 0.80 |
| | WC-C | SS | 1.12 | 611.40 | 1.74 | 834.42 | 2446.88 | 81.56 | 521959.50 | 407.60 | 4.52 | 29.47 | 0.98 |
| | WC-C | CS | 0.67 | 550.20 | 1.87 | 806.51 | 2432.17 | 81.07 | 443665.60 | 407.60 | 4.52 | 29.47 | 0.98 |

Table D.4. Sliding wear and friction test results for Test Condition 4[1].

| Sample pairs | | | μ | $D_M$ | $P_d$ | $A_S$ | $V_S$ ($x10^4$) | **$k_s$ ($x10^{-6}$)** | $A_B$ | $D_B$ | h | $V_B$ ($x10^4$) | **$k_B$ ($x10^{-6}$)** |
|---|---|---|---|---|---|---|---|---|---|---|---|---|---|
| **Test 1** | WC-A | SS | 0.71 | 1304.40 | 1.64 | 1684.95 | 5199.95 | 57.78 | 1255312.60 | 754.10 | 7.73 | 172.64 | 1.92 |
| | WC-A | CS | 0.45 | 754.00 | 1.80 | 1068.72 | 3291.34 | 36.57 | 690291.40 | 468.80 | 2.99 | 25.78 | 0.29 |
| | WC-B | SS | 0.72 | 937.50 | 3.48 | 2560.90 | 7804.84 | 86.72 | 913429.10 | 570.70 | 4.43 | 56.62 | 0.63 |
| | WC-B | CS | 0.28 | 672.60 | 2.37 | 1254.60 | 3799.55 | 42.22 | 631571.00 | 448.40 | 2.73 | 21.57 | 0.24 |
| | WC-C | SS | 0.69 | 1243.20 | 1.63 | 1596.28 | 4936.53 | 54.85 | 1141786.40 | 713.30 | 6.92 | 138.19 | 1.54 |
| | WC-C | CS | 0.43 | 794.90 | 1.64 | 1026.47 | 3121.79 | 34.69 | 690291.40 | 468.80 | 2.99 | 25.78 | 0.29 |
| **Test 2** | WC-A | SS | 0.70 | 1284.00 | 1.60 | 1611.05 | 4940.91 | 54.90 | 1141786.40 | 713.30 | 6.92 | 138.19 | 1.54 |
| | WC-A | CS | 0.38 | 774.40 | 1.70 | 1033.18 | 3122.37 | 34.69 | 690291.40 | 468.80 | 2.99 | 25.78 | 0.29 |
| | WC-B | SS | 0.74 | 1019.00 | 1.89 | 1513.27 | 4670.12 | 51.89 | 1011296.50 | 631.80 | 5.43 | 85.05 | 0.94 |
| | WC-B | CS | 0.26 | 531.40 | 2.34 | 975.04 | 2972.07 | 33.02 | 521959.50 | 407.60 | 2.26 | 14.73 | 0.16 |
| | WC-C | SS | 0.67 | 1222.80 | 1.76 | 1686.38 | 5204.35 | 57.83 | 1141786.40 | 713.30 | 6.92 | 138.19 | 1.54 |
| | WC-C | CS | 0.36 | 774.50 | 2.35 | 1431.24 | 4270.34 | 47.45 | 751621.70 | 489.10 | 3.25 | 30.54 | 0.34 |
| **Test 3** | WC-A | SS | 0.72 | 1263.60 | 1.71 | 1693.06 | 5246.69 | 58.30 | 1187457.90 | 713.30 | 6.92 | 138.19 | 1.54 |
| | WC-A | CS | 0.32 | 774.50 | 1.72 | 1045.97 | 3107.41 | 34.53 | 751621.70 | 489.10 | 3.25 | 30.54 | 0.34 |
| | WC-B | SS | 0.81 | 937.50 | 1.72 | 1264.81 | 3919.53 | 43.55 | 970844.70 | 631.80 | 5.43 | 85.05 | 0.94 |
| | WC-B | CS | 0.26 | 509.50 | 1.71 | 682.89 | 2033.14 | 22.59 | 521959.50 | 407.60 | 2.26 | 14.73 | 0.16 |
| | WC-C | SS | 0.71 | 1222.80 | 1.71 | 1642.34 | 5089.51 | 56.55 | 1233129.40 | 713.30 | 6.92 | 138.19 | 1.54 |
| | WC-C | CS | 0.43 | 876.30 | 1.71 | 1177.52 | 3505.77 | 38.95 | 882111.60 | 529.90 | 3.82 | 42.08 | 0.47 |

Table D.5. Sliding wear and friction test results for Test Condition 5[1].

| Sample pairs | | | μ | $D_M$ | $P_d$ | $A_S$ | $V_S$ ($x10^4$) | **$k_s$ ($x10^{-6}$)** | $A_B$ | $D_B$ | h | $V_B$ ($x10^4$) | **$k_B$ ($x10^{-6}$)** |
|---|---|---|---|---|---|---|---|---|---|---|---|---|---|
| **Test 1** | WC-A | SS | 0.83 | 957.90 | 1.73 | 1300.20 | 4020.84 | 44.68 | 775109.90 | 550.30 | 4.12 | 48.95 | 0.54 |
| | WC-A | CS | 0.32 | 611.40 | 1.88 | 905.12 | 2677.41 | 29.75 | 471068.40 | 387.20 | 2.04 | 11.99 | 0.13 |
| | WC-B | SS | 0.85 | 652.20 | 1.96 | 1004.76 | 3113.67 | 34.60 | 488032.10 | 448.40 | 2.73 | 21.57 | 0.24 |
| | WC-B | CS | 0.32 | 550.30 | 1.82 | 786.13 | 2431.09 | 27.01 | 521959.50 | 407.60 | 2.26 | 14.73 | 0.16 |
| | WC-C | SS | 0.75 | 774.40 | 1.66 | 1011.21 | 3107.76 | 34.53 | 540228.10 | 468.80 | 2.99 | 25.78 | 0.29 |
| | WC-C | CS | 0.44 | 692.90 | 1.83 | 996.86 | 3025.34 | 33.61 | 471068.40 | 387.20 | 2.04 | 11.99 | 0.13 |
| **Test 2** | WC-A | SS | 0.81 | 856.00 | 1.95 | 1308.21 | 4054.05 | 45.05 | 780329.50 | 529.90 | 3.82 | 42.08 | 0.47 |
| | WC-A | CS | 0.31 | 611.40 | 1.80 | 865.19 | 2603.58 | 28.93 | 377115.70 | 346.50 | 1.63 | 7.69 | 0.09 |
| | WC-B | SS | 0.84 | 631.80 | 1.78 | 881.74 | 2760.65 | 30.67 | 574155.40 | 448.40 | 2.73 | 21.57 | 0.24 |
| | WC-B | CS | 0.29 | 550.30 | 1.62 | 700.66 | 2130.92 | 23.68 | 471068.40 | 387.20 | 2.04 | 11.99 | 0.13 |
| | WC-C | SS | 0.79 | 733.70 | 1.98 | 1138.47 | 3498.88 | 38.88 | 685071.90 | 509.50 | 3.53 | 35.96 | 0.40 |
| | WC-C | CS | 0.46 | 754.10 | 1.86 | 1103.85 | 3300.58 | 36.67 | 631571.00 | 448.40 | 2.73 | 21.57 | 0.24 |
| **Test 3** | WC-A | SS | 0.73 | 876.30 | 2.11 | 1448.78 | 4498.91 | 49.99 | 739877.60 | 550.30 | 4.12 | 48.95 | 0.54 |
| | WC-A | CS | 0.33 | 631.70 | 1.69 | 840.34 | 2501.91 | 27.80 | 334054.10 | 326.10 | 1.44 | 6.03 | 0.07 |
| | WC-B | SS | 0.84 | 631.80 | 1.85 | 916.15 | 2844.96 | 31.61 | 575460.40 | 428.00 | 2.49 | 17.91 | 0.20 |
| | WC-B | CS | 0.28 | 570.70 | 2.11 | 946.35 | 2884.18 | 32.05 | 521959.50 | 407.60 | 2.26 | 14.73 | 0.16 |
| | WC-C | SS | 0.77 | 794.50 | 1.88 | 1170.83 | 3605.91 | 40.07 | 750316.80 | 509.50 | 3.53 | 35.96 | 0.40 |
| | WC-C | CS | 0.44 | 672.60 | 1.93 | 1019.60 | 3074.78 | 34.16 | 422787.20 | 366.80 | 1.83 | 9.66 | 0.11 |

[1] Definitions for sliding wear and friction parameters within Table D.1 to D.5 are as follows:

| | |
|---|---|
| $\mu$ | Kinetic coefficient of friction. |
| $D_m$ | Width of the substrate wear track [μm] |
| $P_d$ | Maximum penetration depth Inner [μm] |
| $A_S$ | Calculated cross sectional wear track area [$\mu m^2$] |
| $V_S$ | Total worn volume of substrate [$\mu m^3$] |
| $k_S$ | Dimensional substrate wear coefficient [$mm^3/Nm$] |
| $A_B$ | Worn area of the button [$\mu m^2$] |
| $D_B$ | Average diameter of the worn button area [μm] |
| h | Worn height of spherical button tip [μm] |
| $V_B$ | Total worn volume of button [$\mu m^3$] |
| $k_B$ | Dimensional button wear coefficient [$mm^3/Nm$] |

D.3

The averaged values of Tables D.1 – D.5 is shown in Table D.6, which displays the wear and friction data for each button/substrate pair per test condition.

Table D.6. Averaged sliding wear and friction test results for each button/substrate pair per test condition[1].

| Sample pairs | | | μ | $D_M$ | $P_d$ | $A_S$ | $V_S$ ($x10^4$) | **$k_s$ ($x10^{-6}$)** | $A_B$ | $D_B$ | h | $V_B$ ($x10^4$) | **$k_B$ ($x10^{-6}$)** |
|---|---|---|---|---|---|---|---|---|---|---|---|---|---|
| **Test Condition 1** | WC-A | SS | 0.65 | 1351.87 | 1.80 | 1916.07 | 5882.83 | **39.22** | 1203116.63 | 618.46 | 15.78 | 360.88 | **2.41** |
| | WC-A | CS | 0.35 | 794.80 | 1.67 | 1045.66 | 3205.50 | **21.37** | 657234.03 | 456.36 | 6.49 | 61.22 | **0.41** |
| | WC-B | SS | 0.71 | 985.03 | 1.83 | 1432.57 | 4347.40 | **28.98** | 939527.10 | 544.77 | 9.48 | 140.30 | **0.94** |
| | WC-B | CS | 0.23 | 645.33 | 1.77 | 893.11 | 2673.91 | **17.83** | 541532.97 | 414.40 | 4.69 | 32.22 | **0.21** |
| | WC-C | SS | 0.56 | 1345.10 | 2.72 | 2879.50 | 8753.46 | **58.36** | 1400591.30 | 667.62 | 16.62 | 398.89 | **2.66** |
| | WC-C | CS | 0.31 | 801.70 | 1.72 | 1086.80 | 3305.74 | **22.04** | 780764.43 | 498.45 | 6.69 | 64.74 | **0.43** |
| **Test Condition 2** | WC-A | SS | 0.76 | 1100.53 | 1.72 | 1490.44 | 4593.43 | **51.04** | 868192.67 | 525.39 | 9.72 | 136.69 | **1.52** |
| | WC-A | CS | 0.43 | 706.57 | 1.70 | 944.33 | 2877.20 | **31.97** | 539793.13 | 414.40 | 4.67 | 31.59 | **0.35** |
| | WC-B | SS | 0.77 | 672.57 | 1.82 | 957.22 | 2976.29 | **33.07** | 680722.17 | 465.32 | 5.98 | 51.96 | **0.58** |
| | WC-B | CS | 0.27 | 557.07 | 1.72 | 749.83 | 2286.70 | **25.41** | 354932.43 | 335.78 | 3.97 | 23.52 | **0.26** |
| | WC-C | SS | 0.79 | 978.23 | 1.74 | 1344.72 | 4131.14 | **45.90** | 842964.63 | 516.98 | 8.91 | 117.50 | **1.31** |
| | WC-C | CS | 0.43 | 754.10 | 1.77 | 1049.92 | 3165.40 | **35.17** | 732918.13 | 482.34 | 6.34 | 58.76 | **0.65** |
| **Test Condition 3** | WC-A | SS | 1.17 | 747.27 | 1.79 | 1050.21 | 3065.90 | **102.20** | 598963.97 | 435.70 | 6.72 | 66.00 | **2.20** |
| | WC-A | CS | 0.66 | 529.90 | 1.76 | 730.55 | 2207.84 | **73.59** | 394079.40 | 353.26 | 3.41 | 17.15 | **0.57** |
| | WC-B | SS | 1.18 | 502.70 | 1.79 | 706.49 | 2166.06 | **72.20** | 496731.37 | 394.02 | 4.30 | 28.77 | **0.96** |
| | WC-B | CS | 0.60 | 536.70 | 1.78 | 751.56 | 2266.45 | **75.55** | 395819.27 | 353.26 | 3.42 | 17.55 | **0.58** |
| | WC-C | SS | 1.09 | 645.37 | 1.79 | 908.52 | 2710.01 | **90.33** | 516304.93 | 405.39 | 5.32 | 41.41 | **1.38** |
| | WC-C | CS | 0.63 | 516.30 | 1.83 | 743.91 | 2232.08 | **74.40** | 429746.67 | 369.83 | 3.94 | 22.71 | **0.76** |

Table D.6. Averaged sliding wear and friction test results for each button/substrate pair per test condition conitued[1].

| Sample pairs | | | μ | $D_M$ | $P_d$ | $A_S$ | $V_S$ ($x10^4$) | **$k_s$ ($x10^{-6}$)** | $A_B$ | $D_B$ | h | $V_B$ ($x10^4$) | **$k_B$ ($x10^{-6}$)** |
|---|---|---|---|---|---|---|---|---|---|---|---|---|---|
| **Test condition 4** | WC-A | SS | 0.71 | 1284.00 | 1.65 | 1663.02 | 5129.18 | **56.99** | 1194852.30 | 616.59 | 7.19 | 149.68 | **1.66** |
| | WC-A | CS | 0.38 | 767.63 | 1.74 | 1049.29 | 3173.71 | **35.26** | 710734.83 | 475.54 | 3.07 | 27.36 | **0.30** |
| | WC-B | SS | 0.75 | 964.67 | 2.36 | 1779.66 | 5464.83 | **60.72** | 965190.10 | 554.16 | 5.09 | 75.57 | **0.84** |
| | WC-B | CS | 0.27 | 571.17 | 2.14 | 970.84 | 2934.92 | **32.61** | 558496.67 | 421.20 | 2.42 | 17.01 | **0.19** |
| | WC-C | SS | 0.69 | 1229.60 | 1.70 | 1641.67 | 5076.80 | **56.41** | 1172234.07 | 610.74 | 6.92 | 138.19 | **1.54** |
| | WC-C | CS | 0.40 | 815.23 | 1.90 | 1211.74 | 3632.63 | **40.36** | 774674.90 | 495.92 | 3.35 | 32.80 | **0.36** |
| **Test Condition 5** | WC-A | SS | 0.79 | 896.73 | 1.93 | 1352.40 | 4191.27 | **46.57** | 765105.67 | 493.46 | 4.02 | 46.66 | **0.52** |
| | WC-A | CS | 0.32 | 618.17 | 1.79 | 870.22 | 2594.30 | **28.83** | 394079.40 | 353.26 | 1.70 | 8.57 | **0.10** |
| | WC-B | SS | 0.85 | 638.60 | 1.86 | 934.22 | 2906.43 | **32.29** | 545882.63 | 416.54 | 2.65 | 20.35 | **0.23** |
| | WC-B | CS | 0.30 | 557.10 | 1.85 | 811.05 | 2482.06 | **27.58** | 504995.80 | 400.82 | 2.18 | 13.82 | **0.15** |
| | WC-C | SS | 0.77 | 767.53 | 1.84 | 1106.84 | 3404.18 | **37.82** | 658538.93 | 456.79 | 3.35 | 32.57 | **0.36** |
| | WC-C | CS | 0.45 | 706.53 | 1.88 | 1040.10 | 3133.57 | **34.82** | 508475.53 | 400.82 | 2.20 | 14.41 | **0.16** |

[1] Definitions for sliding wear and friction parameters within Table D.6 are as follows:

| | |
|---|---|
| $\mu$ | Kinetic coefficient of friction. |
| $D_m$ | Width of the substrate wear track [µm] |
| $P_d$ | Maximum penetration depth Inner [µm] |
| $A_S$ | Calculated cross sectional wear track area [$\mu m^2$] |
| $V_S$ | Total worn volume of substrate [$\mu m^3$] |
| $k_S$ | Dimensional substrate wear coefficient [$mm^3/Nm$] |
| $A_B$ | Worn area of the button [$\mu m^2$] |
| $D_B$ | Average diameter of the worn button area [µm] |
| h | Worn height of spherical button tip [µm] |
| $V_B$ | Total worn volume of button [$\mu m^3$] |
| $k_B$ | Dimensional button wear coefficient [$mm^3/Nm$] |

D.4

Table D.7 provides details on the static and kinetic friction response of the button-substrate pairs under the various test conditions. It also indicates the standard deviation between the results obtained.

Table D.7. Static and kinetic friction response of button-substrate pairs.

| | Sample pairs | | Static coefficient of friction | | | | | Kinetic coefficient of friction | | | | |
|---|---|---|---|---|---|---|---|---|---|---|---|---|
| | | | T1 | T2 | T3 | Ave | Std Dev | T1 | T2 | T3 | Ave | Std Dev |
| Test condition 1 | WC-A | SS | 0.75 | 0.85 | 0.91 | 0.84 | 0.07 | 0.69 | 0.59 | 0.67 | 0.65 | 0.04 |
| | WC-A | CS | 0.75 | 0.63 | 0.49 | 0.62 | 0.11 | 0.42 | 0.29 | 0.35 | 0.35 | 0.05 |
| | WC-B | SS | 1.15 | 0.75 | 0.75 | 0.88 | 0.19 | 0.77 | 0.71 | 0.66 | 0.71 | 0.04 |
| | WC-B | CS | 0.42 | 0.31 | 0.21 | 0.31 | 0.09 | 0.19 | 0.28 | 0.21 | 0.23 | 0.04 |
| | WC-C | SS | 0.66 | 0.68 | 1.10 | 0.81 | 0.20 | 0.49 | 0.60 | 0.59 | 0.56 | 0.05 |
| | WC-C | CS | 0.48 | 0.77 | 0.70 | 0.65 | 0.12 | 0.26 | 0.30 | 0.39 | 0.31 | 0.06 |
| Test condition 2 | WC-A | SS | 0.77 | 0.79 | 0.83 | 0.80 | 0.02 | 0.74 | 0.79 | 0.77 | 0.76 | 0.02 |
| | WC-A | CS | 0.75 | 0.49 | 0.48 | 0.57 | 0.12 | 0.43 | 0.45 | 0.42 | 0.43 | 0.02 |
| | WC-B | SS | 0.96 | 0.77 | 0.72 | 0.82 | 0.10 | 0.81 | 0.76 | 0.76 | 0.77 | 0.02 |
| | WC-B | CS | 0.64 | 0.71 | 0.75 | 0.70 | 0.05 | 0.31 | 0.29 | 0.21 | 0.27 | 0.04 |
| | WC-C | SS | 0.82 | 0.66 | 0.76 | 0.75 | 0.07 | 0.79 | 0.80 | 0.77 | 0.79 | 0.01 |
| | WC-C | CS | 0.86 | 0.90 | 0.84 | 0.87 | 0.02 | 0.44 | 0.40 | 0.44 | 0.43 | 0.02 |
| Test condition 3 | WC-A | SS | 1.08 | 1.12 | 1.27 | 1.16 | 0.08 | 1.07 | 1.13 | 1.30 | 1.17 | 0.10 |
| | WC-A | CS | 0.68 | 0.76 | 0.72 | 0.72 | 0.03 | 0.66 | 0.67 | 0.67 | 0.66 | 0.01 |
| | WC-B | SS | 1.13 | 1.04 | 0.60 | 0.92 | 0.23 | 1.25 | 1.16 | 1.13 | 1.18 | 0.05 |
| | WC-B | CS | 0.84 | 0.70 | 0.53 | 0.69 | 0.13 | 0.59 | 0.63 | 0.58 | 0.60 | 0.02 |
| | WC-C | SS | 1.11 | 1.08 | 1.15 | 1.11 | 0.03 | 1.14 | 1.01 | 1.12 | 1.09 | 0.06 |
| | WC-C | CS | 0.57 | 0.59 | 0.62 | 0.59 | 0.02 | 0.67 | 0.56 | 0.67 | 0.63 | 0.05 |
| Test condition 4 | WC-A | SS | 0.96 | 0.88 | 0.91 | 0.92 | 0.03 | 0.71 | 0.70 | 0.72 | 0.71 | 0.01 |
| | WC-A | CS | 0.71 | 0.75 | 0.66 | 0.71 | 0.04 | 0.45 | 0.38 | 0.32 | 0.38 | 0.05 |
| | WC-B | SS | 0.97 | 0.82 | 0.83 | 0.87 | 0.07 | 0.72 | 0.74 | 0.81 | 0.75 | 0.04 |
| | WC-B | CS | 0.95 | 0.87 | 0.56 | 0.79 | 0.17 | 0.28 | 0.26 | 0.26 | 0.27 | 0.01 |
| | WC-C | SS | 0.83 | 0.84 | 0.87 | 0.85 | 0.02 | 0.69 | 0.67 | 0.71 | 0.69 | 0.02 |
| | WC-C | CS | 0.91 | 0.87 | 0.82 | 0.87 | 0.04 | 0.43 | 0.36 | 0.43 | 0.40 | 0.03 |
| Test condition 5 | WC-A | SS | 0.84 | 0.98 | 0.97 | 0.93 | 0.06 | 0.83 | 0.81 | 0.73 | 0.79 | 0.04 |
| | WC-A | CS | 0.84 | 0.74 | 0.74 | 0.77 | 0.05 | 0.32 | 0.30 | 0.33 | 0.32 | 0.01 |
| | WC-B | SS | 0.89 | 0.92 | 0.91 | 0.91 | 0.01 | 0.85 | 0.84 | 0.84 | 0.85 | 0.01 |
| | WC-B | CS | 0.96 | 0.79 | 0.83 | 0.86 | 0.07 | 0.32 | 0.29 | 0.28 | 0.30 | 0.02 |
| | WC-C | SS | 0.98 | 0.98 | 0.88 | 0.95 | 0.05 | 0.75 | 0.79 | 0.77 | 0.77 | 0.02 |
| | WC-C | CS | 0.84 | 0.83 | 0.55 | 0.74 | 0.13 | 0.44 | 0.46 | 0.44 | 0.45 | 0.01 |

D.5

Figures D.2 to D.7 illustrate the individual test results per button/steel pair under test condition 5 (3N, $0.1ms^{-1}$). These graphs were produced by the CSM tribometer software.

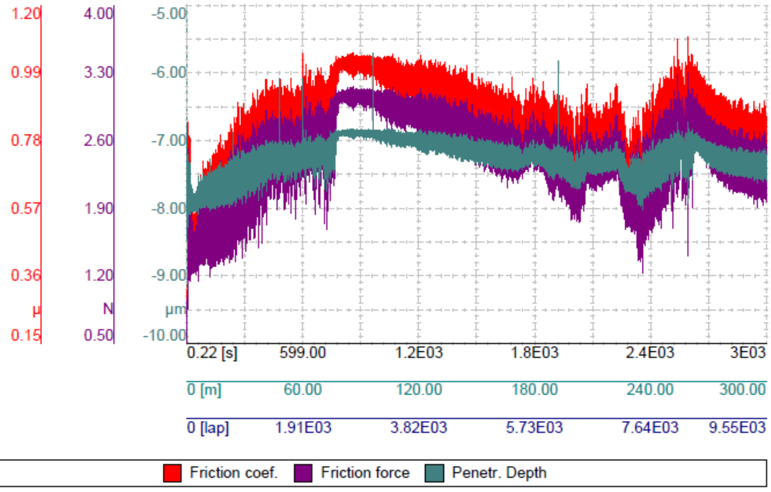


*Test 1*

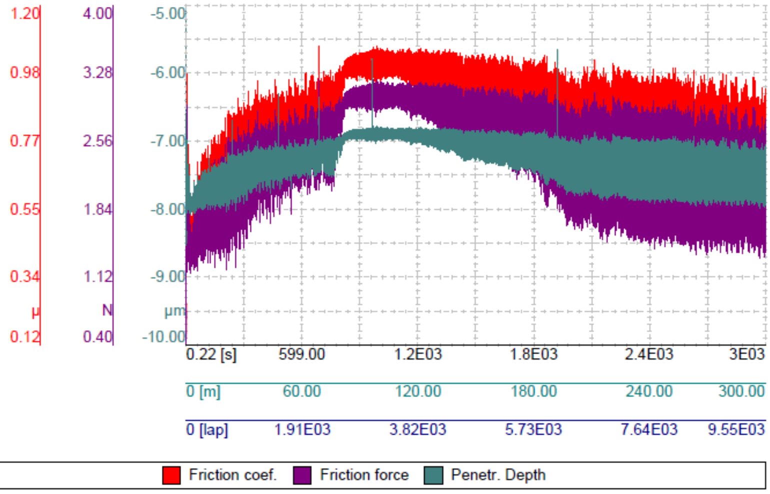


*Test 2*

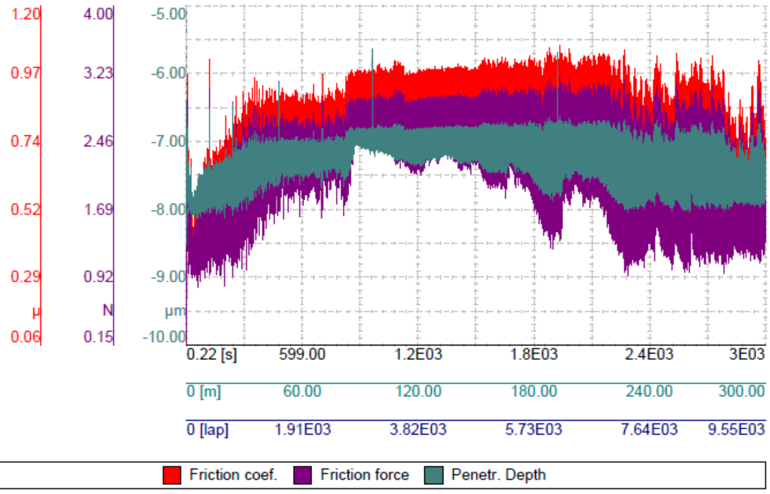


*Test 3*

*Figure D.2. The friction response of three individual tests for cemented carbide grade WC-A paired with a 304 Stainless Steel substrate under test condition 5 (3N, 0.1ms$^{-1}$).*

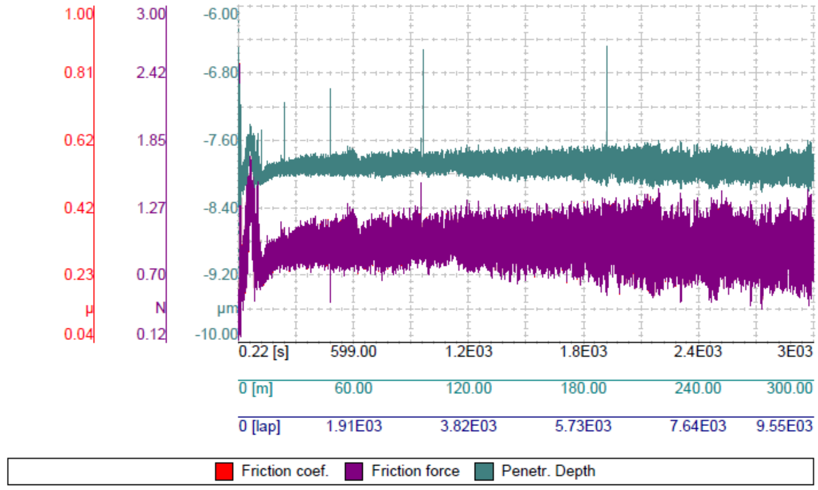


*Test 1*

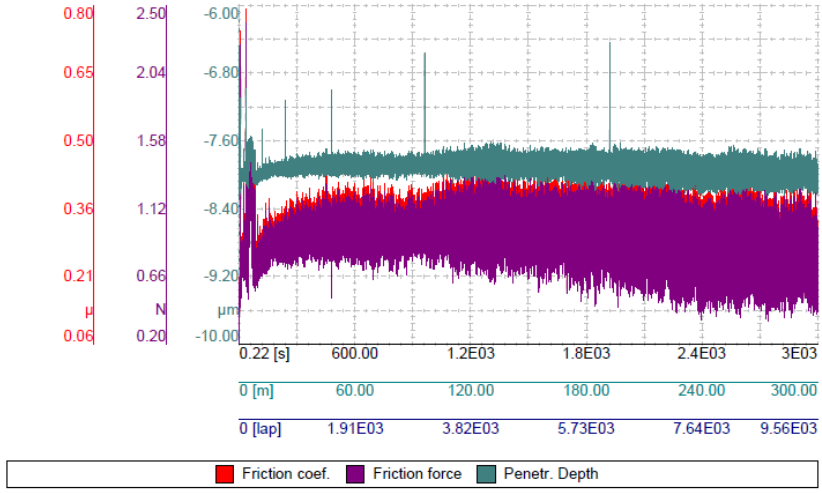


*Test 2*

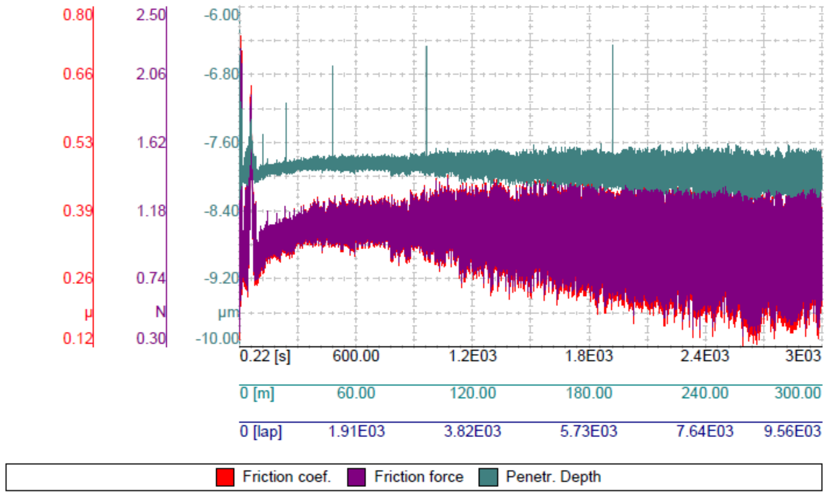


*Test 3*

*Figure D.3. The friction response of three individual tests for cemented carbide grade WC-A paired with a Bright Mild Steel substrate under test condition 5 (3N, 0.1ms$^{-1}$).*

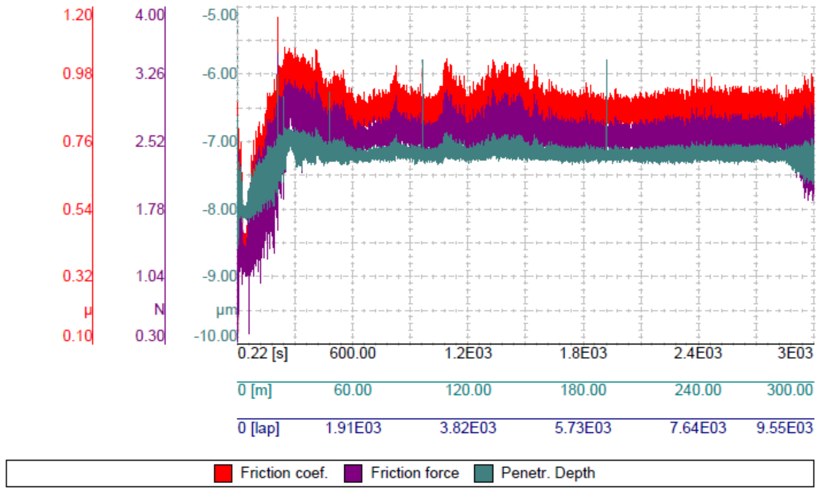


*Test 1*

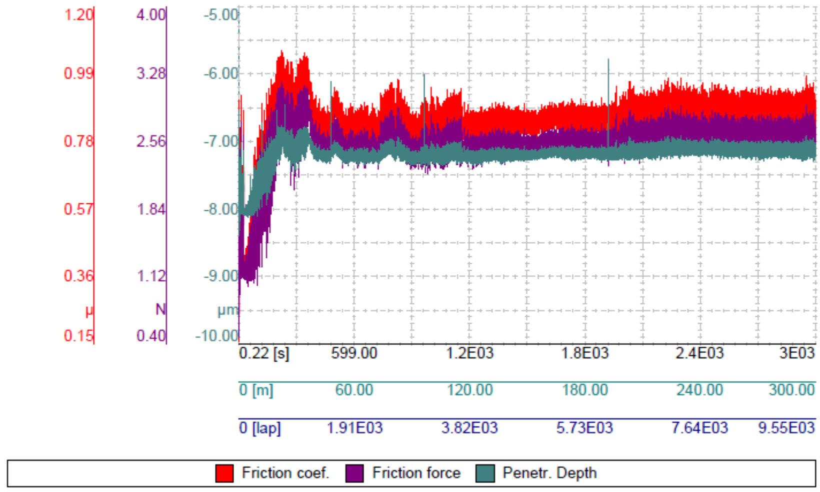


*Test 2*

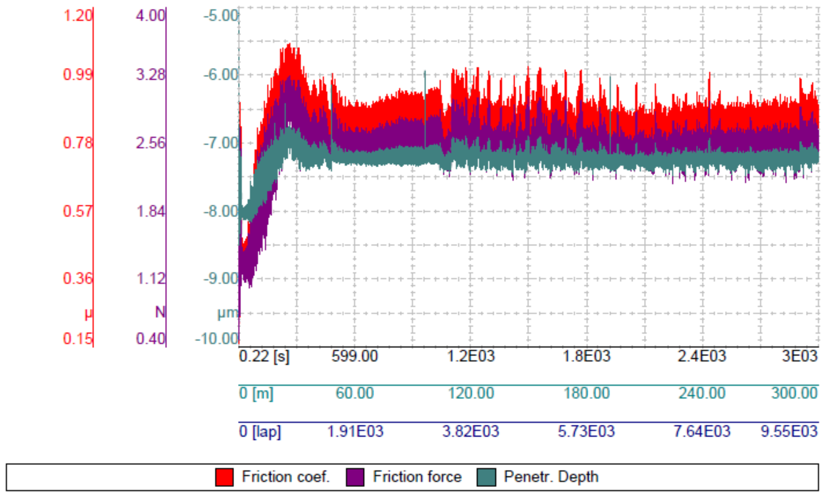


*Test 3*

*Figure D.4. The friction response of three individual tests for cemented carbide grade WC-B paired with a 304 Stainless Steel substrate under test condition 5 (3N, 0.1ms$^{-1}$).*

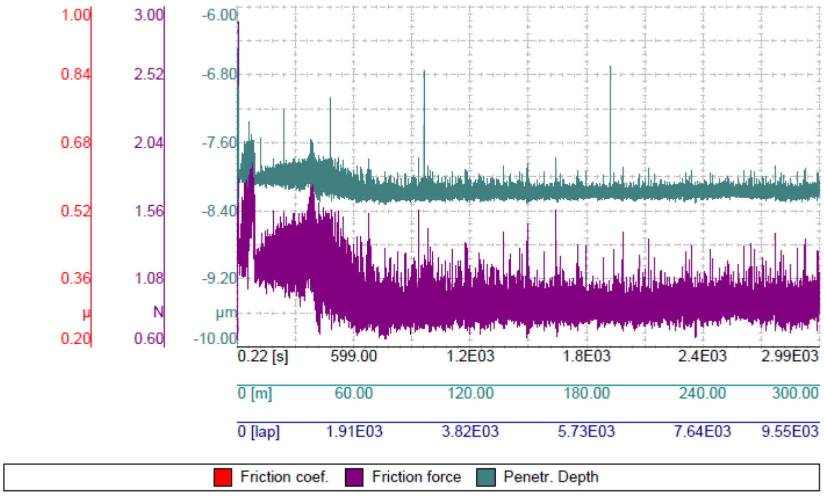


*Test 1*

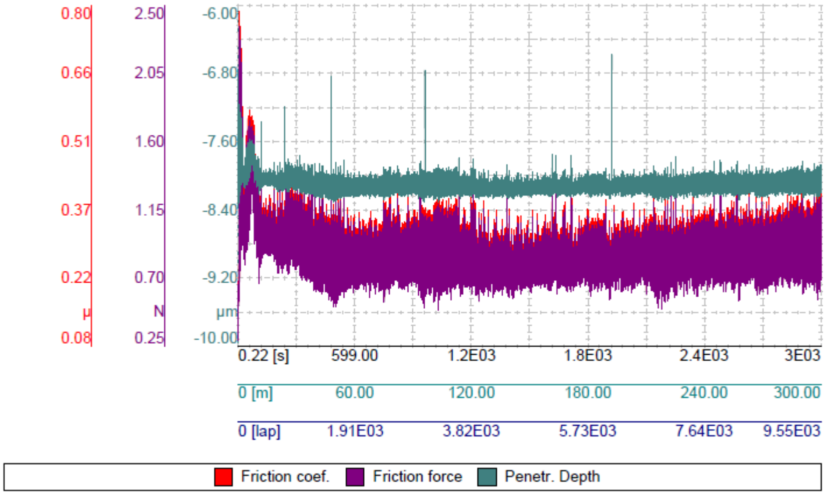


*Test 2*

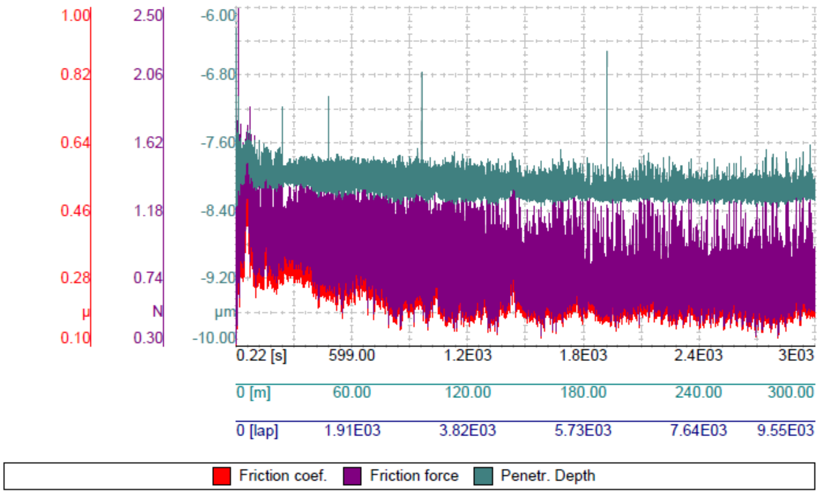


*Test 3*

*Figure D.5. The friction response of three individual tests for cemented carbide grade WC-B paired with a Bright Mild Steel substrate under test condition 5 (3N, 0.1ms$^{-1}$).*

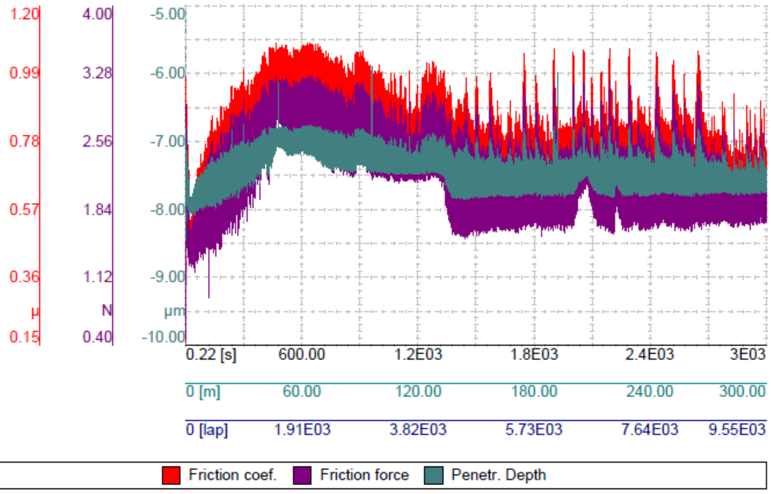


*Test 1*

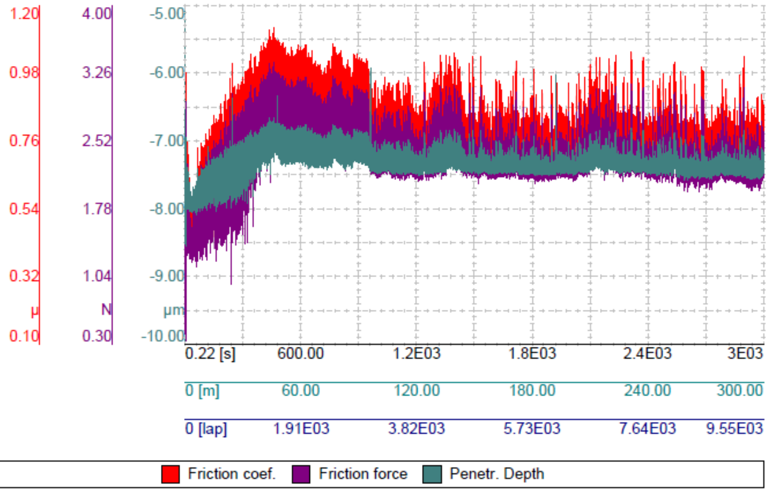


*Test 2*

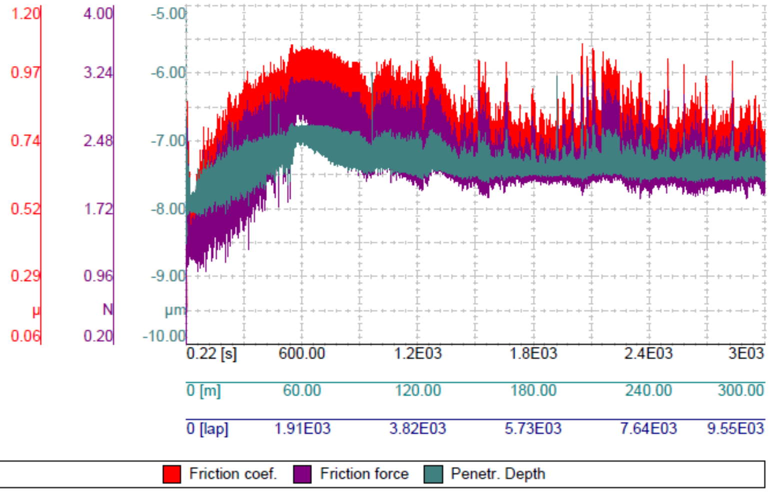


*Test 3*

*Figure D.6. The friction response of three individual tests for cemented carbide grade WC-C paired with a 304 Stainless Steel substrate under test condition 5 (3N, 0.1ms$^{-1}$).*

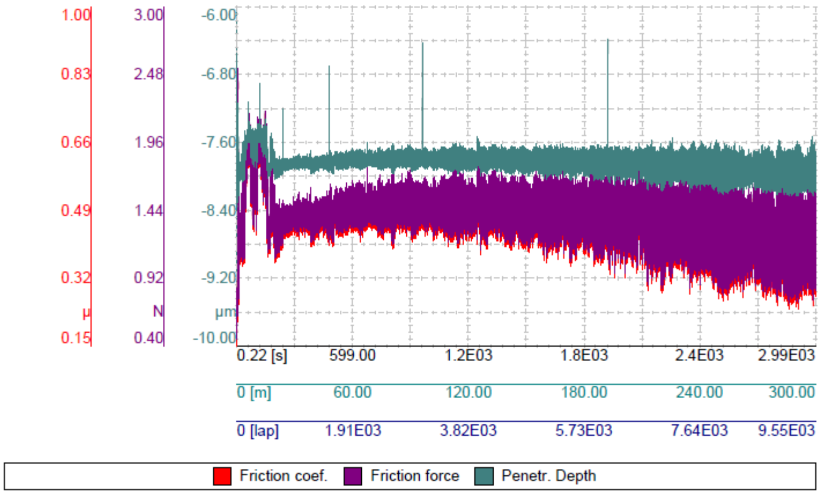


*Test 1*

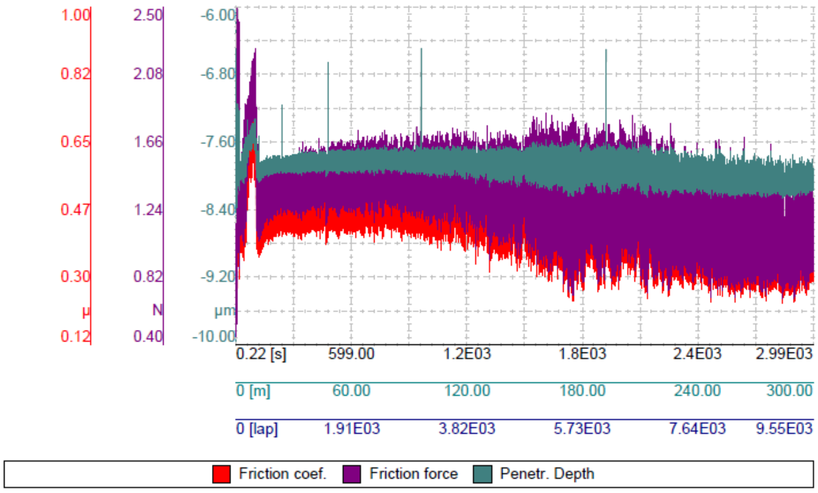


*Test 2*

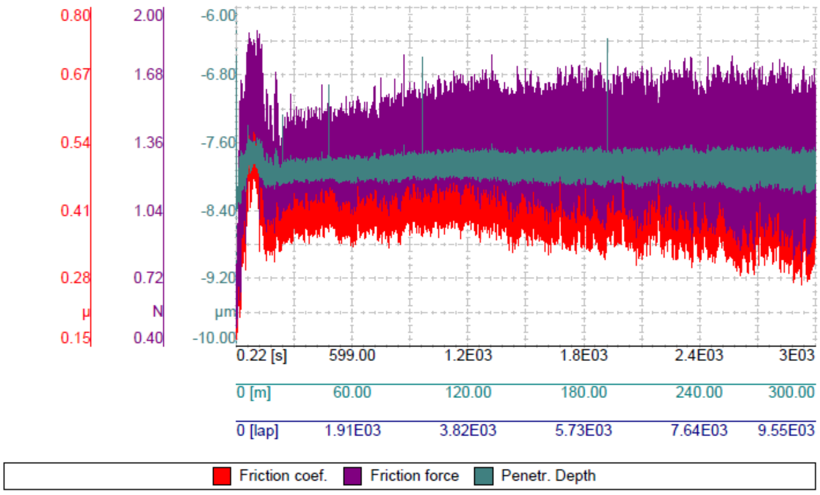


*Test 3*

*Figure D.7. The friction response of three individual tests for cemented carbide grade WC-C paired with a Bright Mild Steel substrate under test condition 5 (3N, 0.1ms$^{-1}$).*

# Appendix E

## Scanning Electron Microscope Images

E.1

SEM images were taken of the wear track on the substrates at a magnification of 250x and have been included here for comparative purposes. The substrates represent one sample from each button-substrate pair of each test condition. Images of the worn area on the corresponding button were also taken and included here at a magnification of 250x. These images were used to identify the wear mechanisms for each button-substrate sliding pair.

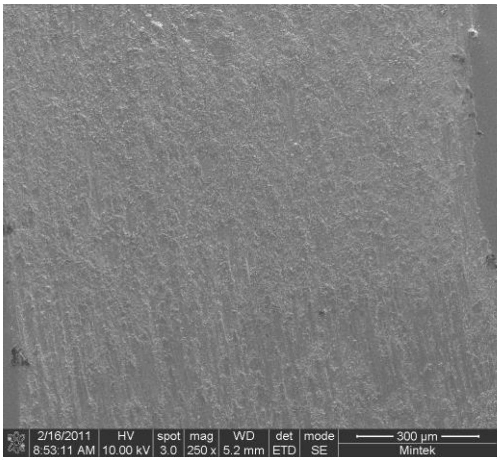


*(a)*

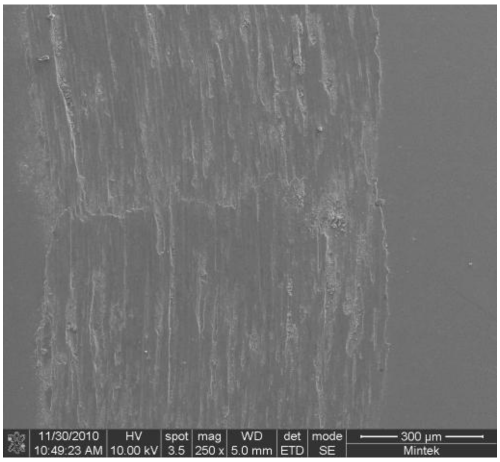


*(b)*

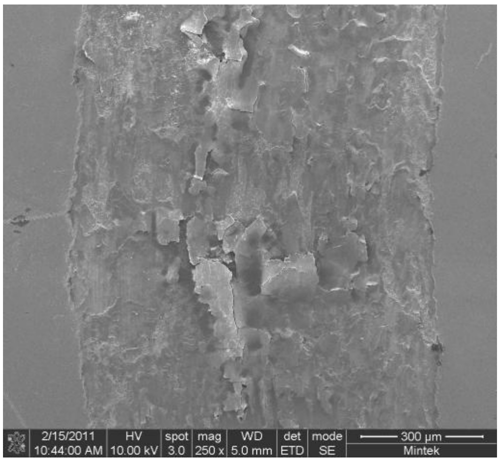


*(c)*

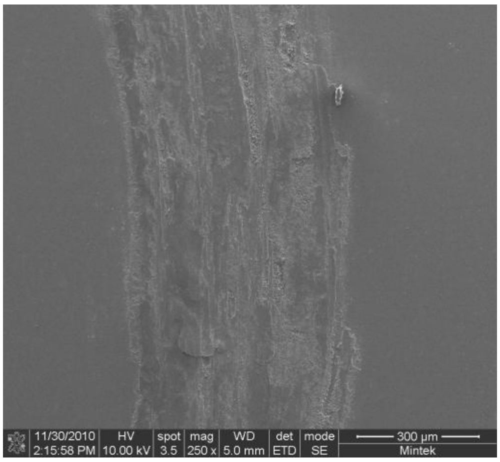


*(d)*

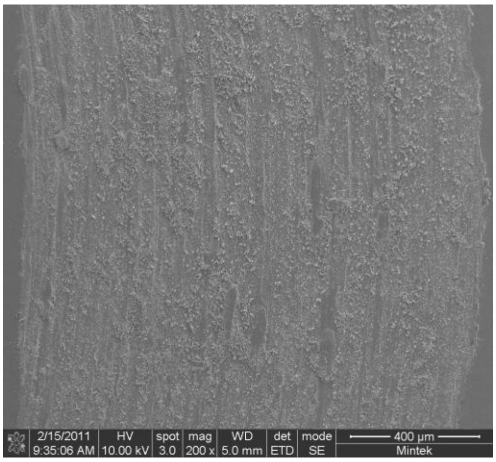


*(e)*

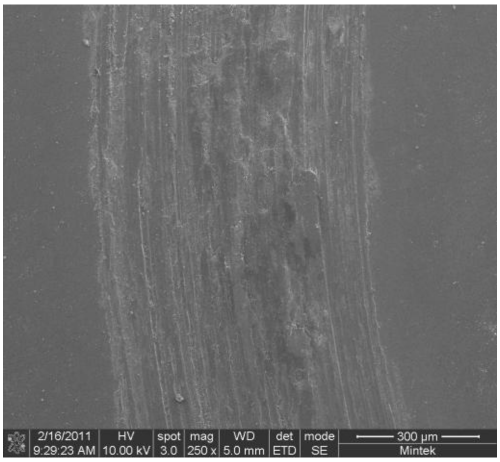


*(f)*

*Figure E.1. SEM images of the wear tracks on 304 Stainless Steel (SS) and Bright Mild Steel (CS) substrates paired as follows: (a) WC-A/SS, (b) WC-A/CS, (c) WC-B/SS, (d) WC-B/CS, (e) WC-C/SS and (f) WC-C/CS under test condition 1 (5N, $0.2ms^{-1}$).*

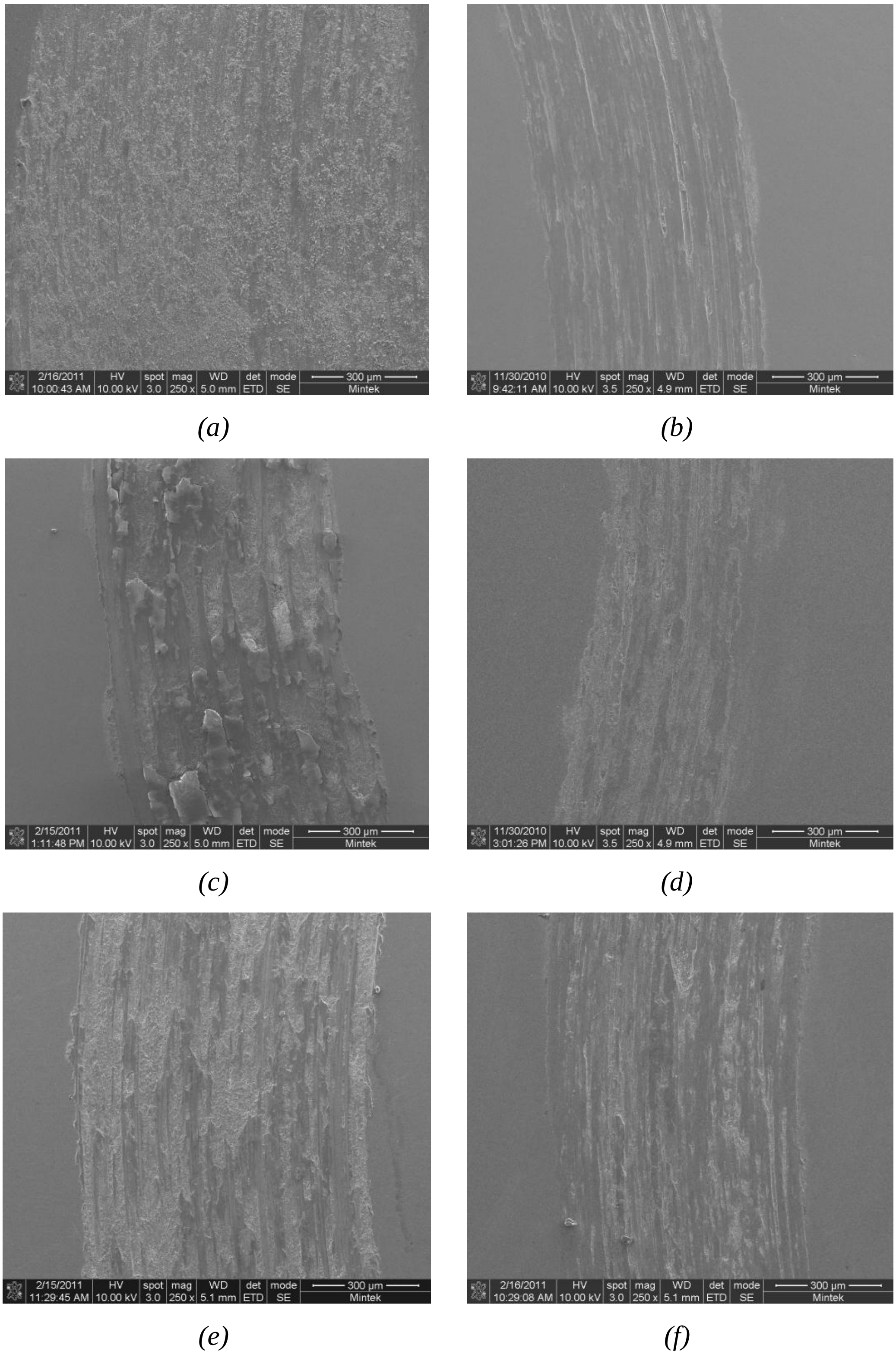


*Figure E.2. SEM images of the wear tracks on 304 Stainless Steel (SS) and Bright Mild Steel (CS) substrates paired as follows: (a) WC-A/SS, (b) WC-A/CS, (c) WC-B/SS, (d) WC-B/CS, (e) WC-C/SS and (f) WC-C/CS under test condition 2 (3N, $0.2ms^{-1}$).*

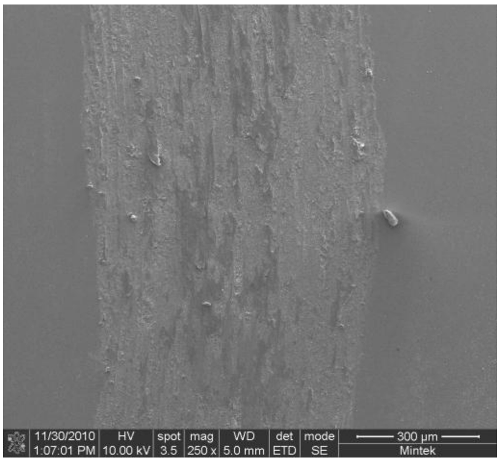


*(a)*

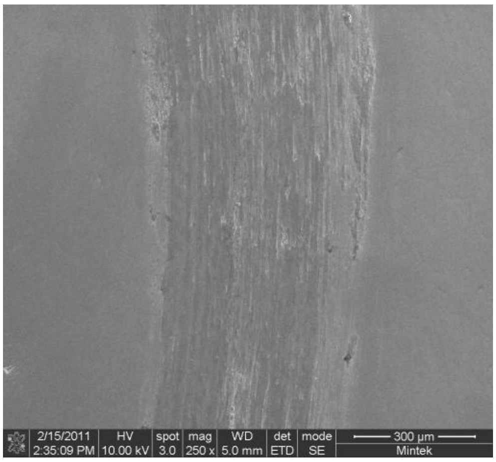


*(b)*

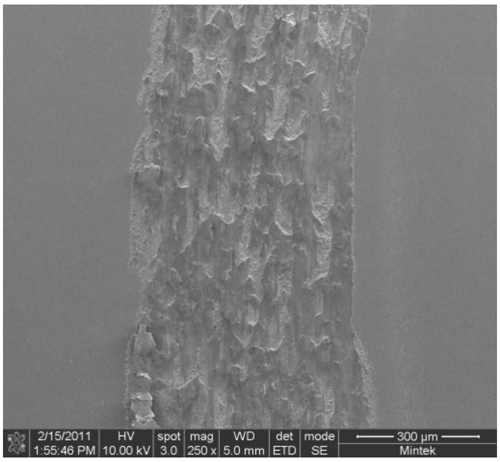


*(c)*

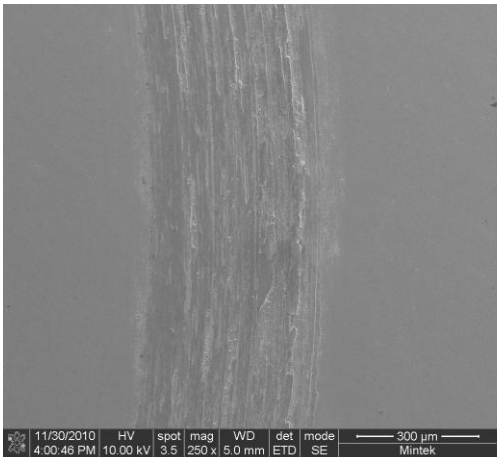


*(d)*

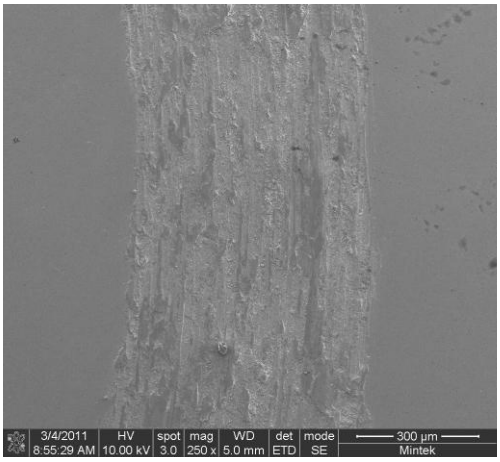


*(e)*

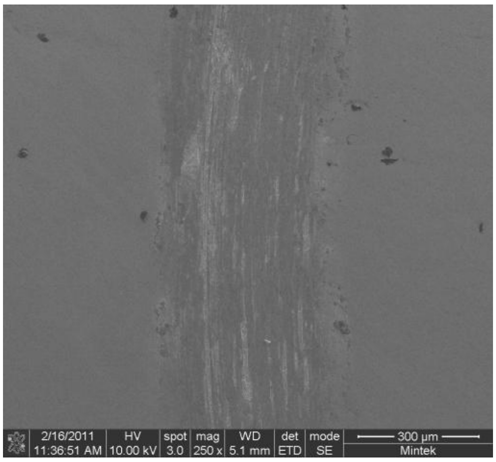


*(f)*

*Figure E.3. SEM images of the wear tracks on 304 Stainless Steel (SS) and Bright Mild Steel (CS) substrates paired as follows: (a) WC-A/SS, (b) WC-A/CS, (c) WC-B/SS, (d) WC-B/CS, (e) WC-C/SS and (f) WC-C/CS under test condition 3 (1N, 0.2ms$^{-1}$).*

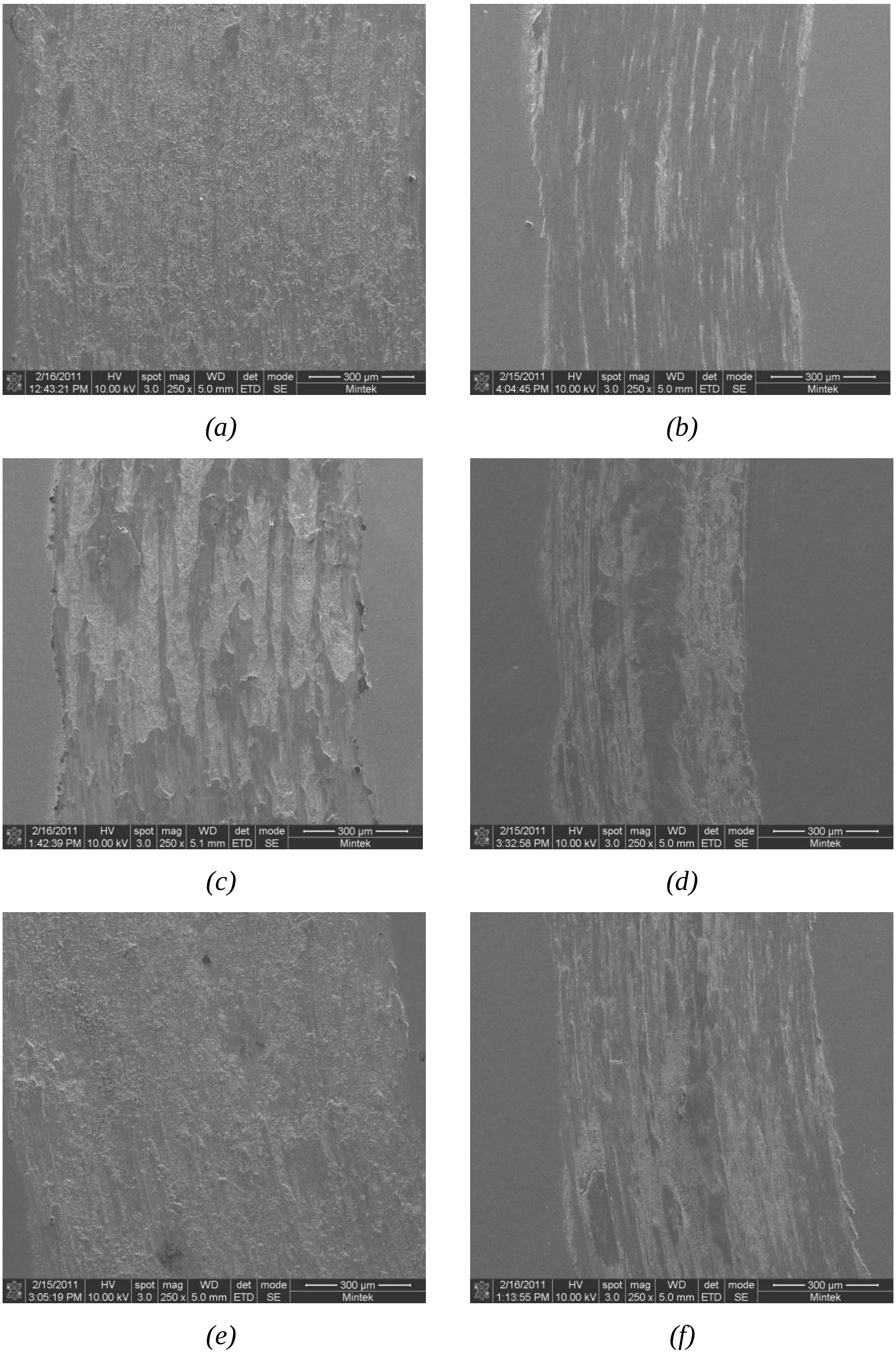


*Figure E.4. SEM images of the wear tracks on 304 Stainless Steel (SS) and Bright Mild Steel (CS) substrates paired as follows: (a) WC-A/SS, (b) WC-A/CS, (c) WC-B/SS, (d) WC-B/CS, (e) WC-C/SS and (f) WC-C/CS under test condition 4 (3N, 0.3ms$^{-1}$).*

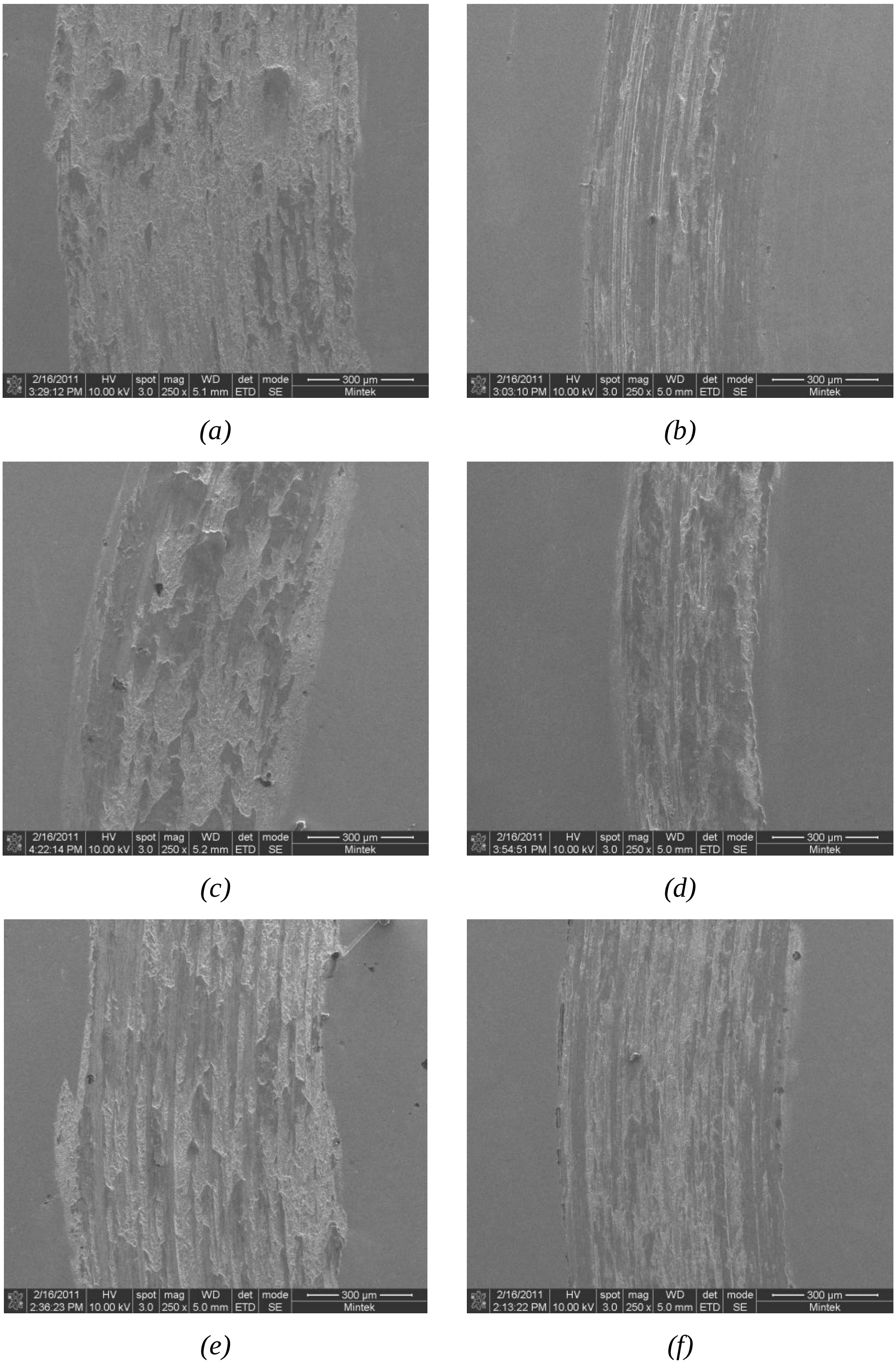


*Figure E.5. SEM images of the wear tracks on 304 Stainless Steel (SS) and Bright Mild Steel (CS) substrates paired as follows: (a) WC-A/SS, (b) WC-A/CS, (c) WC-B/SS, (d) WC-B/CS, (e) WC-C/SS and (f) WC-C/CS under test condition 5 (3N, $0.1ms^{-1}$).*

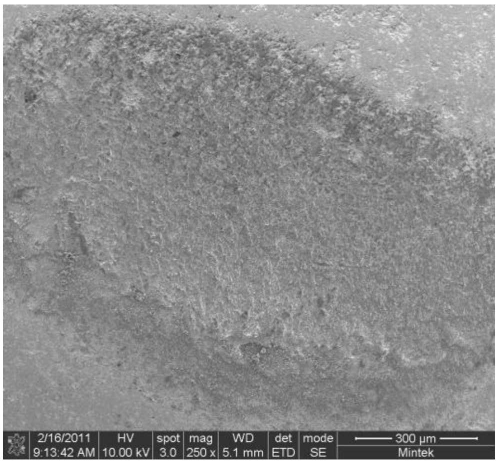


*(a)*

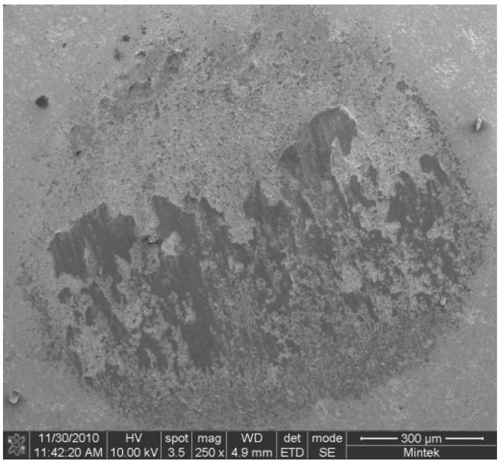


*(b)*

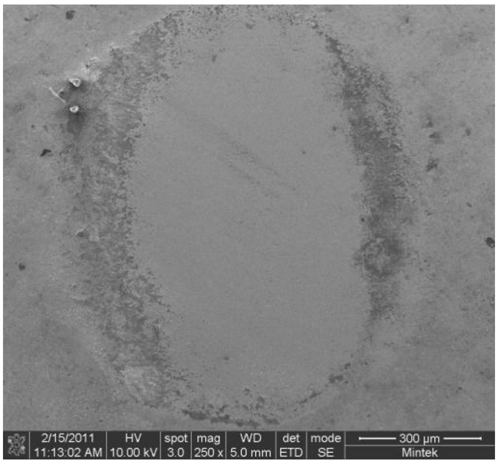


*(c)*

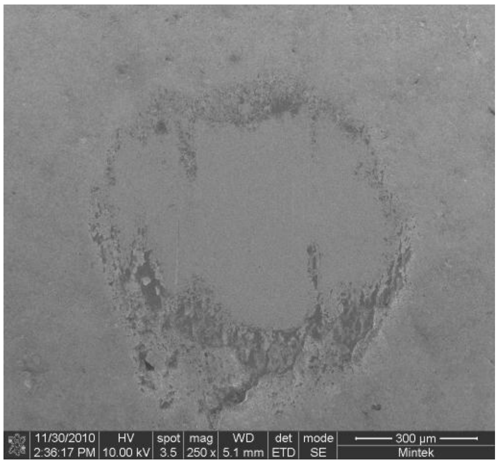


*(d)*

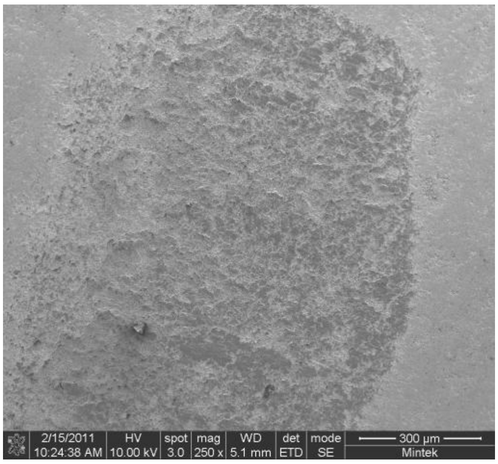


*(e)*

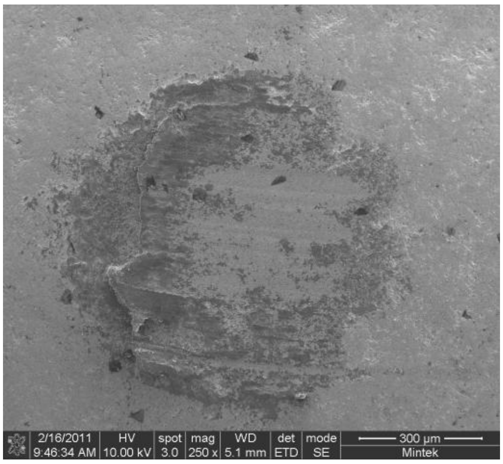


*(f)*

*Figure E.6. SEM images of the wear tracks on cemented carbide buttons paired as follows: (a) WC-A/SS, (b) WC-A/CS, (c) WC-B/SS, (d) WC-B/CS, (e) WC-C/SS and (f) WC-C/CS under test condition 1 (5N, 0.2ms$^{-1}$).*

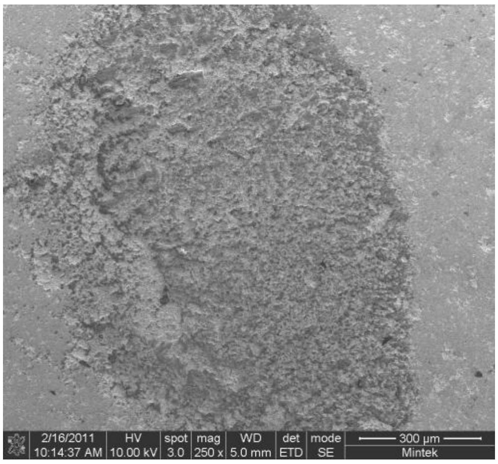


*(a)*

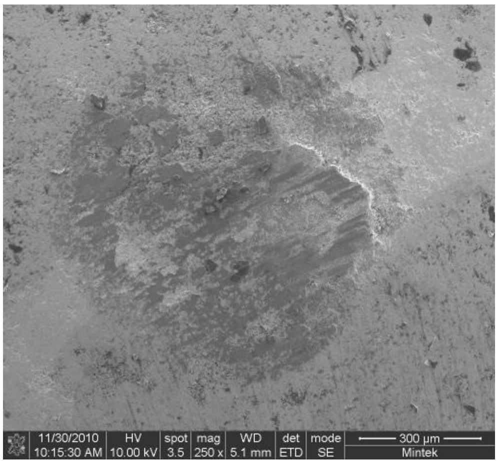


*(b)*

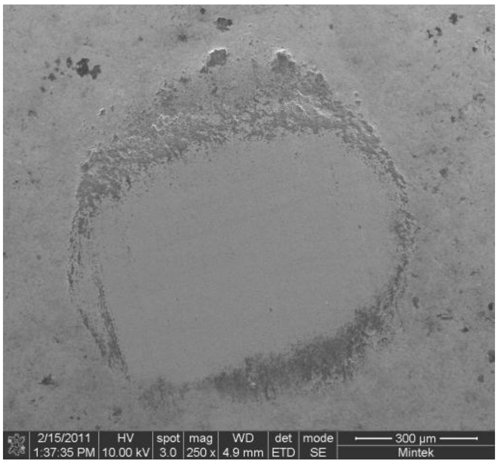


*(c)*

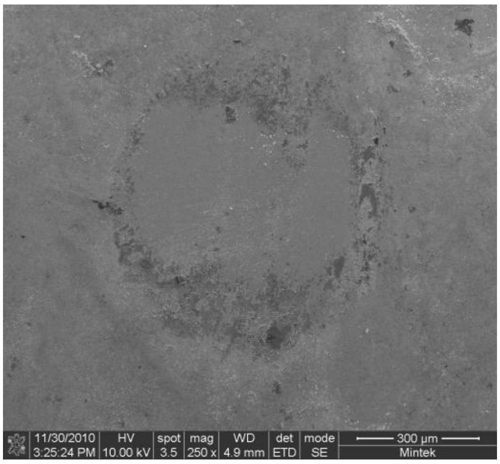


*(d)*

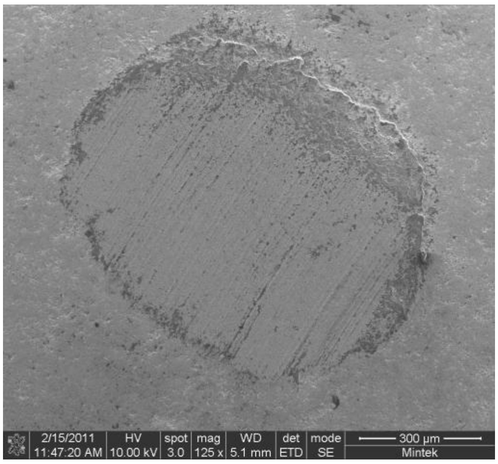


*(e)*

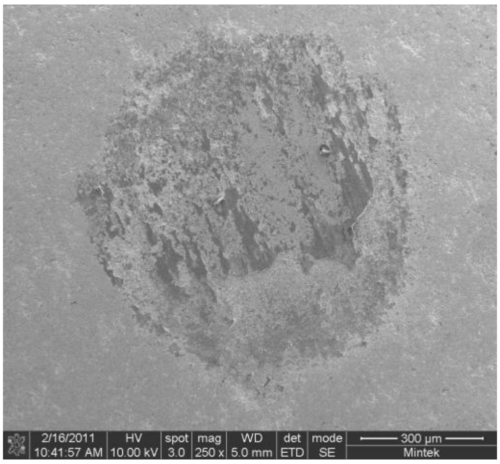


*(f)*

*Figure E.7. SEM images of the wear tracks on cemented carbide buttons paired as follows: (a) WC-A/SS, (b) WC-A/CS, (c) WC-B/SS, (d) WC-B/CS, (e) WC-C/SS and (f) WC-C/CS under test condition 2 (3N, 0.2ms$^{-1}$).*

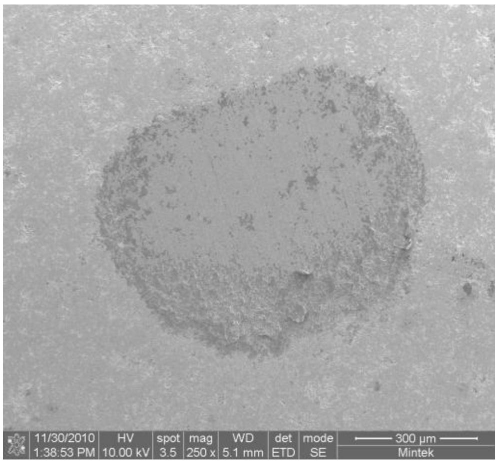


*(a)*

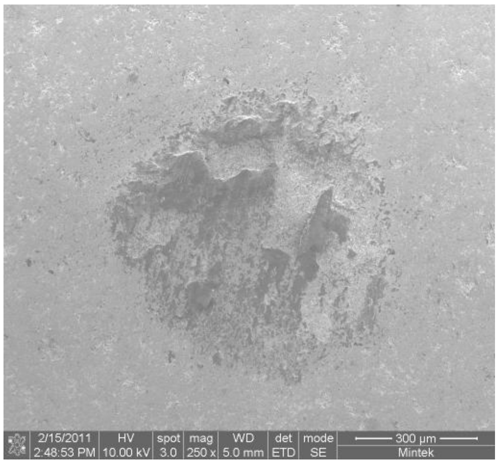


*(b)*

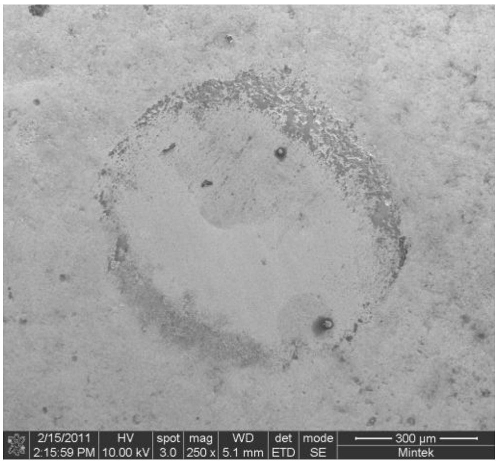


*(c)*

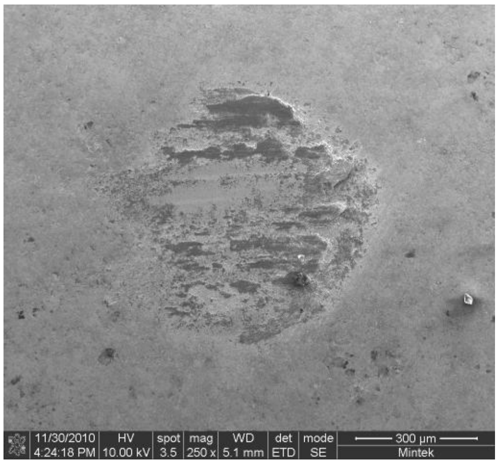


*(d)*

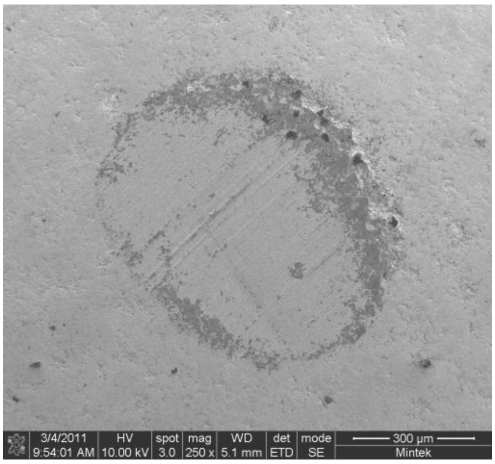


*(e)*

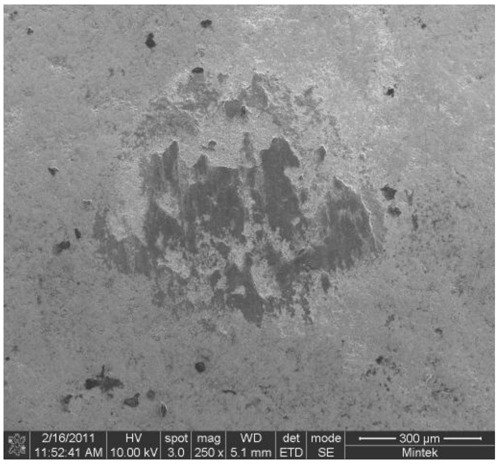


*(f)*

*Figure E.8. SEM images of the wear tracks on cemented carbide buttons paired as follows: (a) WC-A/SS, (b) WC-A/CS, (c) WC-B/SS, (d) WC-B/CS, (e) WC-C/SS and (f) WC-C/CS under test condition 3 (3N, 0.2ms$^{-1}$).*

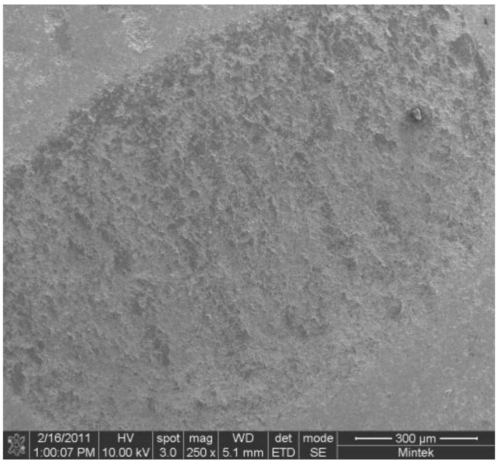


*(a)*

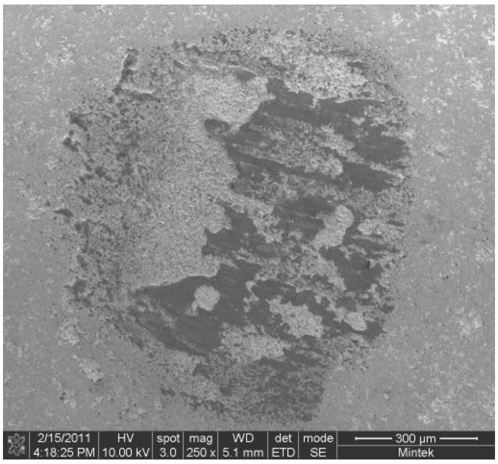


*(b)*

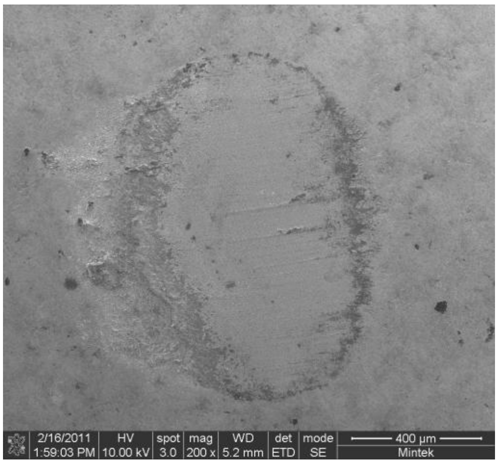


*(c)*

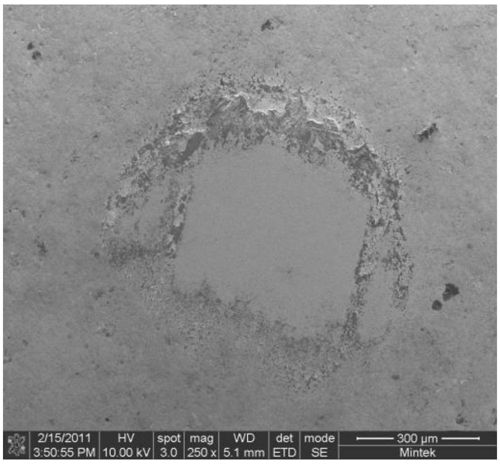


*(d)*

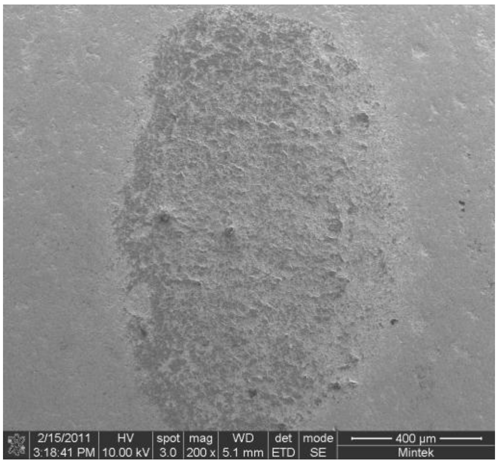


*(e)*

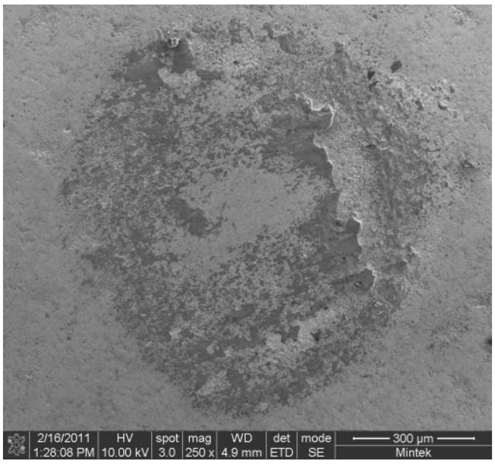


*(f)*

*Figure E.9. SEM images of the wear tracks on cemented carbide buttons paired as follows: (a) WC-A/SS, (b) WC-A/CS, (c) WC-B/SS, (d) WC-B/CS, (e) WC-C/SS and (f) WC-C/CS under test condition 4 (3N, 0.3ms$^{-1}$).*

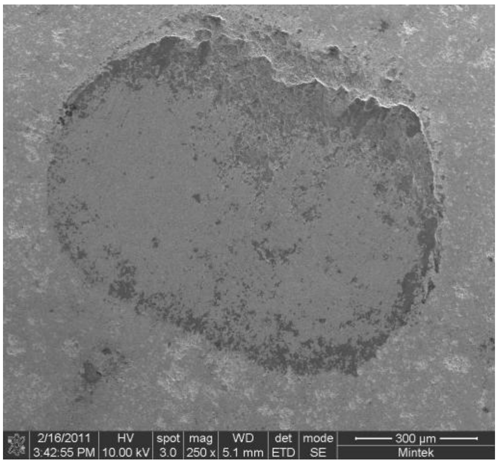


*(a)*

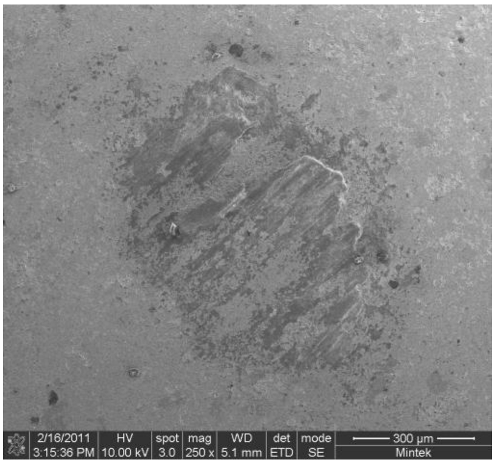


*(b)*

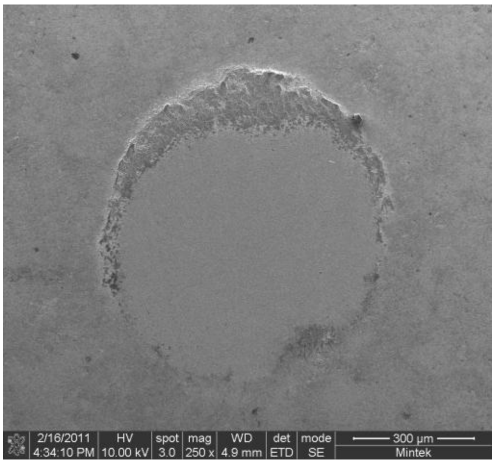


*(c)*

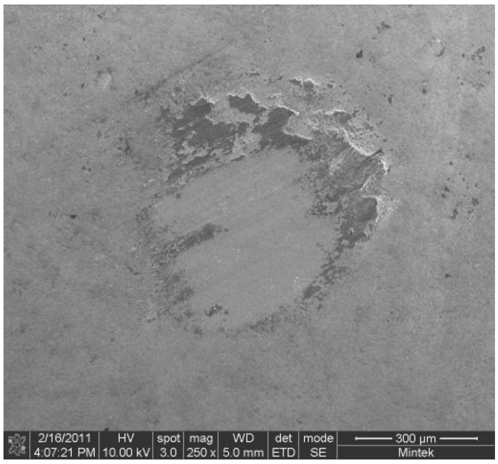


*(d)*

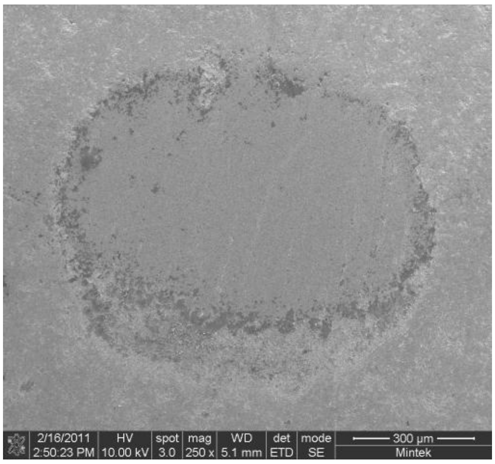


*(e)*

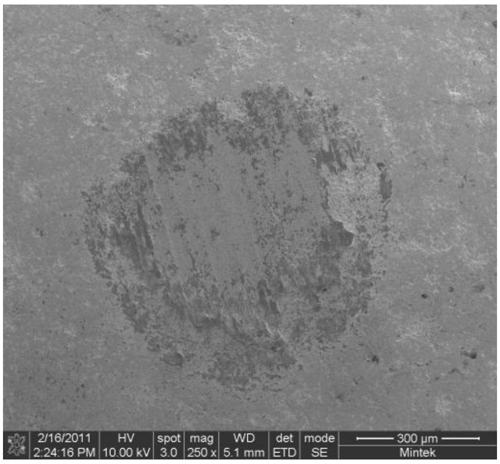


*(f)*

*Figure E.10. SEM images of the wear tracks on cemented carbide buttons paired as follows: (a) WC-A/SS, (b) WC-A/CS, (c) WC-B/SS, (d) WC-B/CS, (e) WC-C/SS and (f) WC-C/CS under test condition 5 (3N, 0.1ms$^{-1}$).*

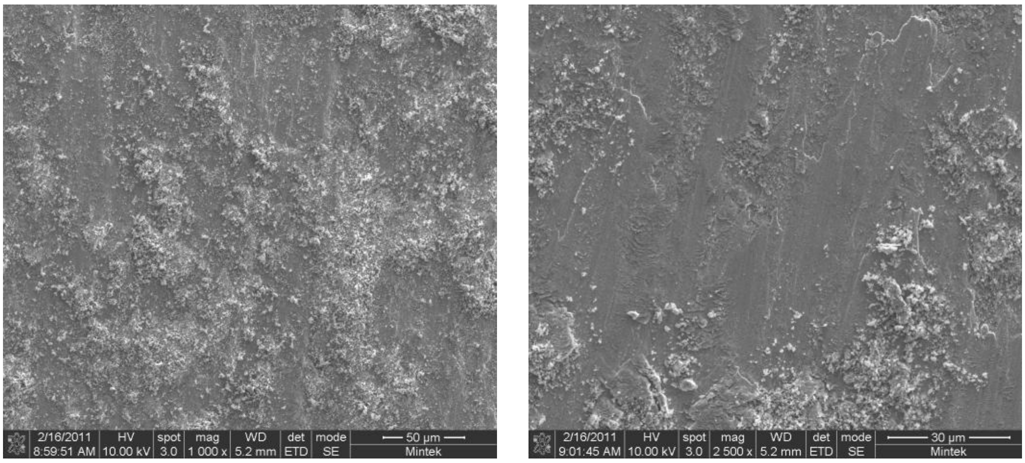


*(a)*

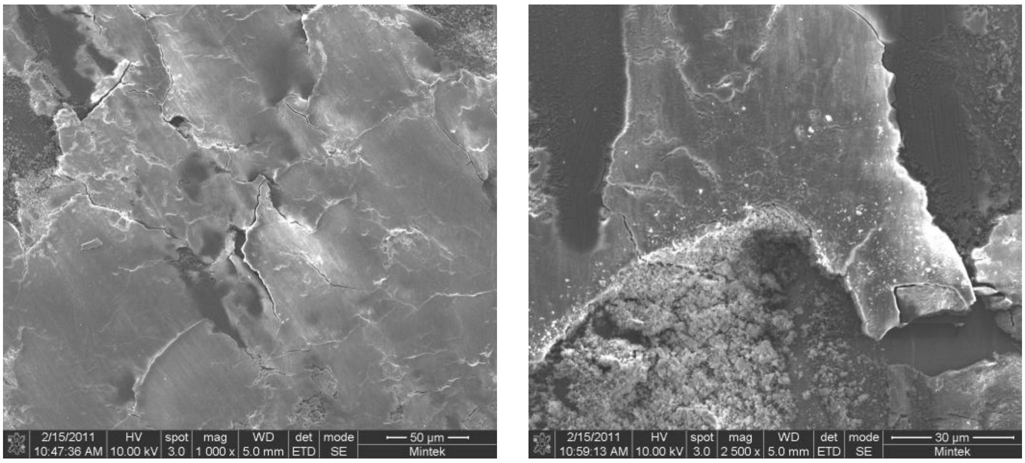


*(b)*

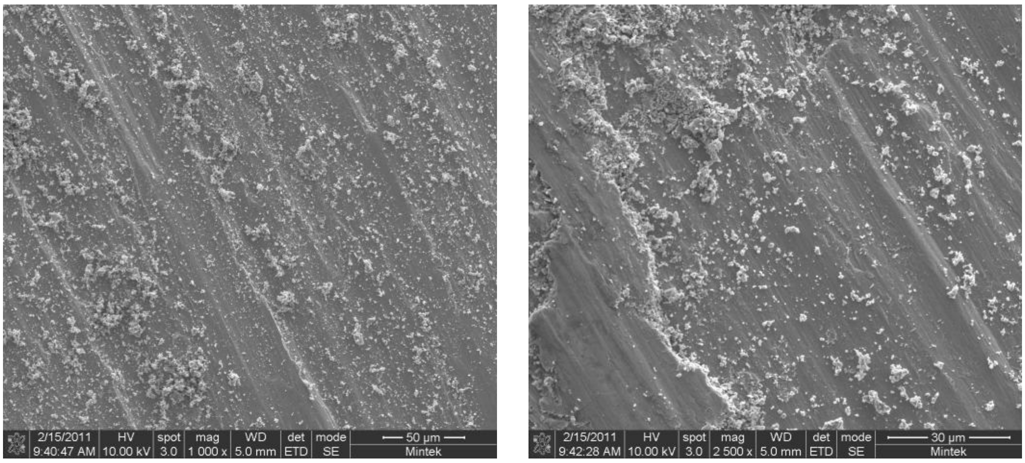


*(c)*

*Figure E.11. SEM images of the 304 Stainless Steel substrate paired with grades (a) WC-A, (b) WC-B and (c), WC-C under the most stringent test condition 1 (5N, 0.2m.s$^{-1}$).*

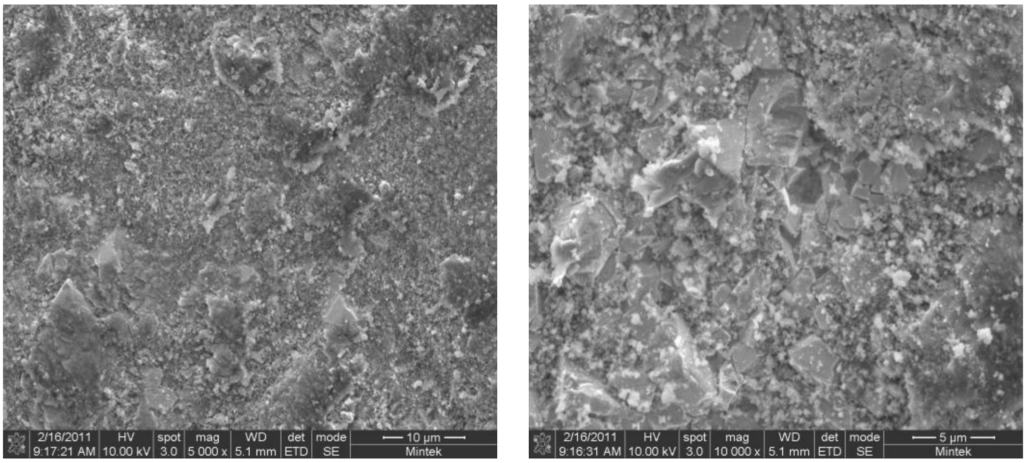


*(a)*

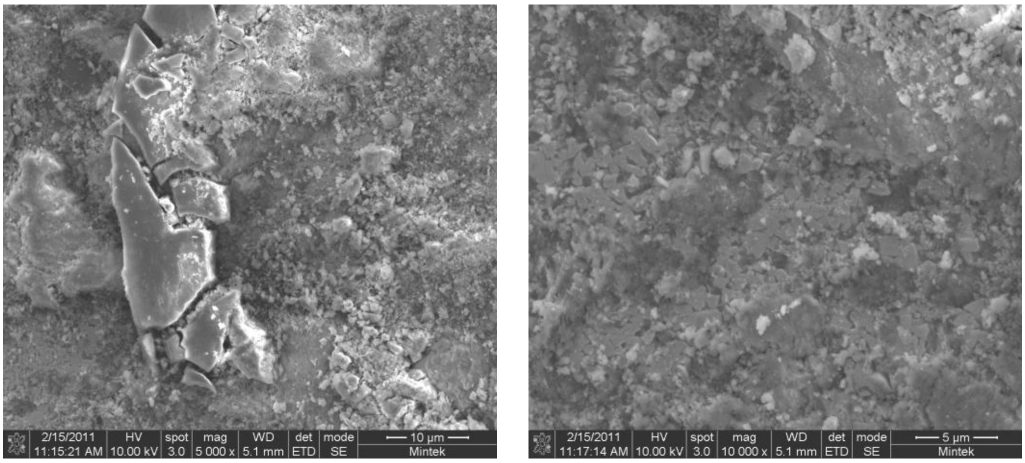


*(b)*

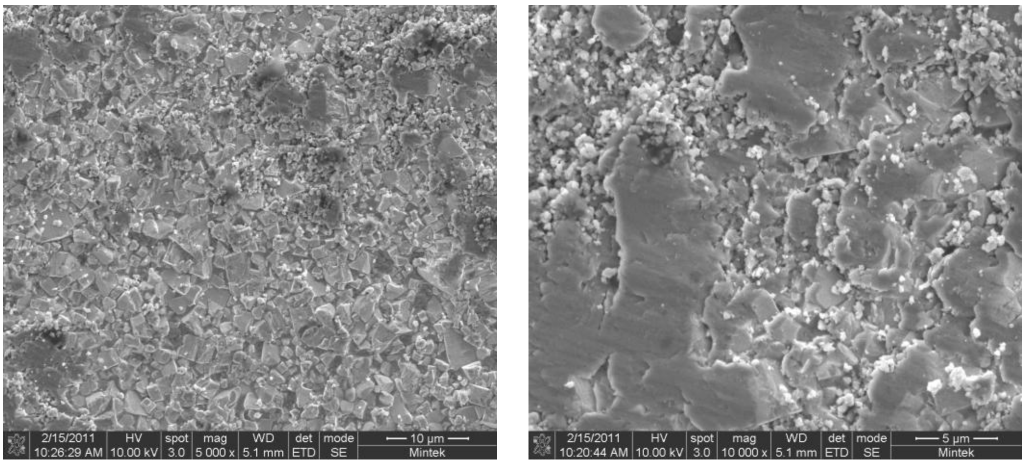


*(c)*

*Figure E.12. SEM images of the button grades (a) WC-A, (b) WC-B and (c), WC-C sliding against 304 Stainless Steel substrate under the most stringent test condition 1 (5N, 0.2m.s$^{-1}$).*

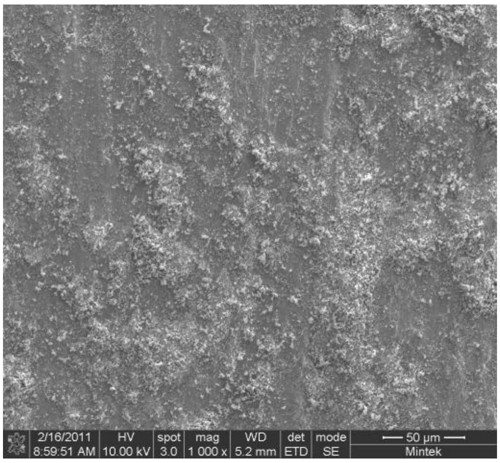


*(a)*

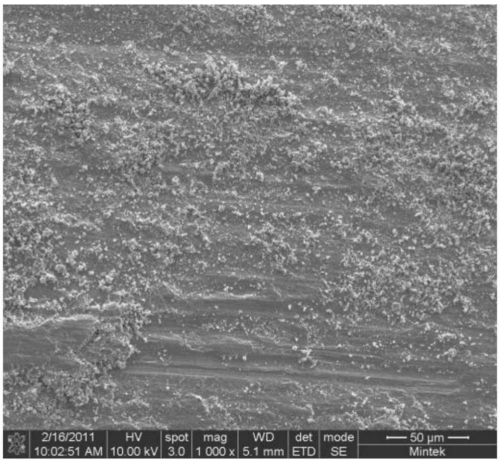


*(b)*

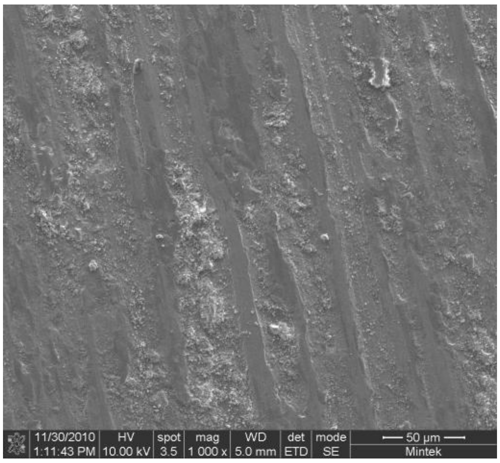


*(c)*

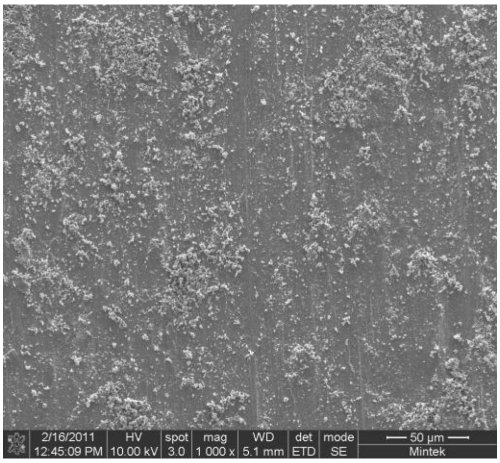


*(d)*

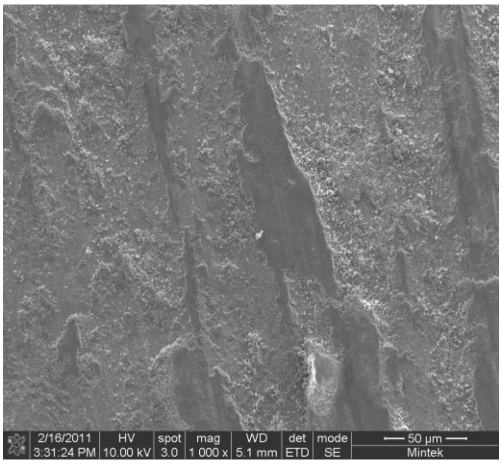


*(e)*

*Figure E.13. SEM images of the 304 Stainless Steel substrate paired with grade WC-A for all the test conditions (a) Test condition 1: 5N, 0.2m.s$^{-1}$ (b) Test condition 2: 3N, 0.2m.s$^{-1}$ (c), Test condition 3: 1N, 0.2m.s$^{-1}$, (d) Test condition 4: 3N, 0.3m.s$^{-1}$ and (e) Test condition 5: 3N, 0.1m.s$^{-1}$.*

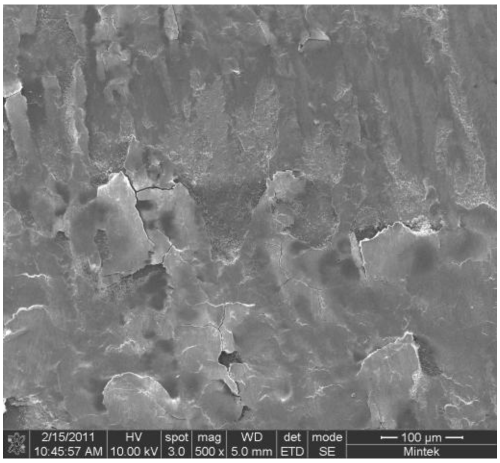


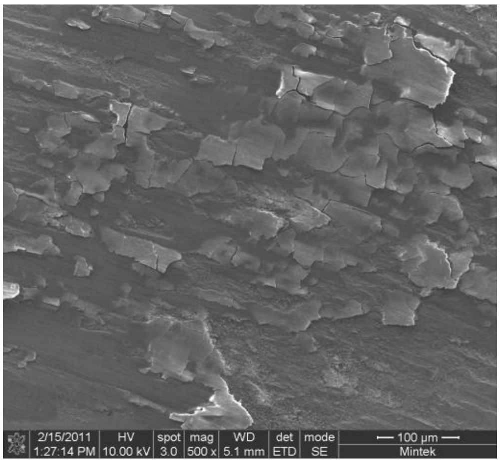


*(a)* *(b)*

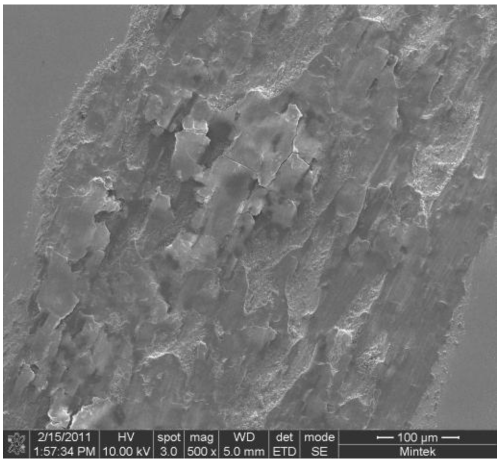


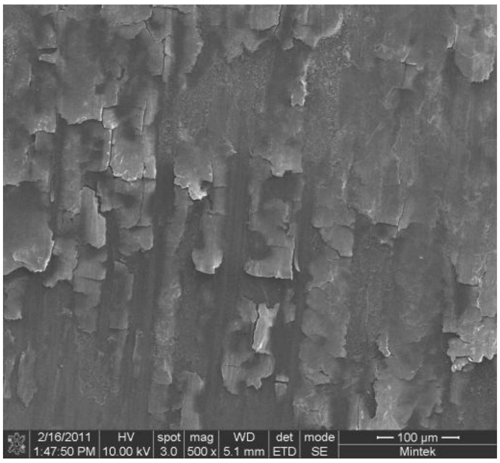


*(c)* *(d)*

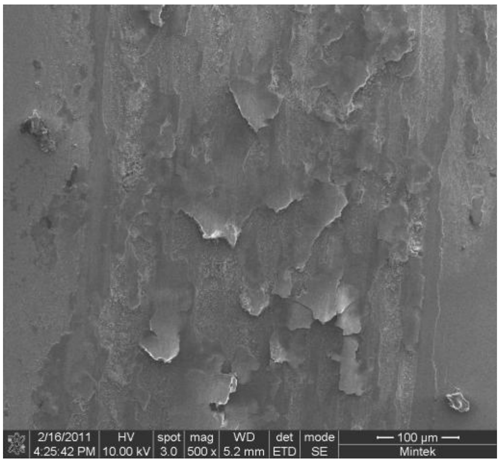


*(e)*

*Figure E.14. SEM images of the 304 Stainless Steel substrate paired with grade WC-B for all the test conditions (a) Test condition 1: 5N, 0.2m.s$^{-1}$ (b) Test condition 2: 3N, 0.2m.s$^{-1}$ (c), Test condition 3: 1N, 0.2m.s$^{-1}$, (d) Test condition 4: 3N, 0.3m.s$^{-1}$ and (e) Test condition 5: 3N, 0.1m.s$^{-1}$.*

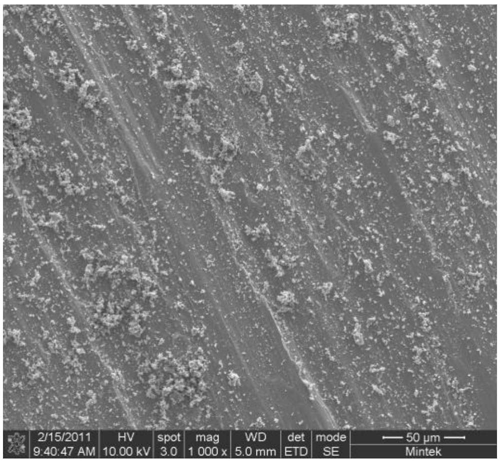


*(a)*

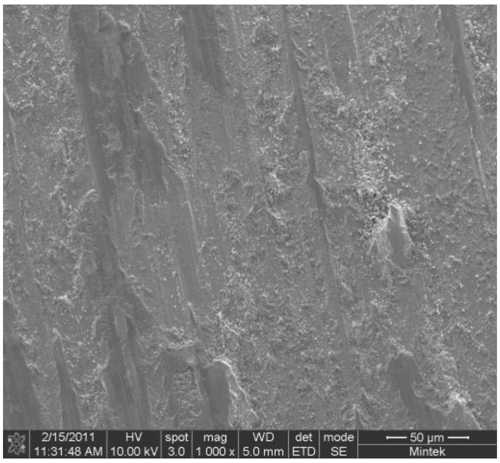


*(b)*

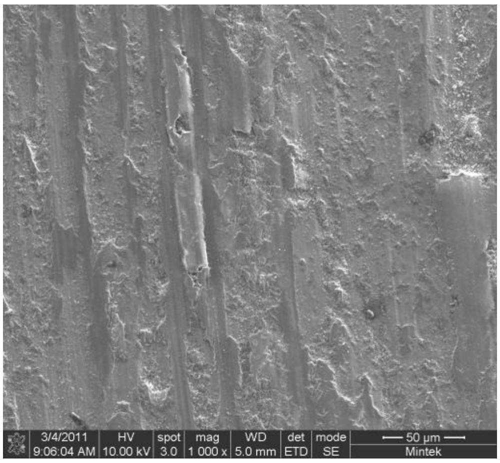


*(c)*

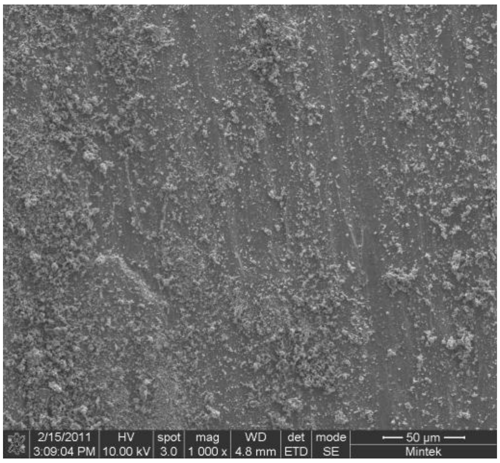


*(d)*

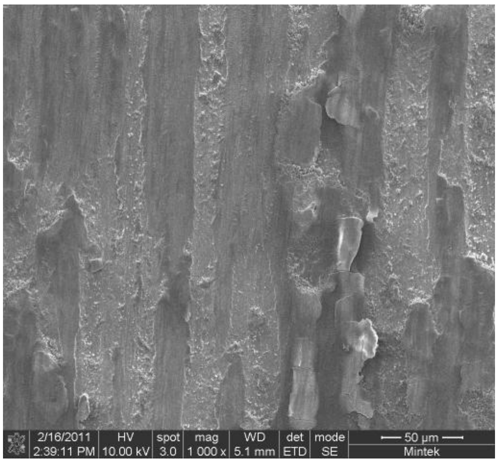


*(e)*

*Figure E.15. SEM images of the 304 Stainless Steel substrate paired with grade WC-C for all the test conditions (a) Test condition 1: 5N, 0.2m.s*$^{-1}$ *(b) Test condition 2: 3N, 0.2m.s*$^{-1}$ *(c), Test condition 3: 1N, 0.2m.s*$^{-1}$*, (d) Test condition 4: 3N, 0.3m.s*$^{-1}$ *and (e) Test condition 5: 3N, 0.1m.s*$^{-1}$*.*

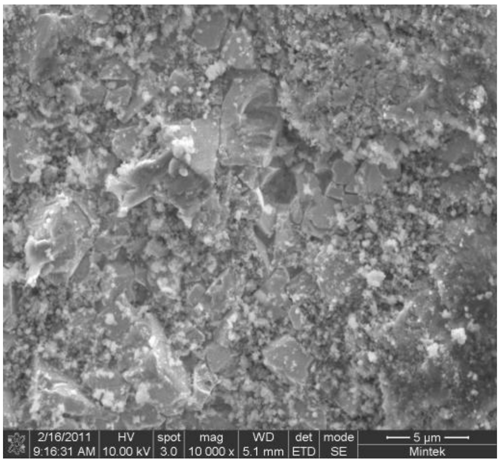


*(a)*

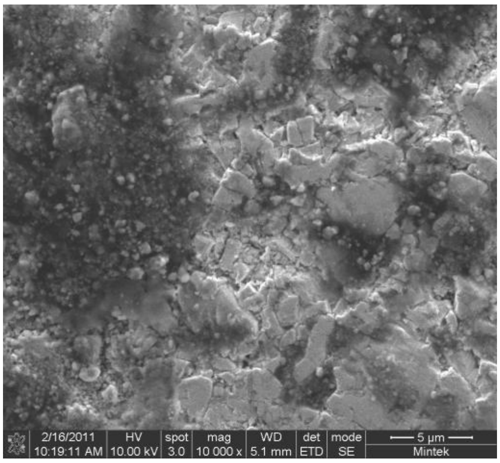


*(b)*

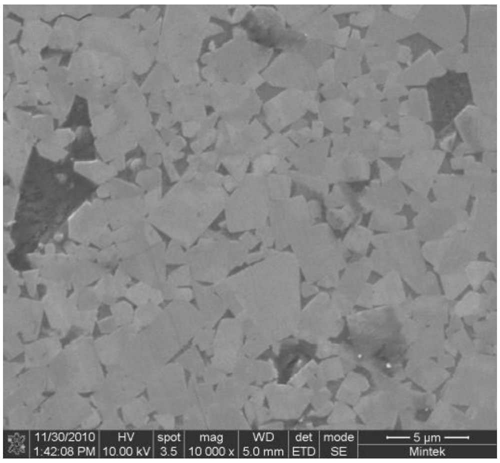


*(c)*

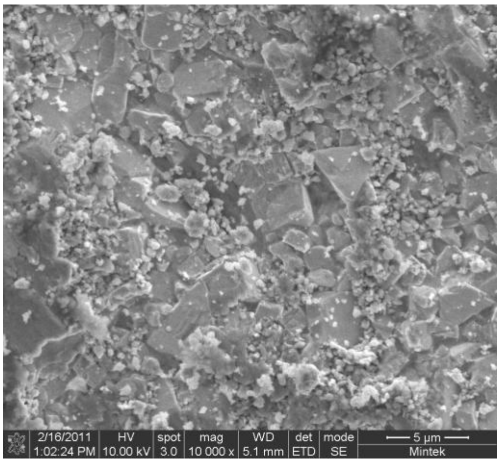


*(d)*

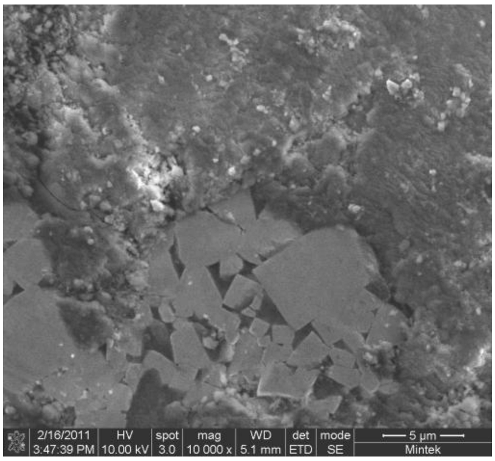


*(e)*

*Figure E.16. SEM images of button WC-A paired with 304 Stainless Steel substrate for all the test conditions (a) Test condition 1: 5N, 0.2m.s$^{-1}$ (b) Test condition 2: 3N, 0.2m.s$^{-1}$ (c), Test condition 3: 1N, 0.2m.s$^{-1}$, (d) Test condition 4: 3N, 0.3m.s$^{-1}$ and (e) Test condition 5: 3N, 0.1m.s$^{-1}$.*

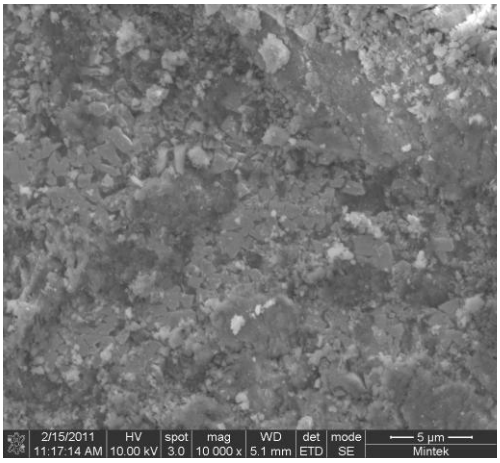


*(a)*

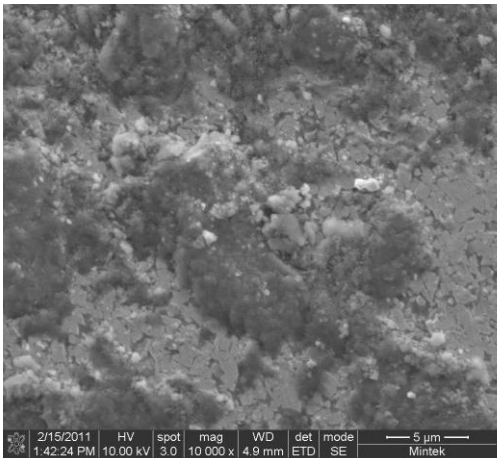


*(b)*

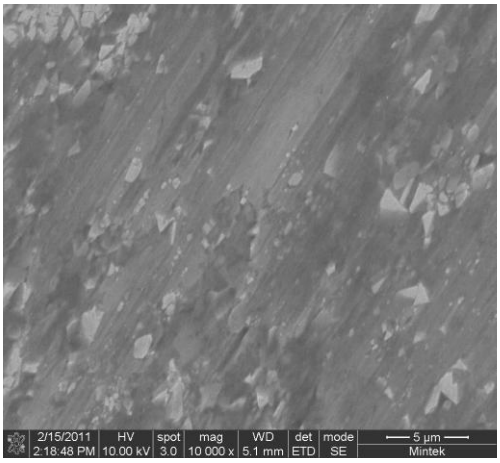


*(c)*

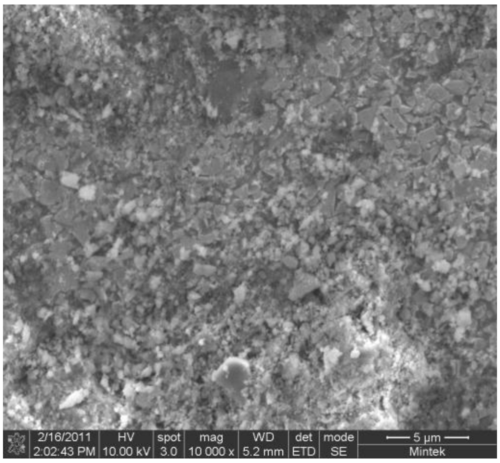


*(d)*

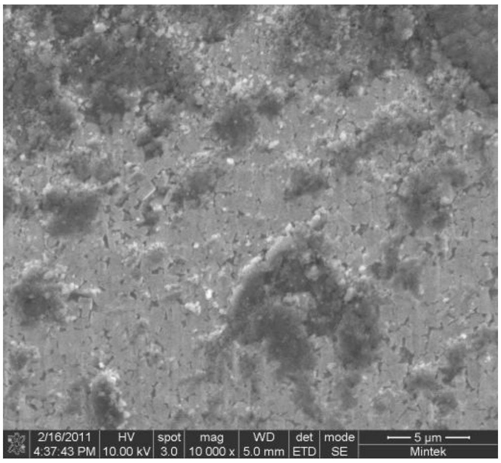


*(e)*

*Figure E.17. SEM images of button WC-B paired with 304 Stainless Steel substrate for all the test conditions (a) Test condition 1: 5N, 0.2m.s$^{-1}$ (b) Test condition 2: 3N, 0.2m.s$^{-1}$ (c), Test condition 3: 1N, 0.2m.s$^{-1}$, (d) Test condition 4: 3N, 0.3m.s$^{-1}$ and (e) Test condition 5: 3N, 0.1m.s$^{-1}$.*

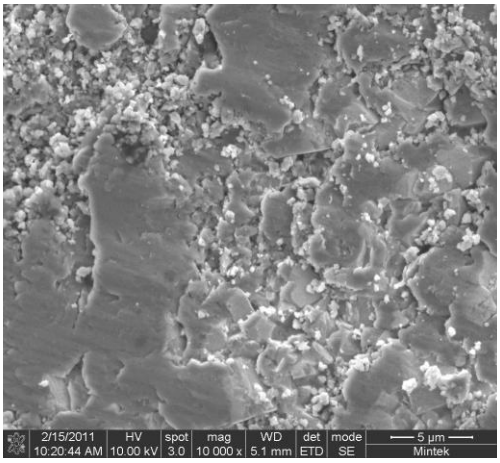


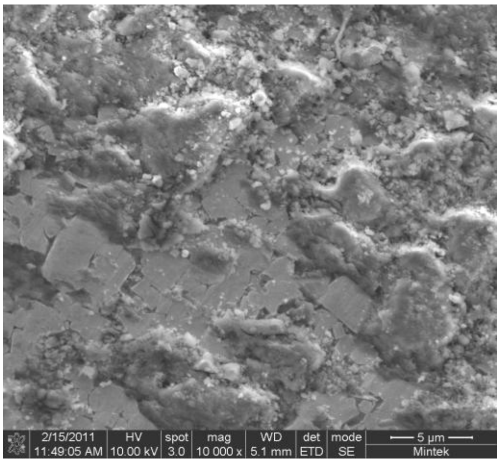


*(a)* *(b)*

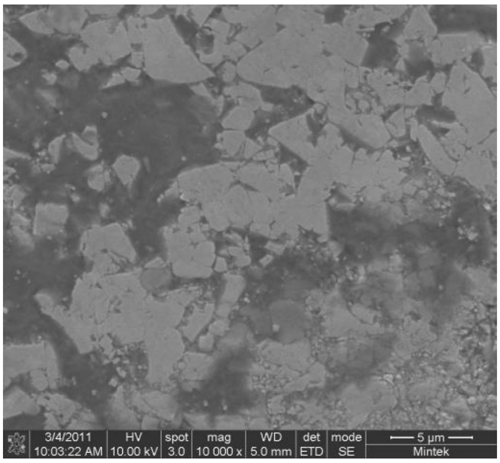


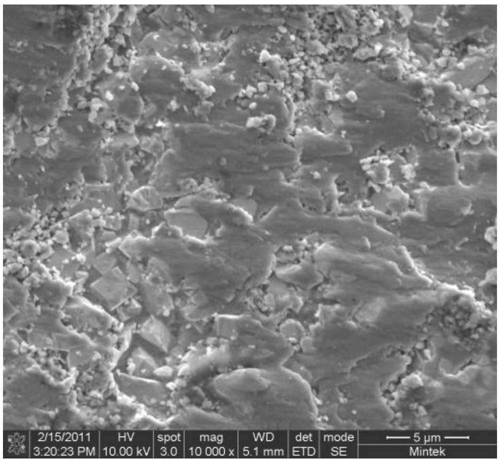


*(c)* *(d)*

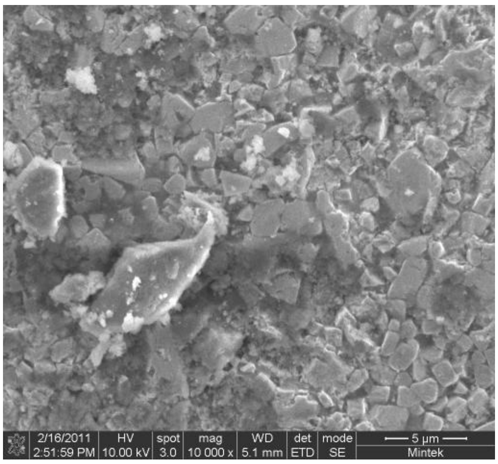


*(e)*

*Figure E.18. SEM images of button WC-C paired with 304 Stainless Steel substrate for all the test conditions (a) Test condition 1: 5N, 0.2m.s$^{-1}$ (b) Test condition 2: 3N, 0.2m.s$^{-1}$ (c), Test condition 3: 1N, 0.2m.s$^{-1}$, (d) Test condition 4: 3N, 0.3m.s$^{-1}$ and (e) Test condition 5: 3N, 0.1m.s$^{-1}$.*

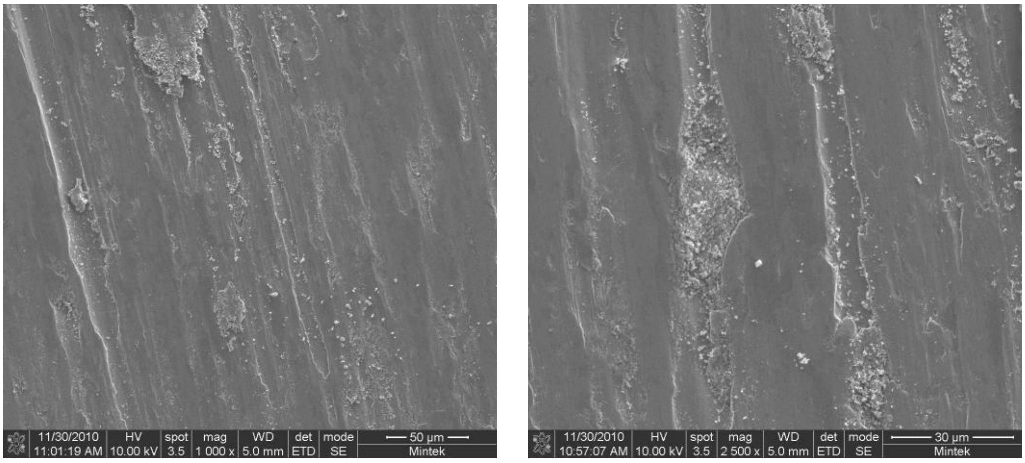


*(a)*

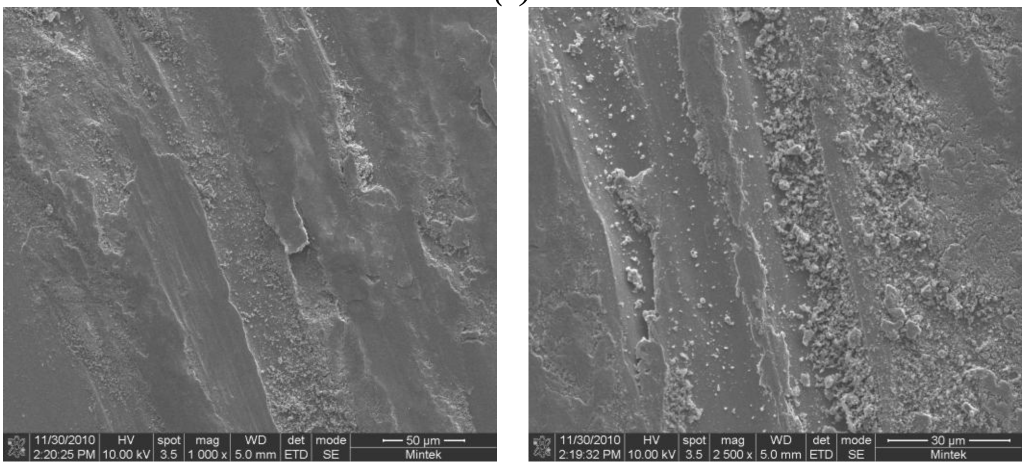


*(b)*

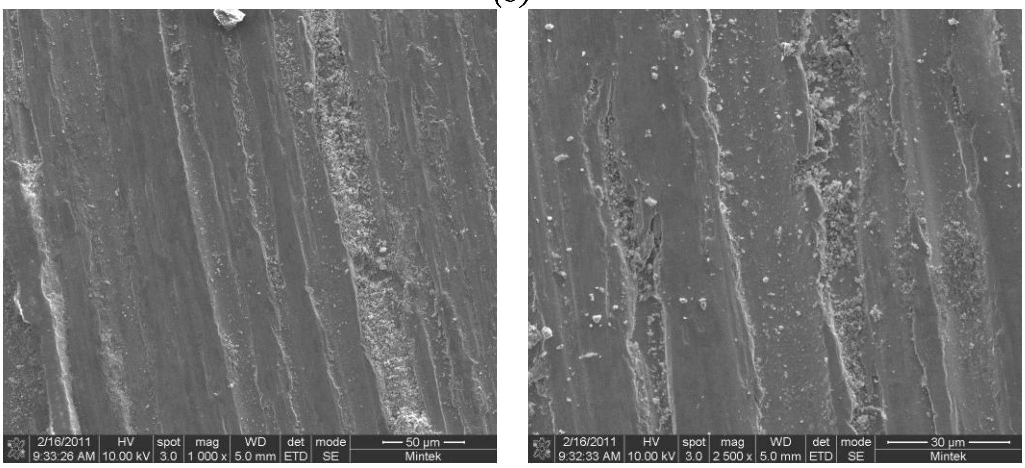


*(c)*

*Figure E.19. SEM images of the Bright Mild Steel substrate paired with grades (a) WC-A, (b) WC-B and (c), WC-C under the most stringent test condition 1 (5N, 0.2m.s$^{-1}$).*

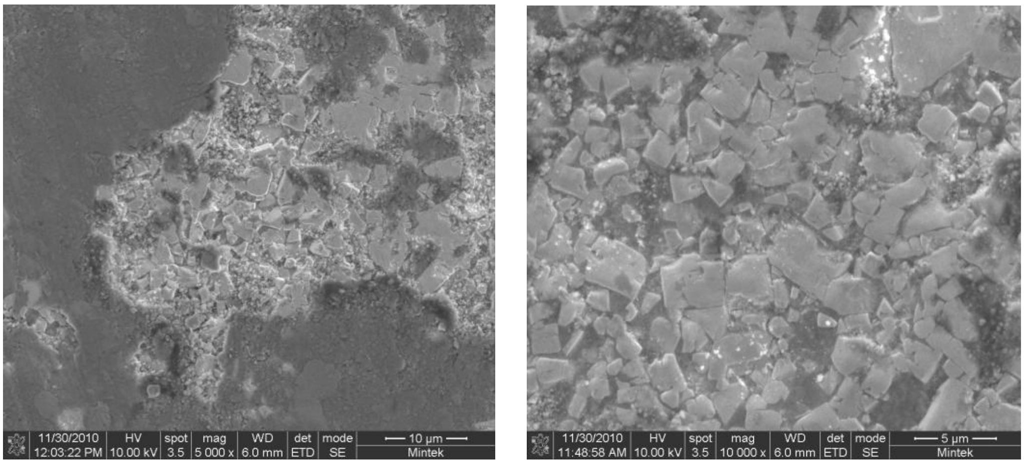


*(a)*

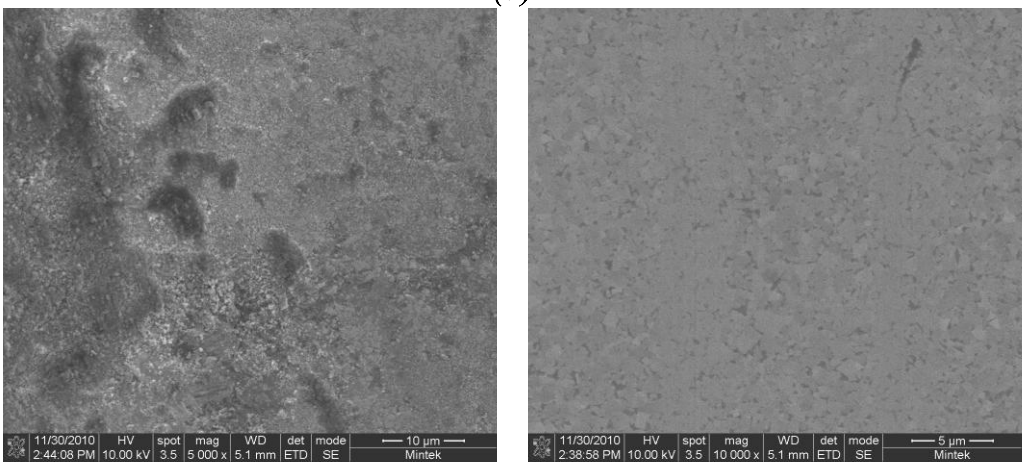


*(b)*

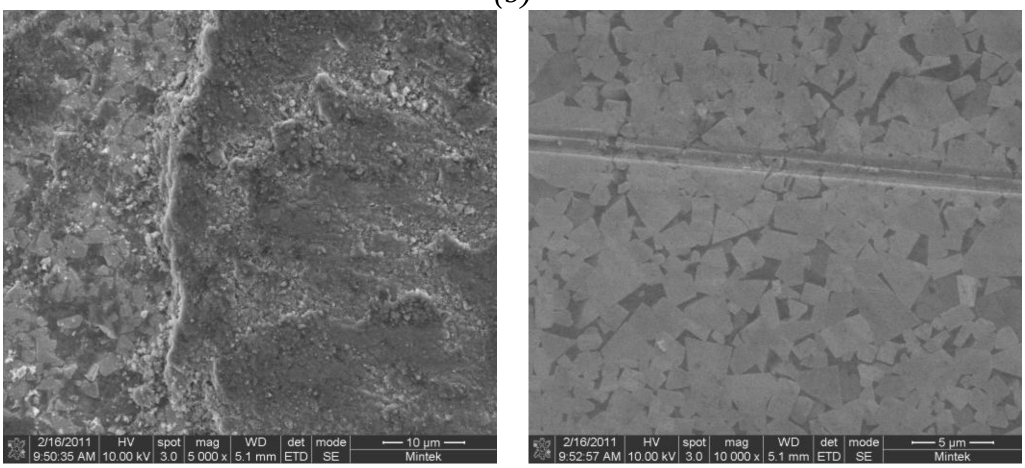


*(c)*

*Figure E.20. SEM images of the button grades (a) WC-A, (b) WC-B and (c), WC-C sliding against Bright Mild Steel substrate under the most stringent test condition 1 (5N, 0.2m.s$^{-1}$).*

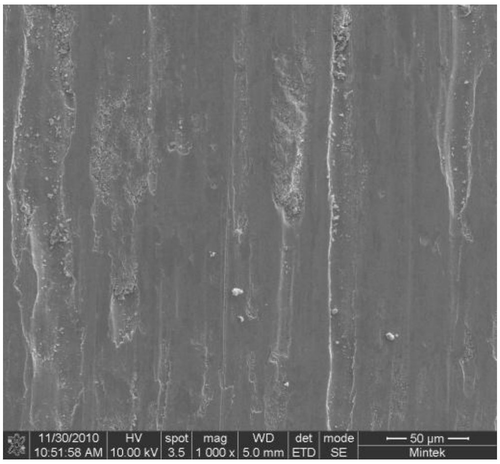


*(a)*

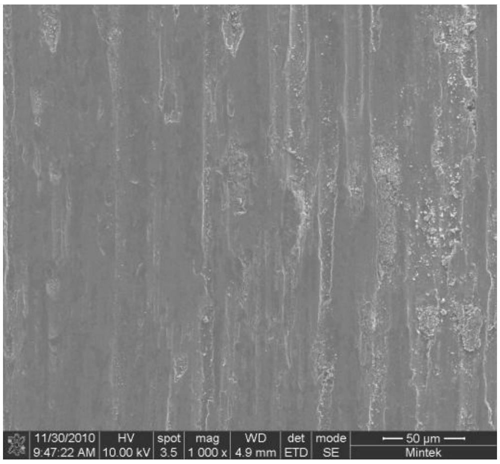


*(b)*

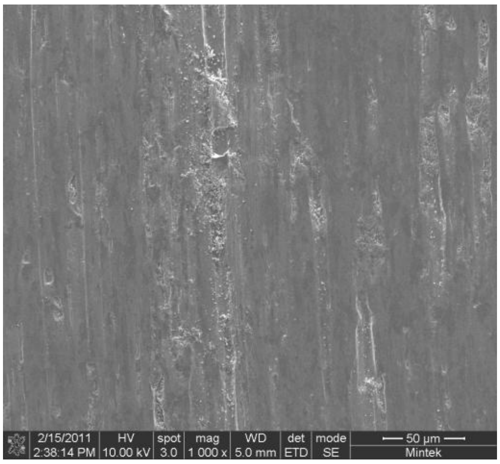


*(c)*

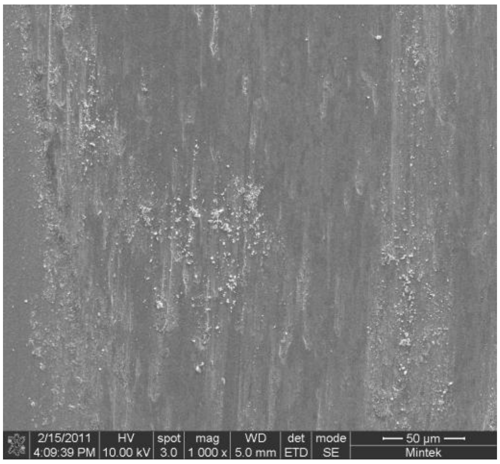


*(d)*

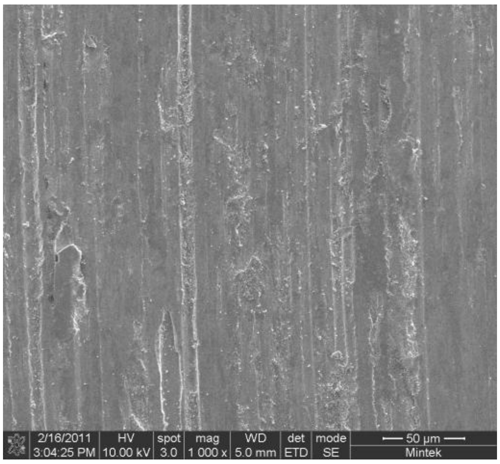


*(e)*

*Figure E.21. SEM images of the Bright Mild Steel substrate paired with grade WC-A for all the test conditions (a) Test condition 1: 5N, 0.2m.s$^{-1}$ (b) Test condition 2: 3N, 0.2m.s$^{-1}$ (c), Test condition 3: 1N, 0.2m.s$^{-1}$, (d) Test condition 4: 3N, 0.3m.s$^{-1}$ and (e) Test condition 5: 3N, 0.1m.s$^{-1}$.*

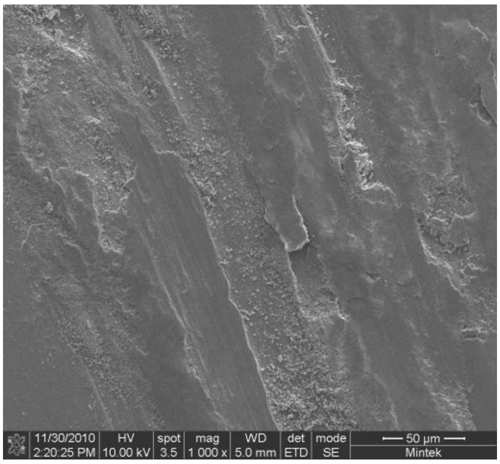


*(a)*

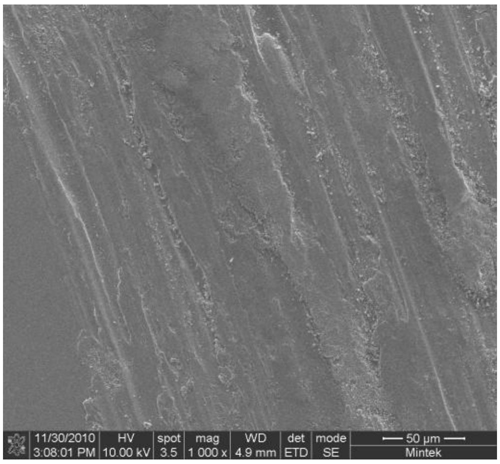


*(b)*

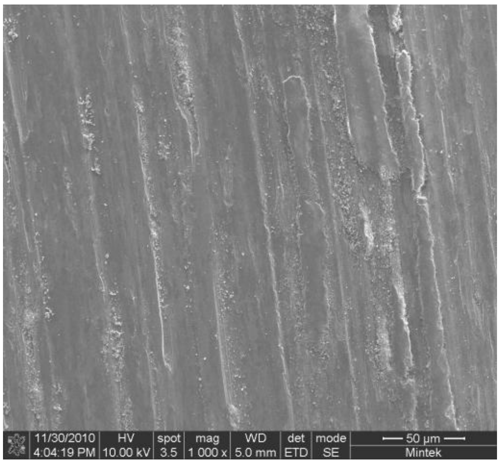


*(c)*

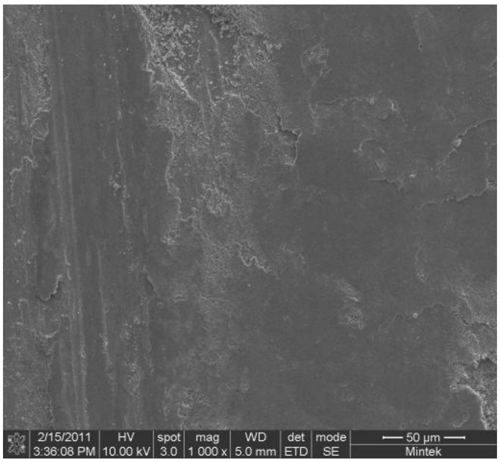


*(d)*

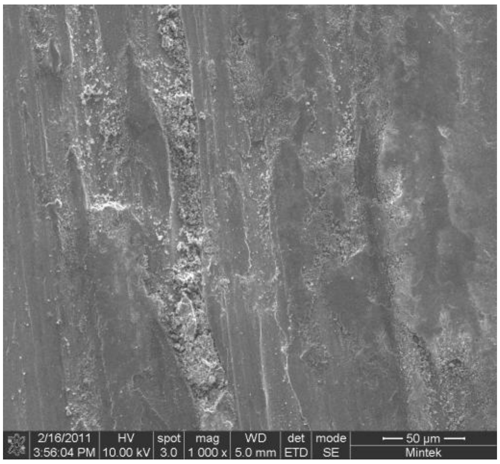


*(e)*

*Figure E.22. SEM images of the Bright Mild Steel substrate paired with grade WC-B for all the test conditions (a) Test condition 1: 5N, 0.2m.s$^{-1}$ (b) Test condition 2: 3N, 0.2m.s$^{-1}$ (c), Test condition 3: 1N, 0.2m.s$^{-1}$, (d) Test condition 4: 3N, 0.3m.s$^{-1}$ and (e) Test condition 5: 3N, 0.1m.s$^{-1}$.*

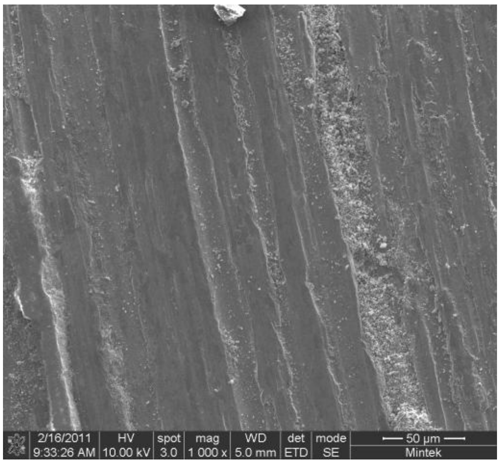


*(a)*

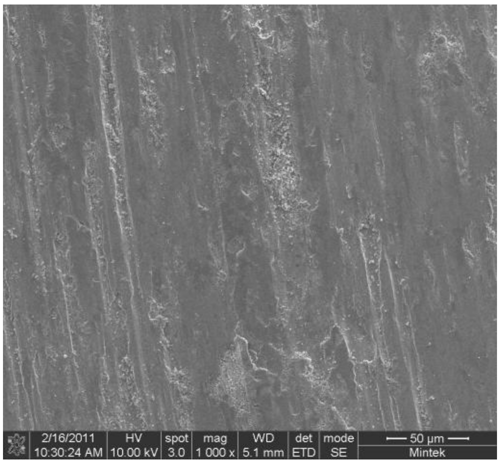


*(b)*

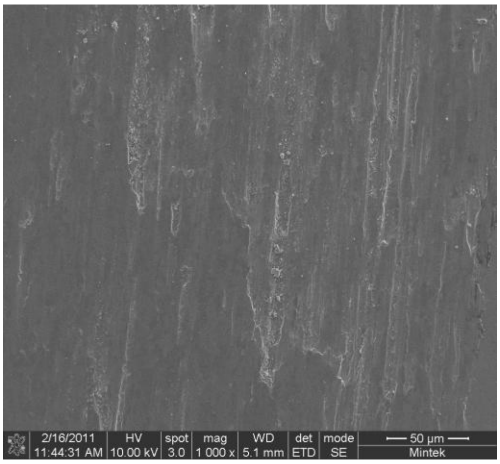


*(c)*

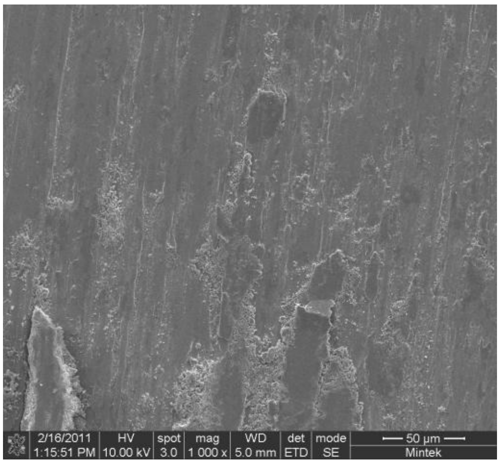


*(d)*

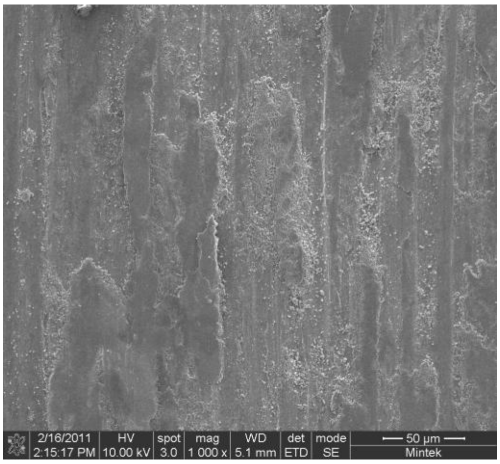


*(e)*

*Figure E.23. SEM images of the Bright Mild Steel substrate paired with grade WC-C for all the test conditions (a) Test condition 1: 5N, 0.2m.s$^{-1}$ (b) Test condition 2: 3N, 0.2m.s$^{-1}$ (c), Test condition 3: 1N, 0.2m.s$^{-1}$, (d) Test condition 4: 3N, 0.3m.s$^{-1}$ and (e) Test condition 5: 3N, 0.1m.s$^{-1}$.*

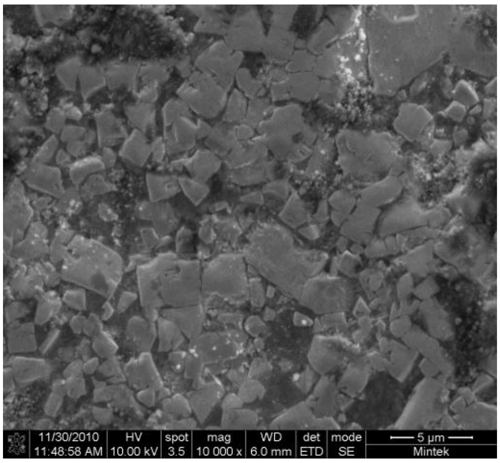


*(a)*

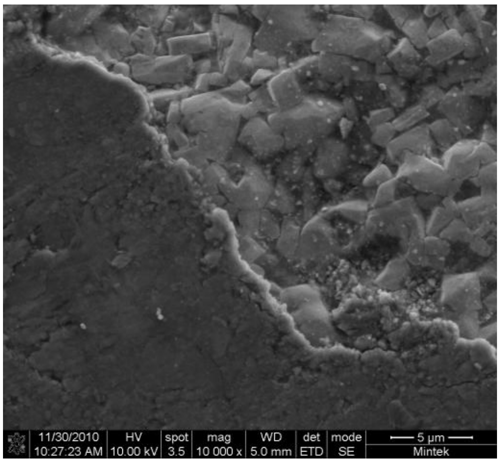


*(b)*

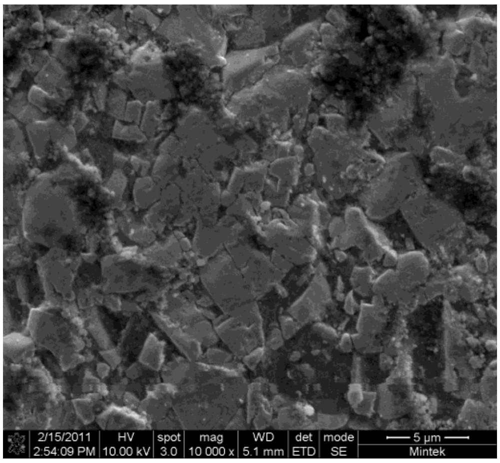


*(c)*

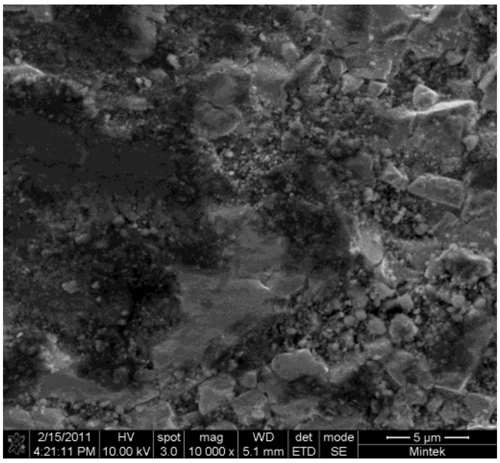


*(d)*

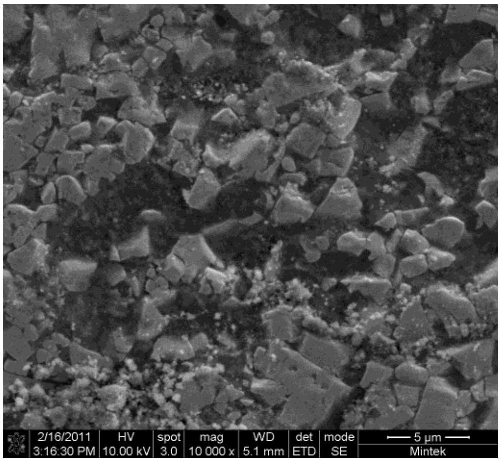


*(e)*

*Figure E.24. SEM images of button WC-A paired with Bright Mild Steel substrate for all the test conditions (a) Test condition 1: 5N, 0.2m.s$^{-1}$ (b) Test condition 2: 3N, 0.2m.s$^{-1}$ (c), Test condition 3: 1N, 0.2m.s$^{-1}$, (d) Test condition 4: 3N, 0.3m.s$^{-1}$ and (e) Test condition 5: 3N, 0.1m.s$^{-1}$.*

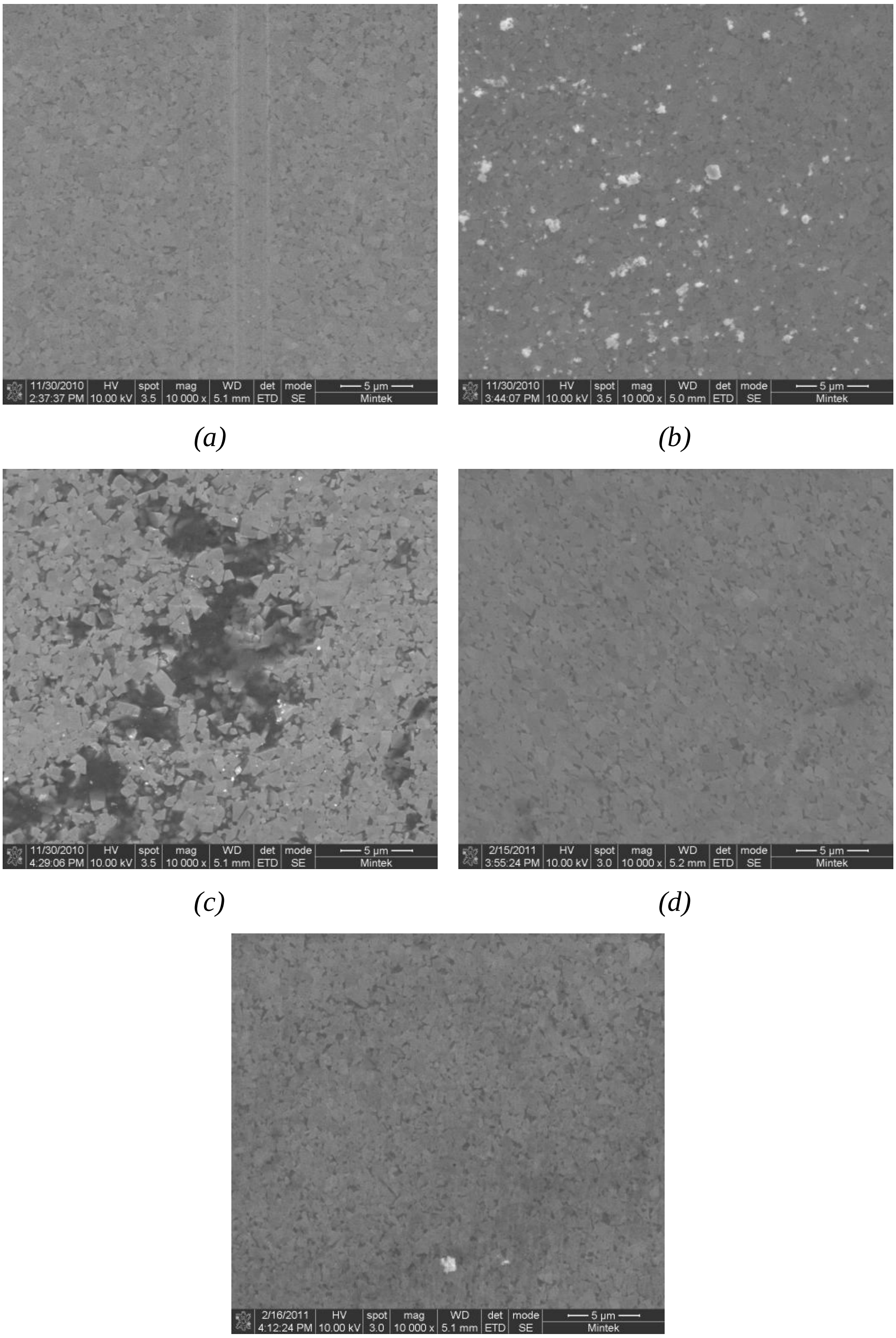

*(a)* *(b)* *(c)* *(d)* *(e)*

*Figure E.25. SEM images of button WC-B paired with Bright Mild Steel substrate for all the test conditions (a) Test condition 1: 5N, 0.2m.s$^{-1}$ (b) Test condition 2: 3N, 0.2m.s$^{-1}$ (c), Test condition 3: 1N, 0.2m.s$^{-1}$, (d) Test condition 4: 3N, 0.3m.s$^{-1}$ and (e) Test condition 5: 3N, 0.1m.s$^{-1}$.*

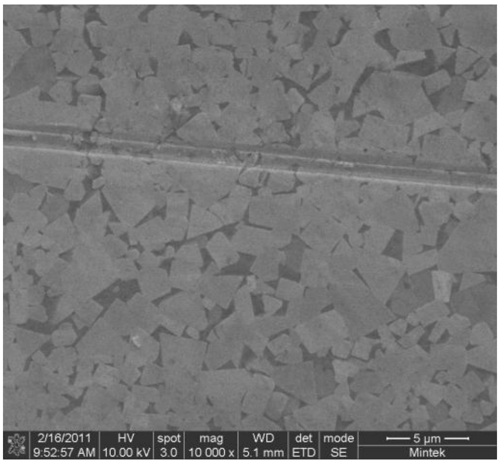


*(a)*

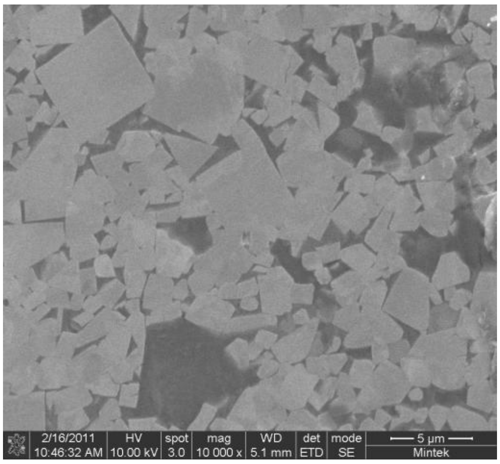


*(b)*

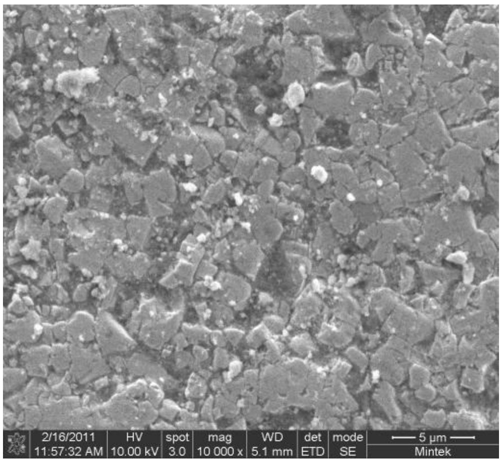


*(c)*

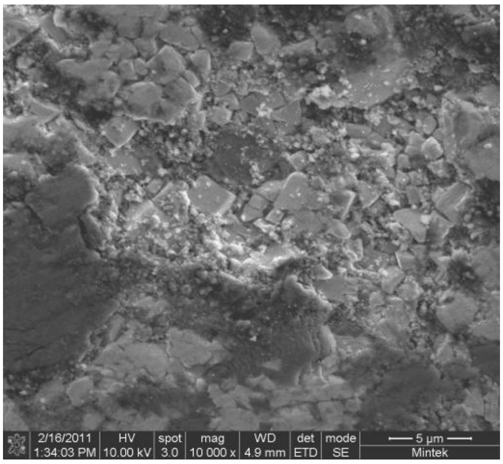


*(d)*

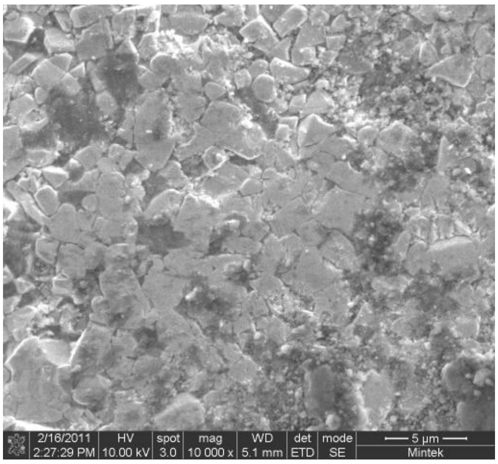


*(e)*

*Figure E.26. SEM images of button WC-C paired with Bright Mild Steel substrate for all the test conditions (a) Test condition 1: 5N, 0.2m.s$^{-1}$ (b) Test condition 2: 3N, 0.2m.s$^{-1}$ (c), Test condition 3: 1N, 0.2m.s$^{-1}$, (d) Test condition 4: 3N, 0.3m.s$^{-1}$ and (e) Test condition 5: 3N, 0.1m.s$^{-1}$.*

# Appendix F

## XPS Data

F.1

Results from the XPS performed on selected sliding pairs are provided below. Table F.1 details the percentage of elements identified on the surface of the substrates. Figures F.1 to F.14 represents the graphical data.

Table F.1. XPS data for the steel substrates under two test conditions.

| | Sample | Atomic Concentration of Elements (%) | | | | | | |
|---|---|---|---|---|---|---|---|---|
| | | C | Fe | O | Cr | Mo | Ni | W |
| | Bright Mild Steel | 1.80 | 95.6 | 2.80 | - | - | - | - |
| | Stainless Steel | 3.80 | 64.5 | 8.60 | 18.10 | 0.40 | 4.60 | - |
| Test Condition 1 | WC-A/CS | 14.4 | 42.8 | 42.8 | - | - | - | - |
| | WC-A/SS | 58.6 | 12.4 | 58.6 | 5.0 | - | 1.1 | - |
| | WC-B/CS | 6.90 | 78.1 | 15.0 | - | - | - | - |
| | WC-B/SS | 27.5 | 21.0 | 41.4 | 9.10 | - | 0.50 | 0.6 |
| | WC-C/CS | 30.9 | 30.5 | 38.6 | - | - | - | - |
| | WC-C/SS | 23.0 | 34.5 | 27.0 | 12.5 | - | 3.0 | - |
| Test Condition 4 | WC-A/CS | 2.9 | 83.6 | 13.6 | - | - | - | - |
| | WC-A/SS | 33.9 | 31.7 | 21.9 | 10.0 | - | 2.5 | - |
| | WC-B/CS | 26.0 | 36.8 | 36.9 | - | - | - | 35.7 |
| | WC-B/SS | 25.8 | 19.7 | 44.1 | 8.0 | - | 1.6 | 0.9 |
| | WC-C/CS | 7.1 | 74.6 | 18.3 | - | - | - | - |
| | WC-C/SS | 15.9 | 36.0 | 31.1 | 13.2 | - | 3.8 | - |

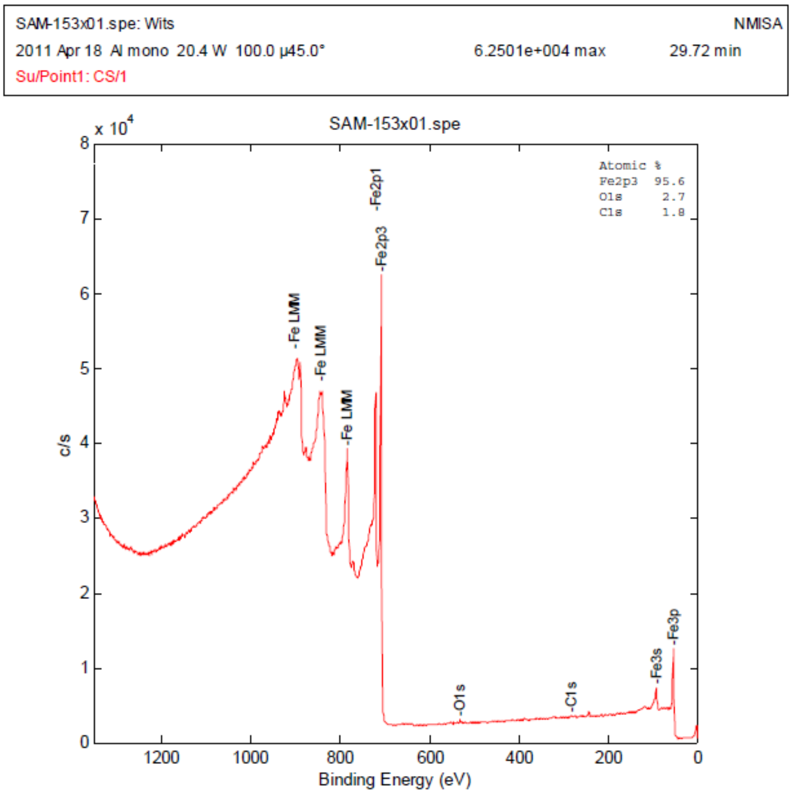


*Figure F.1 XPS results for an unworn bright mild steel substrate.*

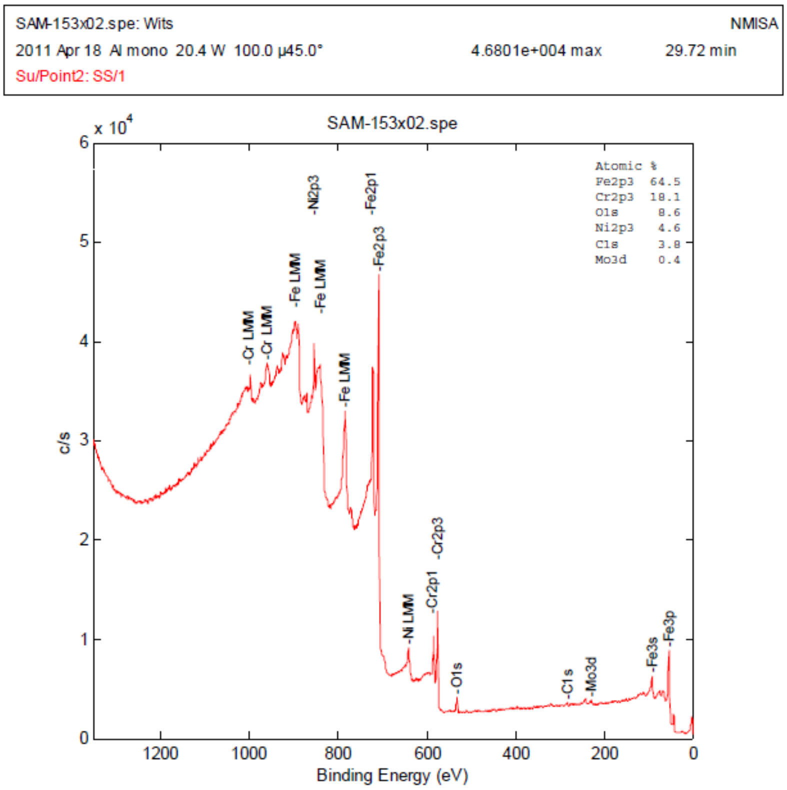


*Figure F.2 XPS results for an unworn 304 stainless steel substrate.*

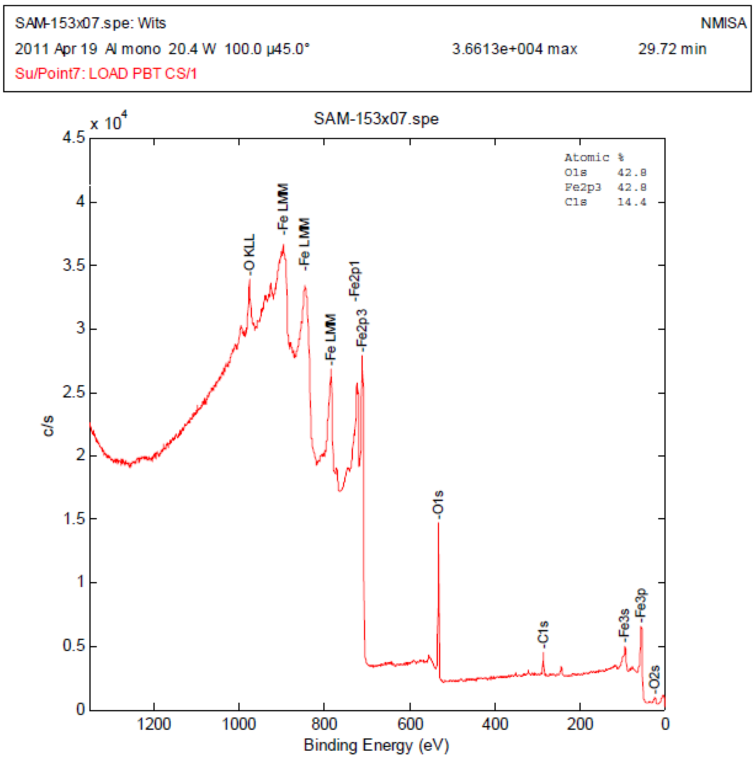


*Figure F.3 XPS results for a mild steel substrate paired with grade WC-A under test condition 1.*

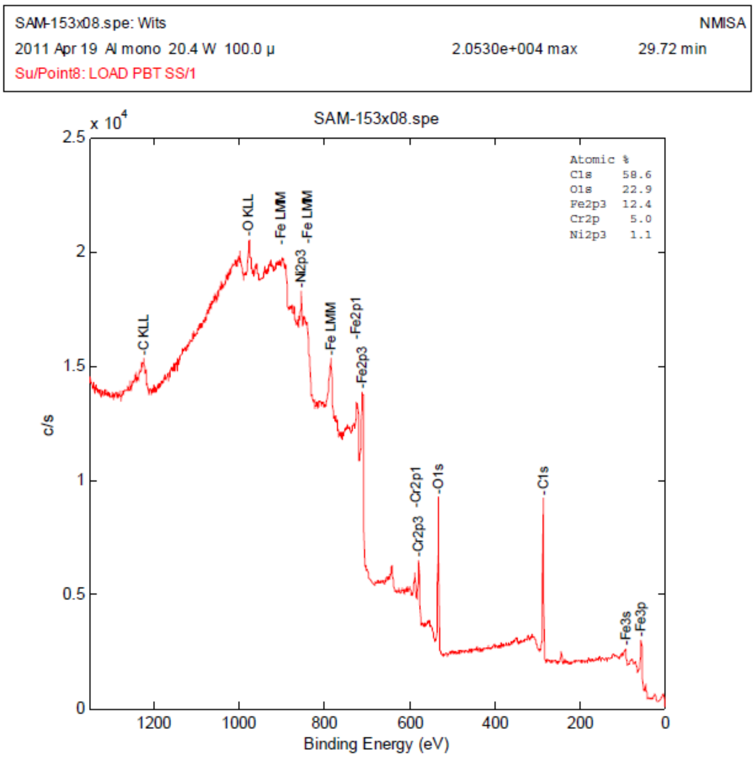


*Figure F.4 XPS results for a 304 stainless steel substrate paired with grade WC-A under test condition 1.*

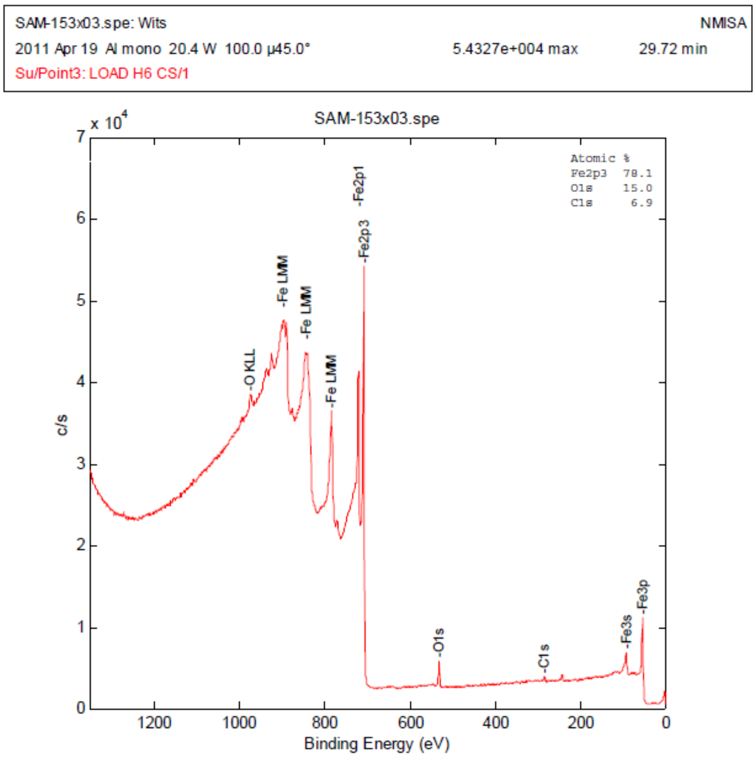


*Figure F.5 XPS results for a mild steel substrate paired with grade WC-B under test condition 1.*

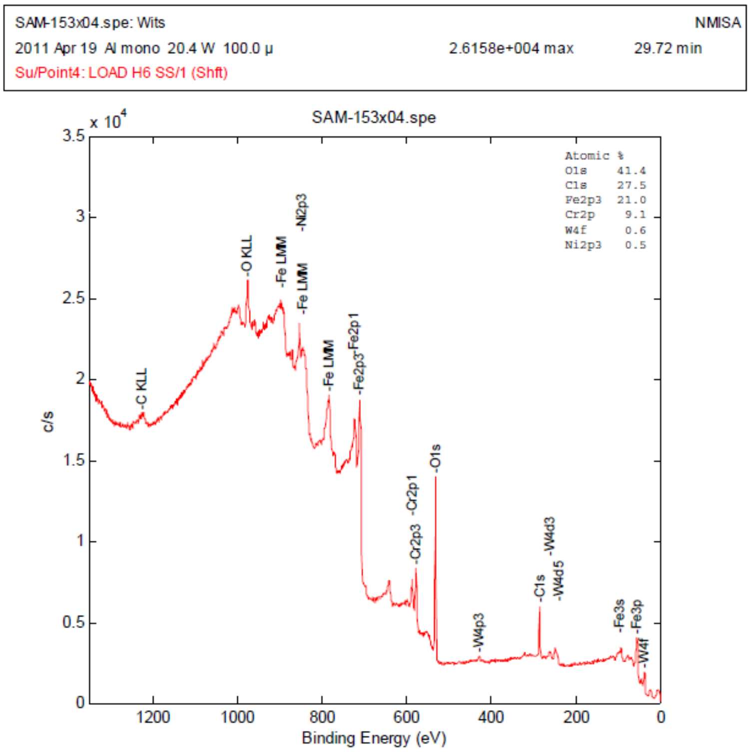


*Figure F.6 XPS results for a 304 stainless steel substrate paired with grade WC-B under test condition 1.*

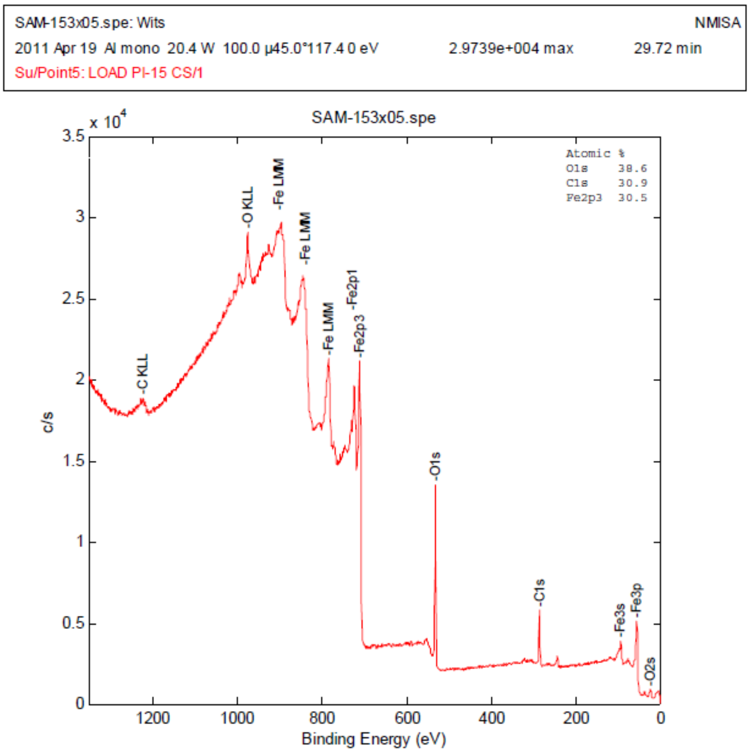


*Figure F.7 XPS results for a mild steel substrate paired with grade WC-C under test condition 1.*

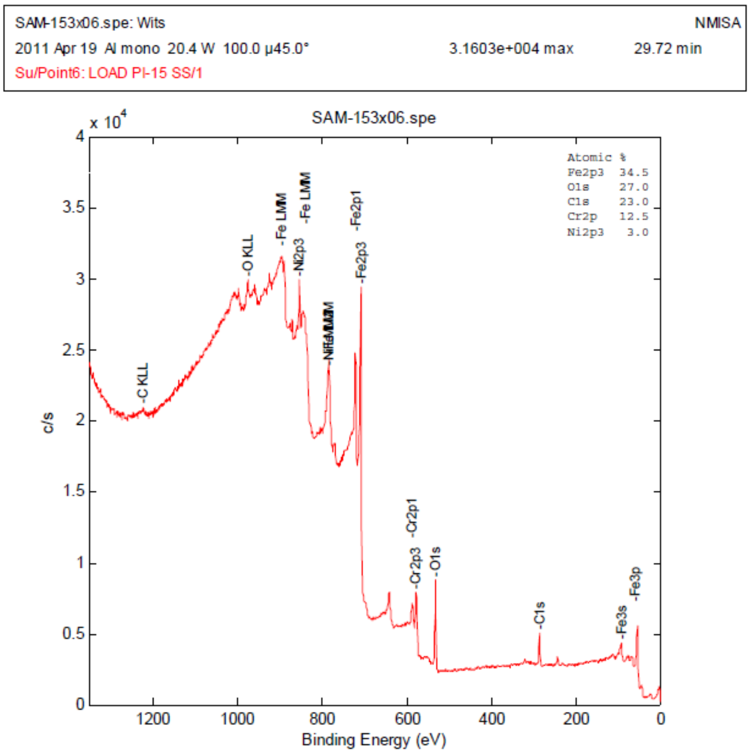


*Figure F.8 XPS results for a 304 stainless steel substrate paired with grade WC-C under test condition 1.*

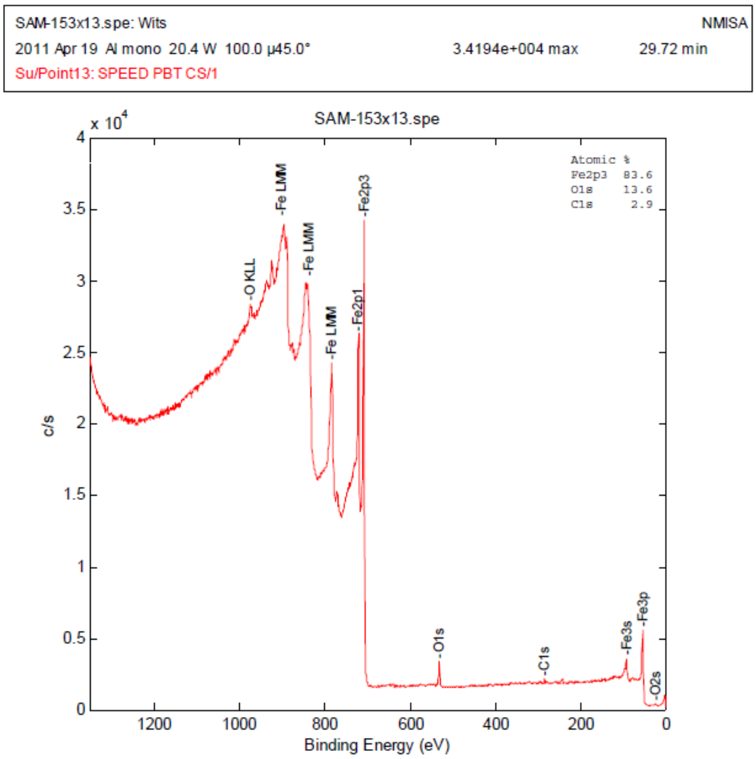


*Figure F.9 XPS results for a mild steel substrate paired with grade WC-A under test condition 4.*

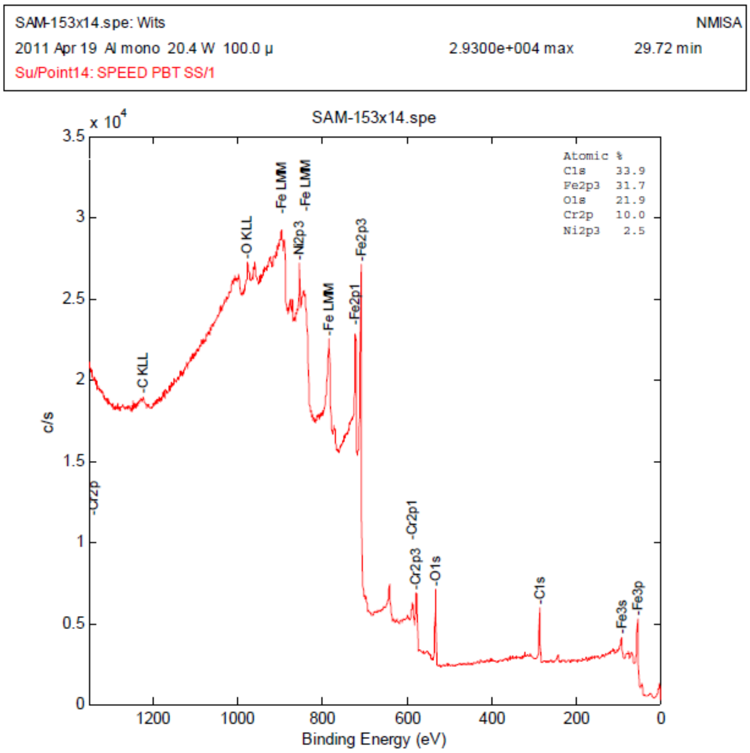


*Figure F.10 XPS results for a 304 stainless steel substrate paired with grade WC-A under test condition 4.*

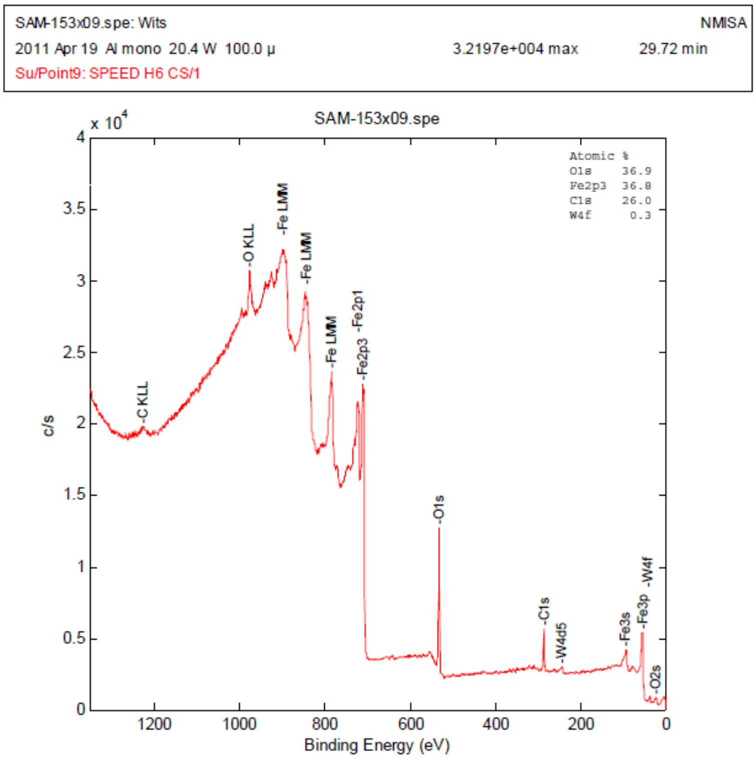


*Figure F.11 XPS results for a mild steel substrate paired with grade WC-B under test condition 4.*

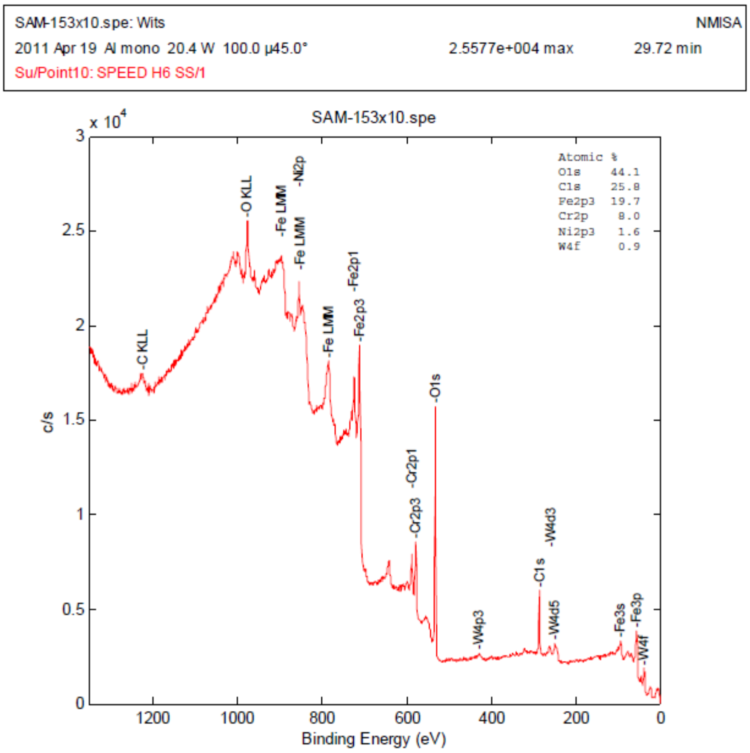


*Figure F.12 XPS results for a 304 stainless steel substrate paired with grade WC-B under test condition 4.*

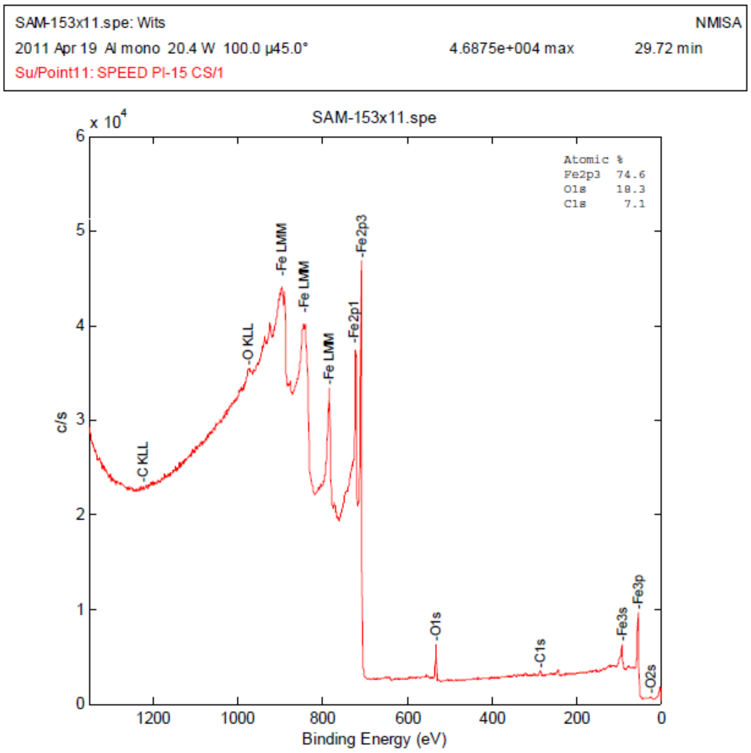


*Figure F.13 XPS results for a mild steel substrate paired with grade WC-C under test condition 4.*

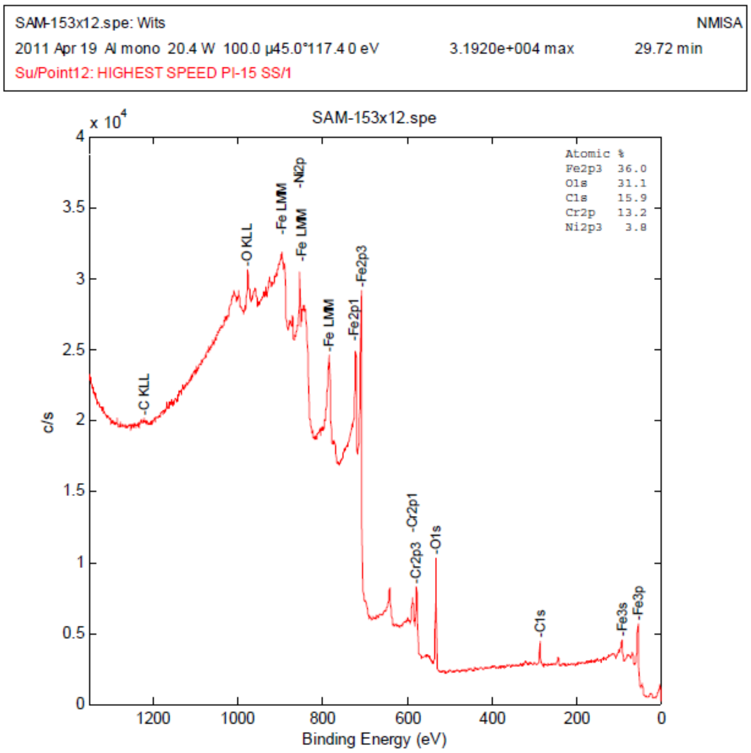


*Figure F.14 XPS results for a 304 stainless steel substrate paired with grade WC-C under test condition 4.*